Evaluating the yield potential of C_4 rice across South and East Asia

DEEPAK POOTHAKUZHIYIL HARIDASAN
July 2021

SUPERVISORS:
Dr. M. T. Marshall
Dr. Ir. C. Van der Tol

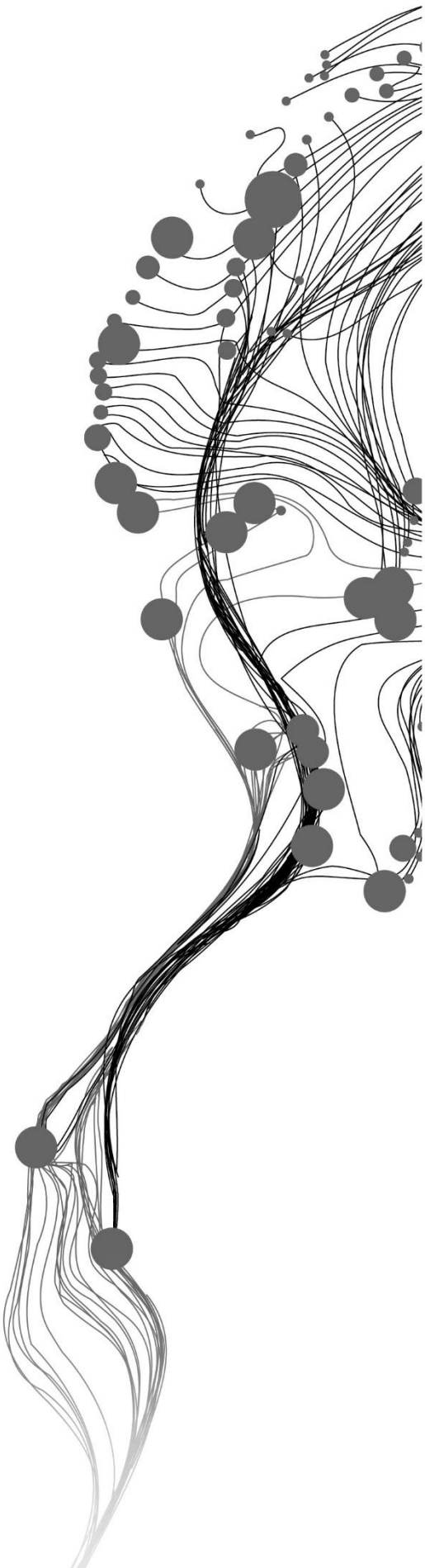

Evaluating the yield potential of C_4 rice across South and East Asia

DEEPAK POOTHAKUZHIYIL HARIDASAN
Enschede, The Netherlands, July 2021

Thesis submitted to the Faculty of Geo-Information Science and Earth Observation of the University of Twente in partial fulfilment of the requirements for the degree of Master of Science in Geo-information Science and Earth Observation.
Specialization: Natural Resources Management

SUPERVISORS:
Dr. M. T. Marshall
Dr. Ir. C. Van der Tol

THESIS ASSESSMENT BOARD:
Dr. Ir. A. Vrieling (Chair)
Dr.Ir. L. Claessens (External Examiner, Wageningen University & Research)

ABSTRACT

The food security for the future humanity is threatened by many factors like climate change, urbanization and soil degradation, etc. To fight against this crisis, new high yielding and resilient crop varieties should be developed. Studies are ongoing to develop such crop varieties like new C_4 rice. But once the variety is developed and ready for cultivation, the community of practice like agricultural researchers, food security analysts, seed companies, etc. may wonder which region and under what agro-climatic conditions these new varieties outperform the traditional varieties and vice versa. In the present study a light use efficiency model (LUE) named Production Efficiency Model Optimized for Crops (PEMOC) was selected to estimate the crop yield for traditional C_3 rice and new C_4 rice across south and east Asia. The study also compared the estimated yield of C_3 and C_4 latitudinally and country-wise corresponding to baseline climatic conditions and future Representative Concentration Pathway (RCP) scenarios. Earlier studies showed that PEMOC can estimate the yield of rice with the coefficient of determination value of 0.75. The model uses only four input parameters such as normalized difference vegetation index, average temperature, solar radiation, and vapour pressure deficit (VPD) and suitable for regional-scale studies. The seasonal average values of NDVI and climatic parameters were calculated from 1982 to 2015 and used as the input parameters for baseline. Also, seasonal average values of the temperature projections corresponding to different RCPs were used for future yield estimation. The result showed that at higher latitudes C_3 crops perform well due to mild temperature and in the mid-latitude around 30^o the difference in yield between C_3 and C_4 is very less. When it comes to the tropic region, the C_4 rice performs better. The country-wise comparison showed that the countries that lie in higher latitude do not get much benefit from C_4 rice in the current climatic condition. But in the future, at elevated temperatures, all countries showed positive responses towards the C_4 rice yield.

Keywords: Crop yield estimation, Food security, PEMOC, C_4 rice, C_3 rice, Photosynthesis, RCP, Optimization, Light use efficiency

ACKNOWLEDGEMENTS

I would like to thank Dr. Michael T. Marshall for the supervision, guidance, and main idea behind the research. He has been very supportive throughout the research period in the difficult times of research and corona lockdown. He has been very patient in explaining the mistakes I made, the solutions for the errors and further steps to procced the research.

I would like to thank Dr. Christiaan van der Tol for his innovative suggestion and support during the research. He has been very kind to attend the supervision meetings within his tight schedule and provided valuable information to conduct the research.

I am very grateful to Dr. Anton Vrieling for clarifying the doubts related to the phenological extraction part of the research. I also express many thanks to Willem Nieuwenhuis and Dr. Andy Nelson for their support.

Thanks to Dr. Michael T. Marshall's wife Dr. Mariana Belgiu and daughter Alexia for the warm and lovely dinner nights at their home.

Finally, I would acknowledge with gratitude the support and love of my family. They all kept me going.

TABLE OF CONTENTS

LIST OF FIGURES

LIST OF TABLES

GLOSSARY OF TERMS AND ABBREVIATIONS

AVHRR	Advanced Very High-Resolution Radiometer
Ca	intercellular CO_2 concentration
CASA	Carnegie–Ames–Stanford Approach
CDS	Copernicus climate data store
CH4	methane
CMIP	Climate Model Intercomparison Project
CO2	Carbon dioxide
D	Total variance
$D(f)$	total variance of the output matric
$D_{12...p}$	all interaction higher than third order
degC	degree Celsius
D_i	first order variance contribution of i^{th} parameter
D_i	variance contribution for parameter i
D_{ij}	second-order contribution of the interaction between parameters i and j
DSSAT	Decision Support System for Agrotechnology Transfer
e_a	actual vapour pressure
ECMWF	European Centre for Medium-Range Weather Forecasts
EOS	end of the season
e_s	mean saturation vapour pressure
EUMETSAT	European Organization for the Exploitation of Meteorological Satellites
FAO	Food and Agricultural Organization of the United Nations
GHGs	greenhouse gases
GIMMS	Global Inventory Monitoring and Modelling System
GPP	Gross Primary Production
HI	Harvest Index
IFS	Integrated Forecast System
IIASA	International Institute for Applied Systems Analysis
IPCC	Intergovernmental Panel on Climate Change
IRRI	International Rice Research Institute
LUE	light use efficiency
MODIS	Moderate Resolution Imaging Spectroradiometer
NASA	National Aeronautics and Space Administration
NASS	National Agriculture Statistics Service
NDVI	Normalized Difference Vegetation Index
NOAA	National Oceanic and Atmospheric Administration
NPP	Net primary production
PAR	Photosynthetically Active Radiation
PAR	photosynthetically active radiation
PEM	production efficiency model
PEMOC	Production Efficiency Model Optimized for Crops
R	proportion of GPP allocated to above-ground productivity
RCP	Representative Concentration Pathway
RMSE	Root mean square error

R-squared	Coefficient of determination
RUE	Radiation use efficiency
SDGs	sustainable development goals
SeaWiFS	Sea-Viewing Wide Field-of-view Sensor
SOS	start of season
T_{max}	daily maximum temperature
T_{min}	daily minimum temperature
T_{OPT}	optimum temperature
UN	United Nations Organizations
US	United States
VPD	vapour pressure deficit
VPM	Vegetation Photosynthesis Model
w	moisture content
WFP	World Food Programme
WHO	World Health Organization
WUE	water use efficiency
F_{GPP}	Conservative fraction for gross daily GPP
F_{Resp}	Fraction for respiration coast
F_{Harv}	Fraction for yield from total biomass produced
ε	ratio of carbon assimilated to the amount of light absorbed by the canopy
ε_{max}	Maximum quantum conversion efficiency
F_{PAR}	Fraction for photosynthetically active radiation
F_T	Fraction for temperature stress
F_M	Short-term moisture stress
F_A	Seasonal moisture stress
Γ	CO_2 compensation concentration
S_i	First-order index
S_{Ti}	Total-order index
°	degree

1. INTRODUCTION

1.1. Background and motivation

Food is one of the essential commodities on the planet to support life as it is the fundamental source of energy and strength. According to the Food and Agricultural Organization of the United Nations (FAO), "food security exists when all people, at all times, have physical and economic access to sufficient safe and nutritious food that meets their dietary needs and food preferences for an active and healthy life" (FAO, 2008). One of the basic components of food security defined by the World Health Organization (WHO) is food availability (*WHO EMRO | Food Security | Nutrition*, n.d.). It refers to the required food available in the right quantities from domestic production or import. But currently, more than 820 million people suffer from hunger (*WHO EMRO | Food Security | Nutrition*, n.d., FAO, 2019). As per studies, the overall food production would be raised by 70 per cent of the current production to feed the increased number of people by 2050 (FAO, 2009). To address this problem, the United Nations Organizations (UN) specially drafted Sustainable Development Goal (SDG) number 2 and called it Zero Hunger (*Goal 2: Zero Hunger – United Nations Sustainable Development*, n.d.). The UN asks all its members to make a profound change to the global food and agricultural system to reduce the number of people who suffer from hunger.

According to World Economic Forum, climate change, urbanization, and soil degradation will be a major threat to arable land and agriculture and consequently food security (*5 Ways to Transform Our Food Systems and Save the Planet | World Economic Forum*, n.d.). Climate change has unprecedented effects on the world's physical and biological systems, including agriculture (Rosenzweig et al., 2008). Some studies predict that increased temperature can considerably reduce yield in the current growing areas for major crops ("Climate Change and Global Warming: Impacts on Crop Production," 2021). Lobell et al., (2011) studied the effect of change of temperature and precipitation on the production of four large commodity crops (wheat , maize, rice and soybean) from 1980 to 2008. The research found out that the temperature trends exceed one standard deviation at most of the growing regions and growing seasons except United States. The study also found that the production of maize and wheat declined by 3.8 and 5.5 %, and for rice and soybean, the increasing and decreasing of yield trends mostly balanced out. Challinor et al., (2014) performed a meta-analysis of crop yield under climate change. The study evaluated the impacts of climate change on yield production of wheat, rice and maize with or without crop level adaptations, such as changes in varieties, planting times, irrigation and residue management. The study's outcome showed that without adaptation, losses could be expected in the production if the temperature is increased by 2^{o}C, whereas with adaptation, the yield production is expected to increase by 7 to 15%, but by the end of current century the production with or without adaptation is predicted to go down.

Historically, farmers performed selective breeding that resulted in the evolution of higher-yielding crop varieties (Ania & Mark, 2012). In the beginning of 1960, new knowledge in the field of crop genetic engineering helped to produce new high yielding crop varieties and seeds that germinate faster. The combination of the new crop varieties with mineral fertilizer, pesticides, irrigation and mechanization caused the agricultural boom (FAO, 2015). But the above-described studies emphasize the importance of developing and adapting new climate-resilient and high yielding crop varieties to battle the future food security crisis. The World Food Programme (WFP) encourages using resilient varieties of crops as one of the five steps to zero hunger (*Zero Hunger | World Food Programme*, n.d.). Some of the methods scientists are working on are increasing the leaf photosynthesis rate of the crops, increasing nitrogen accumulation by crops, increasing the growth rate of individual seeds, developing drought-resilient varieties and introducing higher carbon use efficiency pathway in crops (Sinclair et al., 2004). Many agricultural regions, the crop

production is reached to its peak value, and the existing options are limited (Sage & Zhu, 2011). Therefore, less exploited methods like introduction of higher carbon use efficiency of C_4 photosynthesis in C_3 crops is a possible solution to increase the crop yield.

1.2. Studies on photosynthesis

Some of the studies focused on the photosynthesis process to improve the crop yield already showed positive results (Simkin et al., 2019). Scientists are experimenting with manipulating the existing photosynthesis pathway of some crops like rice, wheat, soybean, etc. Before going into that, it would be better to go through the common photosynthesis pathways in plants. Photosynthesis is the process used by plants to produce food by fixing Carbon dioxide (CO_2). Generally, there are two types of photosynthesis pathways present in the major food crop plants, and they are described below.

1.2.1. C_3 photosynthesis

Barker et al., 1956, discovered this pathway through which plants fix CO_2 into organic acids. Most of the crops on earth, such as barley, oats, rice, wheat, potato, tomato, etc. fix carbon using the C_3 pathway (Meacham-Hensold, 2020). The process in photosynthesis in which CO_2 turns to sugar is called the Calvin cycle with the help of an enzyme called rubisco. The first step of carbon fixation in C_3 photosynthesis is to convert the CO_2 into a 3-carbon compound (3-PGS). This compound then converts into sugar and releases oxygen as a by-product in the presence of sunlight. The entire process occurs inside mesophyll cells in leaves. A schematic diagram of the C_3 pathway is given in figure 1.1.

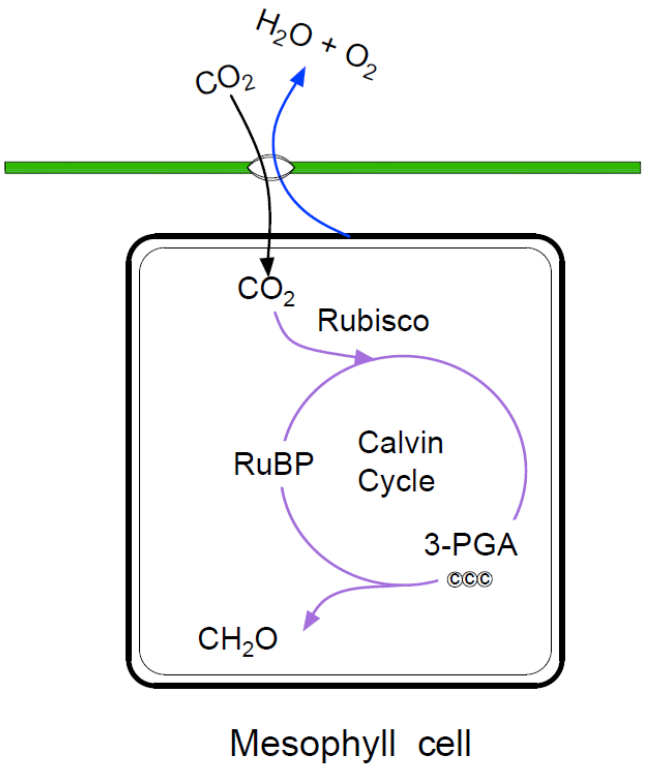

Figure 1.1. Schematic diagram of C_3 photosynthesis. Adapted from Von Caemmerer et al., 2012

A type of respiration called photorespiration exclusively occurs in the presence of light in plants. When a C_3 plant faces temperature stress or water stress, it closes the stomata, and the supply of CO_2 from the atmosphere ceases. But the Calvin cycle continues to fix the absorbed CO_2 and makes higher oxygen concentration inside the cells. Now the rubisco enzyme forces the oxygen, instead of CO_2, to bond with

fixed carbon and releases CO_2. This process is called photorespiration, and it causes wastage of energy (Ehleringer et al., 1991; *Photorespiration (Article) | Photosynthesis | Khan Academy*, n.d.).

1.2.2. C_4 photosynthesis

To prevent energy loss due to photorespiration, some plants like maize and sugarcane evolved into a new photosynthesis pathway called C_4 photosynthesis. In C_4, photosynthesis, the atmospheric CO_2 is initially fixed into a 4 -carbon compound by an enzyme called phosphoenolpyruvate carboxylase (PEP carboxylase) inside mesophyll cells where rubisco is absent (Ehleringer et al., 1991). The second stage of the process (Calvin cycle) occurs at another type of cell called bundle-sheath cells. The 4-carbon compound in mesophyll cells is transported to bundle sheath cells where it is decarboxylated to release CO_2. Then this CO_2 is fixed using rubisco enzyme as in the C_3 plants (Calvin cycle). Since the mesophyll cells continuously pump CO_2 to bundle-sheath cells, the concentration of CO_2 inside the bundle-sheath cells will always remain higher than the oxygen produced. This will prevent energy loss due to photorespiration. A schematic diagram of the C_4 pathway is given in figure 1. 2.

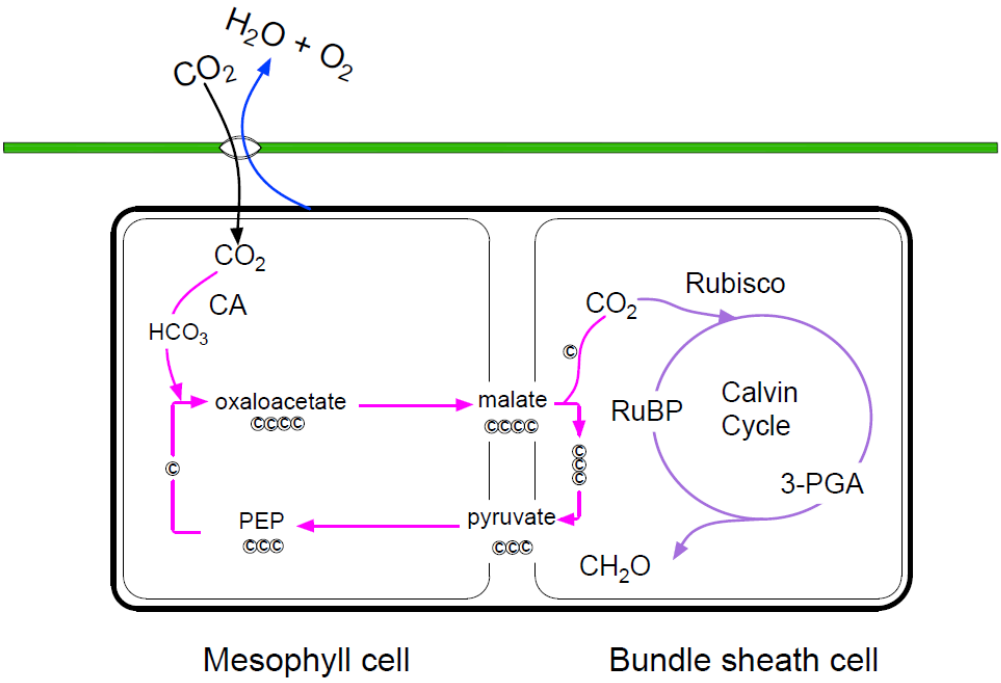

Figure 1.2. Schematic diagram of C_4 photosynthesis. Adapted from Von Caemmerer et al., 2012

1.2.3. Advantages of C_4 crops

In warmer climatic regions, the energy wastage during the photosynthesis in C_3 plants is 40% extra due to photorespiration compared with C_4 crops (Ehleringer et al., 1991). C_4 crops also have higher photosynthetic rate, higher yield, higher water and nitrogen use efficiency, and are more resilient to high temperature (Langdale, 2011; Von Caemmerer et al., 2012). The higher water use efficiency (WUE)of the C_4 crops makes the growing season longer, giving the farmers more flexibility for cultivation (Taylor et al., 2010). The higher water and nitrogen use efficiency can also reduce the farming expense and negative impacts on the environment (Lin et al., 2019). It is observed that C_4 crops are more productive in higher temperature and C_3 crops perform well in the high concentration of CO_2, but when combining with the increase in temperature and WUE, C_4 crops have higher productivity than C_3 crops (Morgan et al., 2011a).

As food security is concerned, one solution to develop a high yielding resilient variety of crops is to introduce C_4 traits to C_3 crops. To conduct this experiment, both species should be closely related and their leaf

anatomy and physiology should be matched (Von Caemmerer et al., 2012). Many experiments were conducted with various species of C_3 and C_4 plants and the researchers found some matches between sorghum and maize (C_4) and rice (C_3) (Lin et al., 2019; Ermakova et al., 2020). To incorporate the C_4 pathway in rice requires a lot of anatomical and biochemical changes and it may take years of experiments to fine-tune and release a high performing variety (Ermakova et al., 2020).

It will be a great relief for the rice farmers and food security analysts if a new high yielding variety of rice arise in the field of agriculture, because rice is one of the most important cereal crops to millions of small farmers and landless workers around the world (IRRI, 2011). Many landless farmers and daily wage workers live their lives using the earning from rice cultivation (Papademetriou, 2000). It is a staple food crop for over half of the population on earth and has the world's second-largest cereal production (FAO, n.d.). Rice is grown in more than 100 countries with an approximate area of 158 million hectares producing more than 700 million tonnes annually (*Rice Productivity - Ricepedia*, n.d.). But for the past few years, the yield returns have ceased to improve with the increase of population through conventional means, and it will soon be plateau (Covshoff & Hibberd, 2012). Therefore, it is very important to develop new resilient, high yielding rice varieties to fight against the future food crisis.

Projects like 'the C_4 rice project' are trying to develop high yielding rice varieties for smallholder farmers by introducing C_4 traits to rice (*The C4 Rice Project*, n.d.). But these experiments are still at the developing and testing stage. But once the varieties are developed and ready to release for public use, the community of practice (e.g.: - food security analysts, agronomists and entrepreneurs) will need to know where and under what conditions they will produce a better yield. Around 90% of total rice production is accounted for from Asia (IRRI, 2011). A huge number of small-scale farmers and landless workers participate in rice cultivation for their day-to-day needs. Also, as described before, global warming can cause considerable reduction of crop yield for normal existing C_3 crop in the current cultivating areas. So, it is good to know what kind of crops can grow better in the coming times using climatic projections. The information can also use for scenario building and develop new policies and practices related to rice production in the region.

1.3. Crop yield estimation models

Since the C_4 rice is a new breed of rice with no cultivation experience before, it is better to understand which agroclimatic region and condition produce more C_4 rice than C_3 rice and vice versa. This concerns related to C_4 rice crop yield and growing conditions can be answered and mapped using crop yield estimation models. Models have been used in food and agricultural related studies in various domains like plant growth, leaf photosynthesis, crop yield estimation, food security analysis and many more (Morgan et al., 2011b; Marshall et al., 2018; Yang et al., 2020). According to Lobell, (2013), satellite data with or without the combination of climatic and other ancillary data or models can accurately measure crop yield mainly in three different ways. The first approach was the empirical model in which the relationship is established between the yield measured in the field and spectral-based vegetation indices, such as the Normalized Difference Vegetation Index (NDVI), obtained through remote sensing. But the transfer of empirical models to other location may not produce reliable results because they are tuned to estimate biomass in a particular area and prone to overfitting (Michael Marshall et al., 2018). In Fully process-based approaches, crop simulation models are integrated with remote sensing data using data assimilation. This process needs a lot of input parameters and suitable for field level studies. It requires simplifications for regional analysis, which questions their validity because of the high risk of propagation of errors and may require trial and error methods which also make it more time consuming. Another approach that will be suitable to predict the yield for regional scale is the light use efficiency model(LUE) or production efficiency model (PEM) approach, first conceived by Monteith, (1977). In this approach, the Gross Primary Production (GPP) is estimated from Photosynthetically Active Radiation (PAR) weighted by the fraction of photosynthetically active radiation absorbed by the canopy (F_{PAR}) and energy to dry matter or quantum conversion efficiency

(ε). GPP is defined as the amount of carbon uptake by vegetation through photosynthesis (X. Li et al., 2016). . ε is the ratio of carbon assimilated to the amount of light absorbed by the canopy. Then the GPP is converted to yield using the harvest index.

According to Dong, Lu, Wang, Ye, & Yuan, (2020), LUE models are efficient and reliable method to estimate crop yield. Xin et al., (2013) also used an LUE model to estimate crop yield for both corn and soybean and found out that the output has good correlation with the field data (0.77 and 0.66 respectively). Empirical models tend to assume linear relationships between abiotic factors and yield, but the LUE models can be used to estimate the GPP regional or global scale without the problem of non-linearity between ecosystem process and environmental variables (Running et al., 2000). The advantages of using LUE models are simple model structure, limited number of parameters and integration of remote sensing data (Zan et al., 2018), making it suitable for regional-scale studies. The simple structure of the model also reduces the computation time considerably. Marshall, Tu, & Brown, (2018), introduced a new production efficiency model (PEM) called Production Efficiency Model Optimized for Crops (PEMOC) for regional-scale yield estimation for different crops (corn, rice, soybean, and winter wheat) using earth observation data and geospatial climate data for the United States (US). The model was optimized for above mentioned crops in the study area of US and proven to be suitable to estimate crop yields. The model show improvements in results compared with another model called MOD17 (Moderate Resolution Imaging Spectroradiometer GPP/NPP product). PEMOC requires only four inputs and appears accurate and robust. The required input parameters are normalized difference vegetation index (NDVI), solar radiation flux, vapour pressure and average temperature. The research uses different values for the quantum conversion efficiency (ε) for C_3 and C_4 crops because, as described earlier, the C_3 photosynthesis is depend on temperature and CO_2 concentration , while C_4 metabolism is not (Collatz et al., 1991.;G. Collatz et al., 1992). PEMOC is also suitable for regional-scale studies with less computational time. Therefore, the best option to conduct this study is to use PEMOC.

PEMOC can also be used to evaluate the effect of global warming on crop yield. For this, the crop yield corresponds to temperature projections based on different Representative Concentration Pathways (RCPs) can be estimated and compared. RCPs are scenarios that include time series of emissions and concentrations of greenhouse gases (GHGs), aerosols, chemically active gases and change of land use/ land cover (IPCC, 2014). These external drivers of climate change cause change in the net, downward minus upward, radiative flux (expressed in Watts per square metre; W m^{-2}) called radiative forcing. Four RCPs produced from Integrated Assessment Models were selected from the published literature and are used in the Fifth Intergovernmental Panel on Climate Change (IPCC) assessment as a basis for the climate predictions and projections (Stocker et al., 2013). RCPs usually refer to the portion of the concentration pathway extending up to 2100. The details of the four major pathways are given below (IIASA, 2015).

- RCP 2.6: One pathway where radiative forcing peaks at approximately 3 W m^{-2} before 2100 and then declines (the corresponding ECP assuming constant emissions after 2100). The projection for atmospheric CO_2 concentration for year 2050 is 442.70 ppm and for the year 2100 is 420.89 ppm.
- RCP 4.5 and RCP6.0: Two intermediate stabilization pathways in which radiative forcing is stabilized at approximately 4.5 W m^{-2} and 6.0 W m^{-2} after 2100 (the corresponding ECPs assuming constant concentrations after 2150). The projection for atmospheric CO_2 concentration for year 2050 is 486.54 ppm and for year 2100 is 538.36 ppm corresponds to RCP 4.5. For RCP 6.0, the CO_2 concentration are 477.67 ppm and 669.72 ppm for years 2050 and 2100 respectively.
- RCP 8.5: One high pathway for which radiative forcing reaches greater than 8.5 W m^{-2} by 2100 and continues to rise for some amount of time (the corresponding ECP assuming constant emissions after 2100 and constant concentrations after 2250). As per RCP 8.5, the projected atmospheric CO_2 concentrations are 540.54 ppm and 935.87 ppm for the years 2050 and 2100 respectively.

RCP 8.5 usually considered as the high emission scenario and RCP 2.6 is the lowest emission scenario. The RCP scenarios are widely used in climate and agricultural research (Ahmadi et al., 2021; Müller et al., 2015; van Vuuren et al., 2011). It can also incorporate with PEMOC to see the effect of future climate on the C_3 and C_4 rice yield production.

1.4. Problem statement

LUE models are suitable for crop yield estimation regional scale. PEMOC is an optimization LUE model, which can estimate yield using NDVI and climatic parameters such as average temperature, vapour pressure and solar radiation flux. Many studies are available to estimate the crop yield of various crops of both C_3 and C_4 pathways covering local and regional scale using various models with remote sensing (Hoefsloot et al., 2012; Peng et al., 2014; Wang et al., 2020; Xin et al., 2013; Yuan et al., 2015; Zhou et al., 2017). Many research articles were published related to the development of C_4 rice, but the estimation of crop production of C_4 rice in local or regional scale for present or future has not been done yet (Covshoff & Hibberd, 2012; Langdale, 2011; Von Caemmerer et al., 2012).

Since the C_4 rice variety is not developed yet, there is no information about any of the plant's biological or biochemical process or properties, only the information about the pathway is known (Von Caemmerer et al., 2012). Therefore the value of quantum conversion efficiency of C_4 rice has to be taken as the same as that used in the previous study with PEMOC (Michael Marshall et al., 2018). The model is optimized for the rice and other crops cultivated in the US. But it is recommended to optimize the model before yield estimation using the yield or GPP data available anywhere from the study area.

It is highly informative to understand which parameter of the model inputs is the most influencing at various places in the study area, especially when the study area is large scale. It can help to make the predictions more reliable and help to improve the results. Therefore, a sensitivity analysis can also be used to answer this question and may help to interpret the results of yield estimations across the study area.

Climatic researchers developed various scenarios predicting the future climatic conditions considering global warming and GHGs emissions (*Socio-Economic Data and Scenarios*, 2019). To battle with future food crisis and help farmers, it is always useful to know which crop produce higher in the future conditions. The researchers can use the information about the crop to optimize the management practices, assist in breeding programmes and develop new crop rotation methods (Asseng et al., 2015). This research also aims to analyse the crop yield of C_3 and C_4 rice in probable future scenarios for the year 2050 and 2099.

About 77% of world's rice production comes from South and East Asia (FAOSTAT, n.d.). Nine out of top ten rice-producing countries are from Asia, considering the average production from 1994 to 2019 (FAOSTAT, n.d.). They are China, India, Indonesia, Bangladesh, Vietnam, Thailand, Myanmar, Philippines, Japan in the descending order of rice production. Many farmers and landless workers depend on rice cultivation in this region (IRRI, 2011). Therefore, the study area is selected as South and East Asia covering all the above stated countries. The aim of the research is to provide a basic understanding of the yield potential of the new C_4 rice variety in South and East Asia in the current rice cultivating areas. Since the study area is vast and covers a large variability in climate when moving from northern latitude of study area to southern latitude, it is expected to see a change of yield in C_3 and C_4 yield production as per the research of Morgan et al., (2011b). At the northern latitudes the temperature is less and the C_3 productivity is expected more than C_4 rice. When comes to the tropical region the C4 rice is expected to perform well. A conceptual diagram depicting the research description is given in figure 1.3.

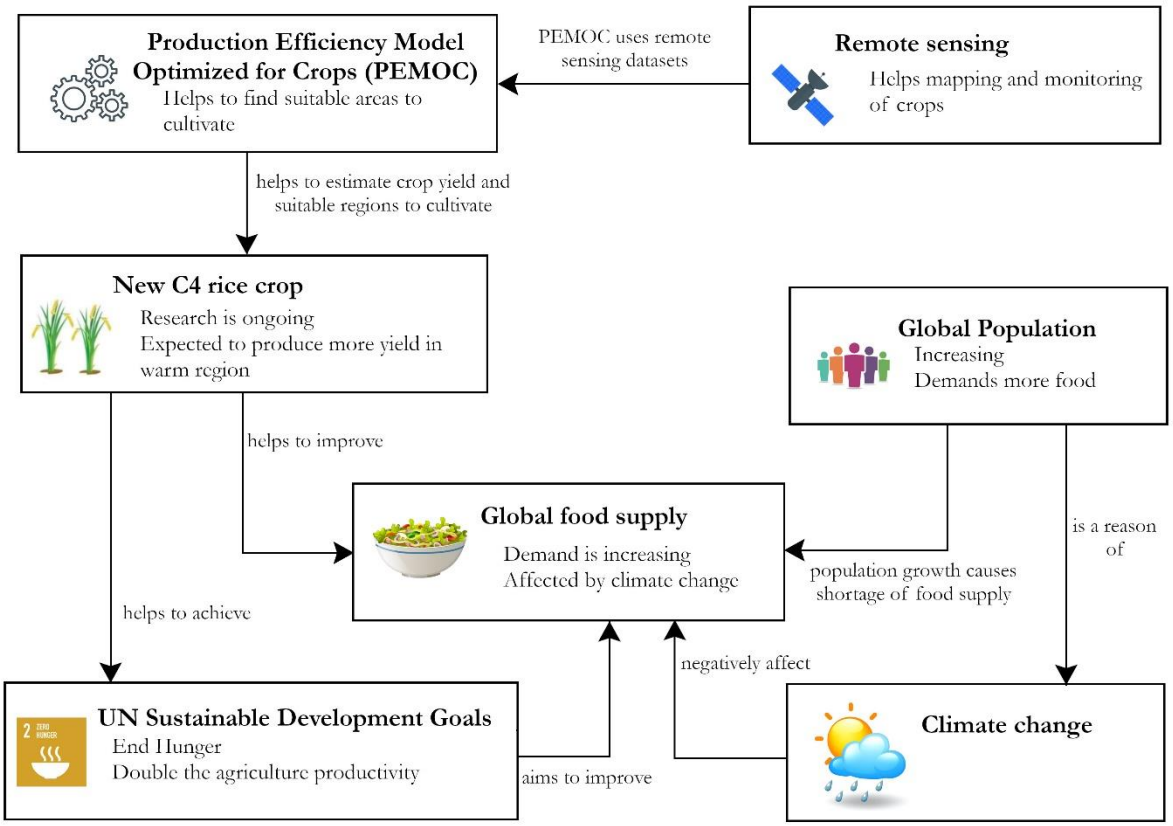

Figure 1.3. Conceptual diagram of the research.

Centre of the figure is global food security, which is negatively affected by global population and climate change. The UN tries to improve the situation by implementing new policies like UN sustainable development goals (SDGs) (especially goal number 2: Zero hunger). New research like C_4 rice development is ongoing and expected to improve global food security and help to achieve UN goals. Model alike PEMOC can be used to estimate the crop yield of the crops using remote sensing datasets. It can also provide valuable information like where and under which conditions the new C_4 crop varieties can perform better.

1.5. Research Objectives and Questions

Before releasing a new crop variety, it is better to understand the prior knowledge about the optimum conditions and suitable place for cultivating it. This helps the researchers, policymakers, and farmers to plan the practices better and helps to battle the future food crisis. Some of the ways to do this are increasing the seed production to supply enough seed to farmers, aware the farmers and increase their participation in new crop cultivation, improving the policies and legislation for the new varieties, etc. As discussed in the previous section, LUE modelling techniques can be used to get insight of crop productivity on the regional scale. Since South and East Asia is the biggest producer and consumer of rice globally (Papademetriou, 2000), the same is considered the study area. Therefore, this research is focused on estimating the yield potential of C4 rice in South and East Asia and compare it with the current C_3 rice crop with the help of the light use efficiency model PEMOC.

The research also examines the effect of future temperature on C_3 and C_4 rice yield production. C_3 and C_4 rice crop yield for the current climatic conditions will be estimated and compared according to different RCP scenarios. These results will explain how the crops will perform in the future in different agro-climatic regions. The research will also check which climatic variable in the model, which is mostly influencing the output in different region in the study area.

The specific objectives of the study are given below.

1. To estimate the difference in crop yield for C_3 and C_4 rice on a pixel-by-pixel basis for the current average climatic conditions of 34 years (1982 to 2015) in South and East Asia using the PEMOC model.
2. To estimate the difference in crop yield for C_3 and C_4 rice on a pixel-by-pixel basis for the future three RCP scenarios (4.5, 6.0 and 8.5) for the years 2050 and 2099 in South and East Asia using the PEMOC model.
3. To characterize the growth conditions where crop yield for C_3 rice is higher than C_4 rice and vice versa.
4. To check the sensitivity of the model for C_3 and C_4 pathways to various input parameters, namely NDVI, photosynthetically active radiation (PAR), average temperature (Ta) and vapour pressure deficit (VPD).

The following questions will be answered to achieve the stated objectives,

1. What is the spatial distribution of differences in estimated C_3 and C_4 rice yield pathways in the following climatic condition?
    a. Current climatic condition
    b. Three RCP scenarios (4.5, 6.0 and 8.5) for the year 2050
    c. Three RCP scenarios (4.5, 6.0 and 8.5) for the year 2099
2. Under what agroclimatic conditions is C_4 rice yield higher than C_3 rice yield?
3. What input parameters are the model most sensitive to and what is the spatial variability of model to different parameters?

1.6. Expected results

Based on the above literature and objectives of the research the expected results of this study are given below.

1. At higher latitudes (northern) the model is sensitive to temperature and at tropics the model is sensitive to radiation.
2. Both C_3 and C_4 rice produce comparatively less at northern latitudes and the productivity increases when moving towards the tropical region (near equator)
3. The difference in crop yield between C_3 rice and C_4 rice is minimum at northern latitudes and the difference increases moving towards the tropical region (near equator)
4. The productivity of C_4 rice is comparatively more than that of C_3 rice for current and future climatic scenarios in current rice-growing areas.

2. REVIEW OF LITERATURE

Information about the crop production and crop area plays an important role in the agriculture sector (FAO, 2017). This information acts as a fundamental input to the planners and policymakers responsible for formulating efficient agricultural policies and making important decisions regarding procurement, storage, public distribution, import, export, and other related issues. FAO also describes various field methods to estimate crop yield, such as whole plot harvest method, crop cut method, farmer's recall, sampling of harvest units, simple crop modelling (empirical-statistical) and complex crop modelling based on crop physiology.

All of the above methods have its own advantages and disadvantages. Methods like the whole plot harvest method and crop cut method are very accurate, but they are time-consuming and covers small areas. Farmer's recall and sampling of harvest units are very fast and less labour-intensive, but they may not be accurate, and chances of biasing is also more. Simple and complex crop models using the field data are suitable for local scale, but, for regional-scale prediction other methods like crop estimation models using remote sensing must be used(Weiss et al., 2020). Some of the advantages of using remote sensing data in crop yield estimation are given below.

1. Many high-resolution satellite images and vegetation products are freely available (European Environment Agency, 2017; NOAA, n.d.). Therefore, it is very cost-effective.
2. The acquisition of satellite is very frequent. For example, Landsat satellite has a 16-day revisit time and sentinel-2 has a 5-day revisit time at the equator.
3. The image capturing process is very consistent and the product covers globally. Therefore, it is suitable for regional scale analysis.

2.1. Crop yield estimation using remote sensing

According to Lobell, (2013), crop yield estimation using remote sensing is less accurate than field-based measures, but remote sensing helps to predict yield for very large areas and for longer period. He also explained about various approach using remote sensing data to predict crop yield. The first approach is simply finding an empirical relationship between any of the vegetation indices like leaf area index (LAI) or normalized difference vegetation index (NDVI) and measured yield from the ground (Delécolle et al., 1992a; Paul C Doraiswamy et al., 2003). This method is suitable to explain the yield variability within a field, but it is difficult to transfer to another region and period. Secondly, he explained about the light use efficiency (LUE) approach developed by Monteith, (1977). This approach assumes that the crop yield is proportional to the photosynthetically active radiation (PAR) during the crop growing period. There are other approaches, like the crop condition and crop simulation model using Landsat and Modis (P. C. Doraiswamy et al., 2004) and Decision Support System for Agrotechnology Transfer (DSSAT) (Hoogenboom et al., 2019). These methods often need more model functions as inputs, and which adds complexity and computation time also difficult to parametrize over large areas.

2.2. Light use efficiency (LUE) models

As per the reviews of David B. Lobell, (2013) , Delécolle et al., (1992b) and Doraiswamy et al., (2003) LUE modelling is an appropriate method to conduct the current study. The cropland net primary production (NPP) of the United States was estimated by D. B. Lobell et al., (2002) using an LUE model called the Carnegie–Ames–Stanford Approach (CASA) for the period of 1982 to 1998. The modelled NPP were then compared with field estimates based on harvest data from United States Department of Agriculture National Agriculture Statistics Service (NASS) county statistics. The study suggests that use of remote sensing data for such analysis can be carried out faster, with less complexity and large area coverage.

Chen et al., (2014) used CASA to estimate the global cropland GPP for the year 2000 using satellite data, eddy covariance flux measurements and field survey data. The study was conducted for 26 crop types. The study found out Asia produce one-third of global cropland GPP. When comparing with the observed GPP in the field with the modelled GPP, the correlation coefficient was found out to be 0.85 ± 0.14.

Yuan et al., (2007) developed an LUE model to measure gross primary production (GPP) for regional scale using eddy covariance (EC) measurements and named the model EC-LUE. The assumptions made during model development were photosynthetically active radiation (PAR) is a linear function of NDVI, and light use efficiency is controlled by air temperature or soil moisture, whichever is most limiting. The outputs were validated and compared against Moderate Resolution Imaging Spectroradiometer (MODIS) GPP and found that the model is reliable across biomes and geographic region. The model is independent of landcover types and the input variables can be obtained from satellite data or weather observation networks, which made the model flexible and transferable. Another study was conducted on EC-LAU model by Yuan et al., 2015 and confirmed that the model is robust and reliable to predict the primary productivity of crops.

Dong et al., (2020), estimated the winter wheat yield based on EC-LAU model across Kansas state, U.S.A, from 2008 to 2017. He derived NDVI from Landsat 5, 7 and 8 images. The other input parameters like photosynthetically active radiation (PAR), air temperature, net radiation, relative humidity, and surface pressure were obtained from the Modern-Era Retrospective Analysis for Research and Applications, version 2 (MERRA-2). The research was able to explain 82% of the inter-annual yield variation.

In another research, the crop yields of corn and soybean were estimated using a production efficiency model (PEM) with MODIS data and GPP algorithm in the Midwestern United States (Xin et al., 2013). The model outputs for both crops were compared with NASS data and found coefficient of determination (R-squared) = 0.77; and root mean square error, (RMSE)= 0.89 MT/ha for corn and R-squared = 0.66; RMSE = 0.38 MT/ha for soybean. The study also found out that the use of proper crop-type efficiency factor to estimate the yield is very important in the process.

Nguy-Robertson et al., (2015), modelled GPP for maize and soybean near Nebraska, the U.S.A, using diffuse and direct sunlight light, temperature, water stress, and phenology. The model used in the study was derived from an LUE model called Vegetation Photosynthesis Model(VPM) developed by Xiao et al., (2004). The outputs were validated with field data with an RMSE of 2.6 $gCm^{-2}\ d^{-1}$.

The MODIS NPP algorithms were combined with another model called Eight-day NPP model to predict rice yield estimation in Liling County, China by Peng et al., (2014). The study also used radiation use efficiency (RUE) and harvest index (HI) to estimate crop yield. Then the outputs were validated with field data and found out relative error and RMSE of less than 5% and 5×10^4 kg respectively.

Marshall et al., (2018) presented a new production efficiency model called Production Efficiency Model Optimized for Crops (PEMOC) for macro scale yield estimation for various crops, including C_3 crops (rice, soybean and winter wheat) and C_4 crop (maize). The result of validation for rice has R-squared = 0.75 and RMSE =17.47 g $CO_2\ d^{-1}$. The model was able to estimate crop yield for six crops across the Contiguous United States. The data from eddy covariance flux towers was used to optimize the model. The model uses only few parameters (NDVI, incoming shortwave radiation, temperature, and the vapour pressure deficit (VPD)) and can be easily be adapted to other ecosystems. The study showed the yield estimation improved mainly because of simulating C_3 and C_4 separately.

3. METHODOLOGY

3.1. Study area

The stydy area was chosen as South and East Asia. 59.51% of the world population live in Asia (• *Global Population - Distribution by Continent 2019 | Statista*, n.d.), and 70% of the world's poor population (people who earn less than $1.90 per day) also live in Asia (IRRI, 2011; Roser, Max and Ortiz-Ospina, 2013). For these people, rice is one of the important food commodities in their daily life. About 92% of the world's rice production comes from Asia (IRRI, 2011), and 77% from South and East Asia (FAOSTAT, n.d.). Nine out of top ten rice-producing countries are from Asia, considering the average production from 1994 to 2019 (FAOSTAT, n.d.). They are China, India, Indonesia, Bangladesh, Vietnam, Thailand, Myanmar, Philippines, Japan in the descending order of rice production and Brazil is in the tenth position, which is the only country outside Asia (FAOSTAT, n.d.). Most of the rice cultivated in the area is based on irrigated low land cultivation (*Where Is Rice Grown? - Ricepedia*, n.d.; *FAOSTAT*, n.d.). The extent of the study area lies within 57° 50' 0.0024" to 168° 4' 59.9988" in longitude while - 16° 49' 59.9988" to 55° 55' 0.0012" in latitude. The extent is determined based on the extend of map showing rice cultivation areas obtained from International Rice Research Institute (IRRI).

Since the area covers a large portion of Asia, it covers many agro-climatic zones (Dando, 2005). The area near the Himalayan mountains is cold and the temperature drops to below freezing point during winter and reaches an average of 15 degC during summer. North, northeast and central parts of China are temperate zones. But in Northern and central part of china no rice is grown. The northern part of India, south, south-east and south-west parts of China are sub-tropical regions. The coastal regions of south and east Asia are tropical areas.

To understand the changes in temperature and precipitation across the rice cultivation regions in the study area, sixty-one points were picked randomly across the study area from countries Bangladesh, Cambodia, China, India, Indonesia, Japan, Laos, Malaysia, Myanmar, North Korea, Pakistan, Philippines, South Korea, Thailand and Vietnam. The points were selected using the rice cultivation map obtained from IRRI. The global monthly average temperature (degC) and precipitation (mm) data from 1970-2020 was downloaded from www.worldclim.org (Fick & Hijmans, 2017). The download file is a zip file consist of twelve tiff files for average values of temperature and precipitation for each month from January to December. The resolution of the file is 10 minutes (approximately 340 km^2) and projected on WGS 1984 coordinate system. The average values of temperature and precipitation at selected points in the rice cultivation areas were extracted and plotted. The selected points with rice cultivation area are shown in figure 3.1. The monthly average temperature (degC) and precipitation (mm) in the selected points are shown in figure 3.2 and 3.3.

From the figure 3.2, it is clear that at all selected locations the temperature reached above 15 degC during summer from May to August and most of the places it is above 20 degC, which is suitable for rice cultivation (JICA, 2010) . But in some areas like northern China, Japan, North Korea and South Korea, the temperature falls below 5 degC in the months of December- January (winter) and that is not good for rice. But selected locations in the tropical region do not have many fluctuations in temperature, it varies between 25 to 35 degC.

When looking at the precipitation in figure 3.3, the points at the higher latitude have very low precipitation. But the points at the tropics have high precipitation at different months of the yaer. Points at Indonesia receive high rainfall from November to February. Other places like Philippines, Thailand, Myanmar, Bangladesh receive high rainfall from May to September.

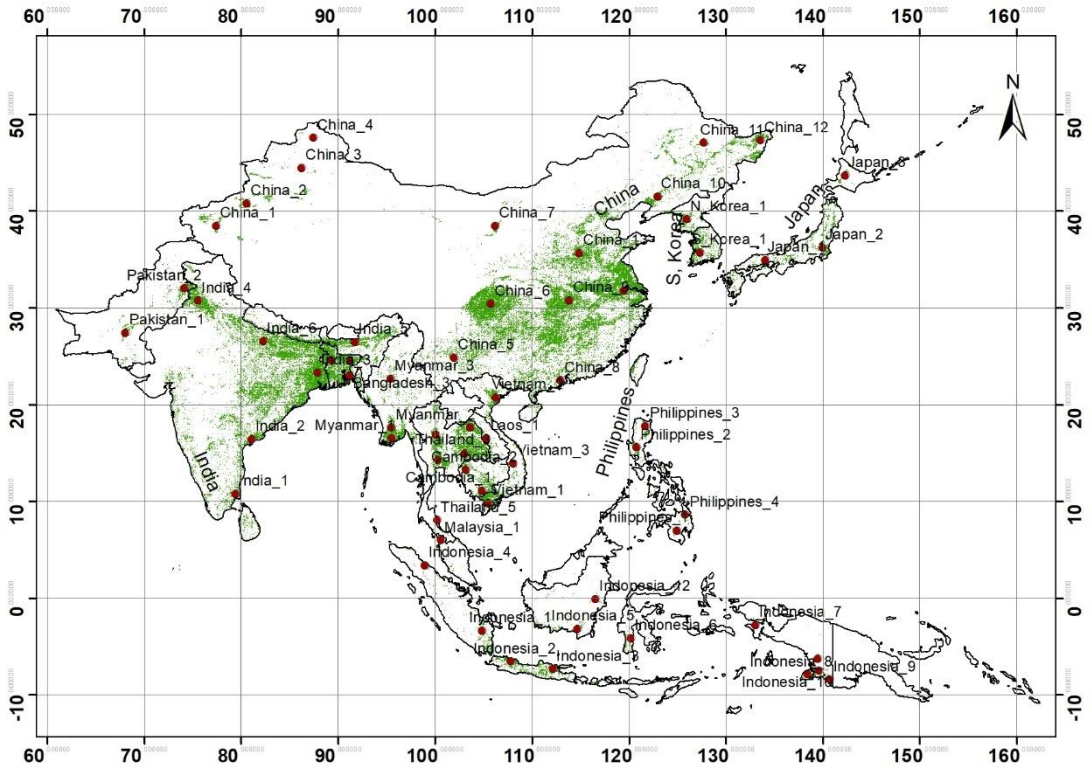

Figure 3.1. Study area. The green patches in the map showing the rice growing regions. The red dots are randomly selected points to extract and plot monthly average temperature and precipitation.

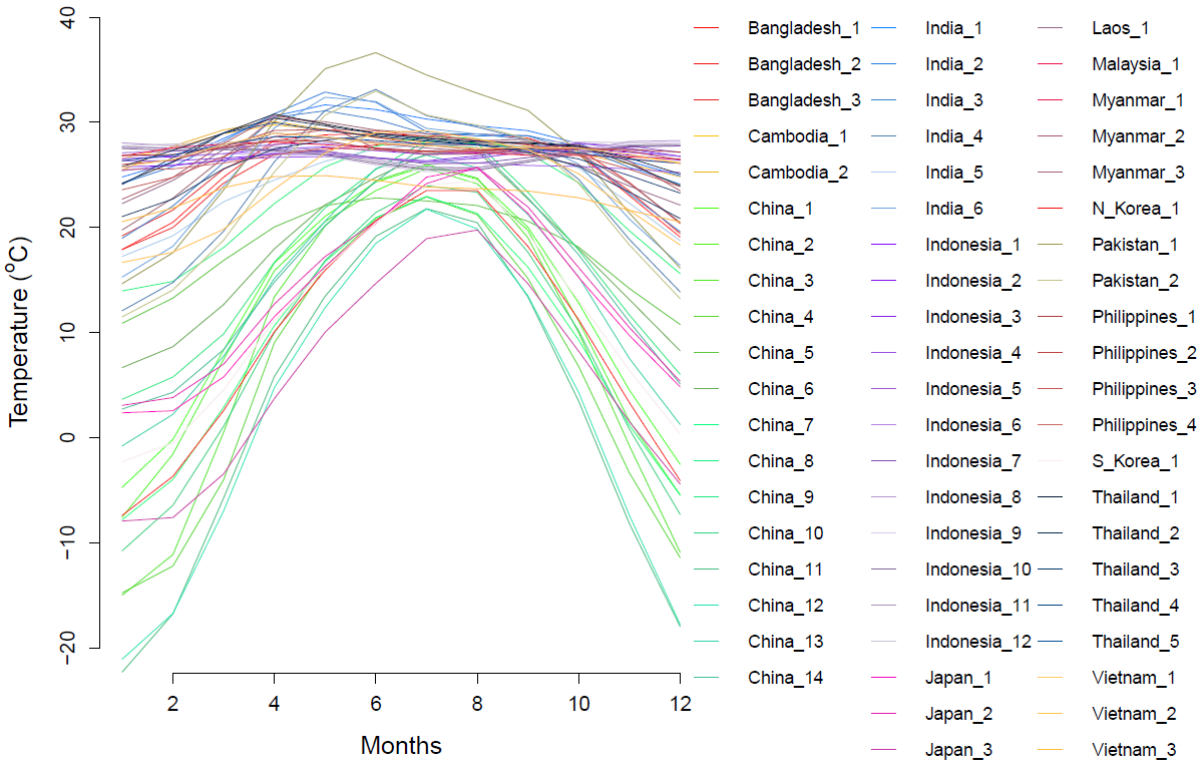

Figure 3.2. Monthly average temperature at the selected locations in the study area. The points selected are shown on the right side with the country name and point number.

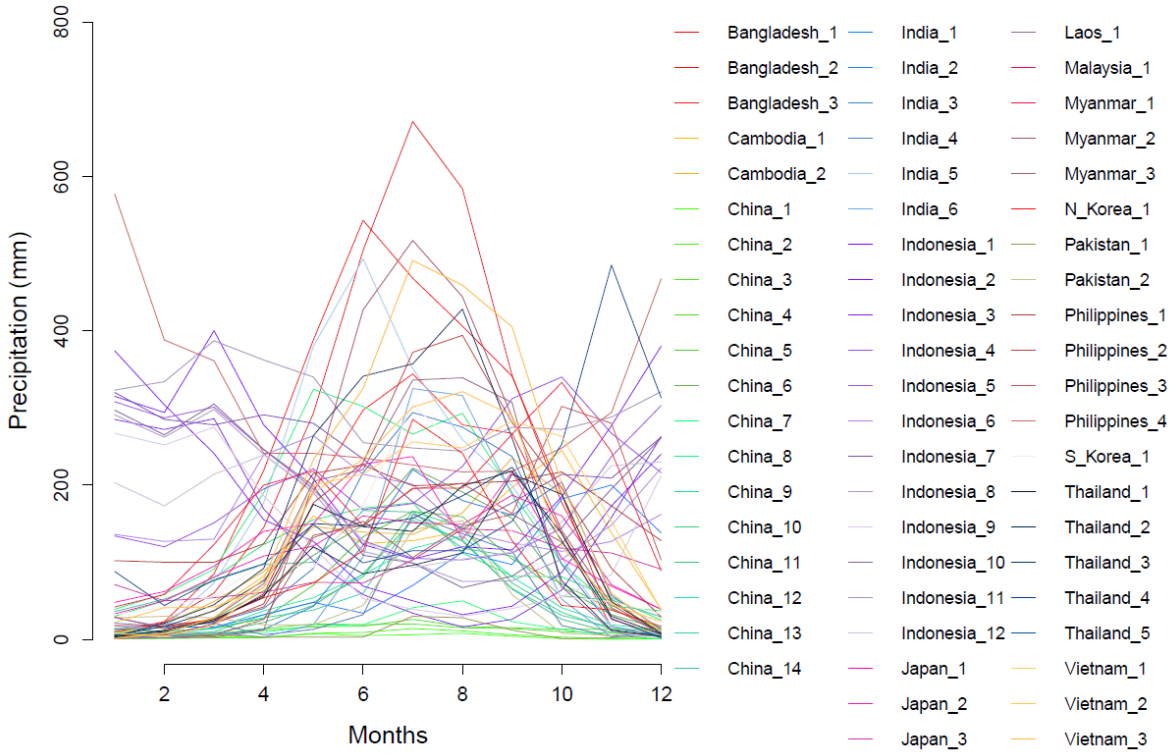

Figure 3.3. Monthly average precipitation at the selected locations in the study area. The points selected are shown on the right side with the country name and point number.

3.2. Data

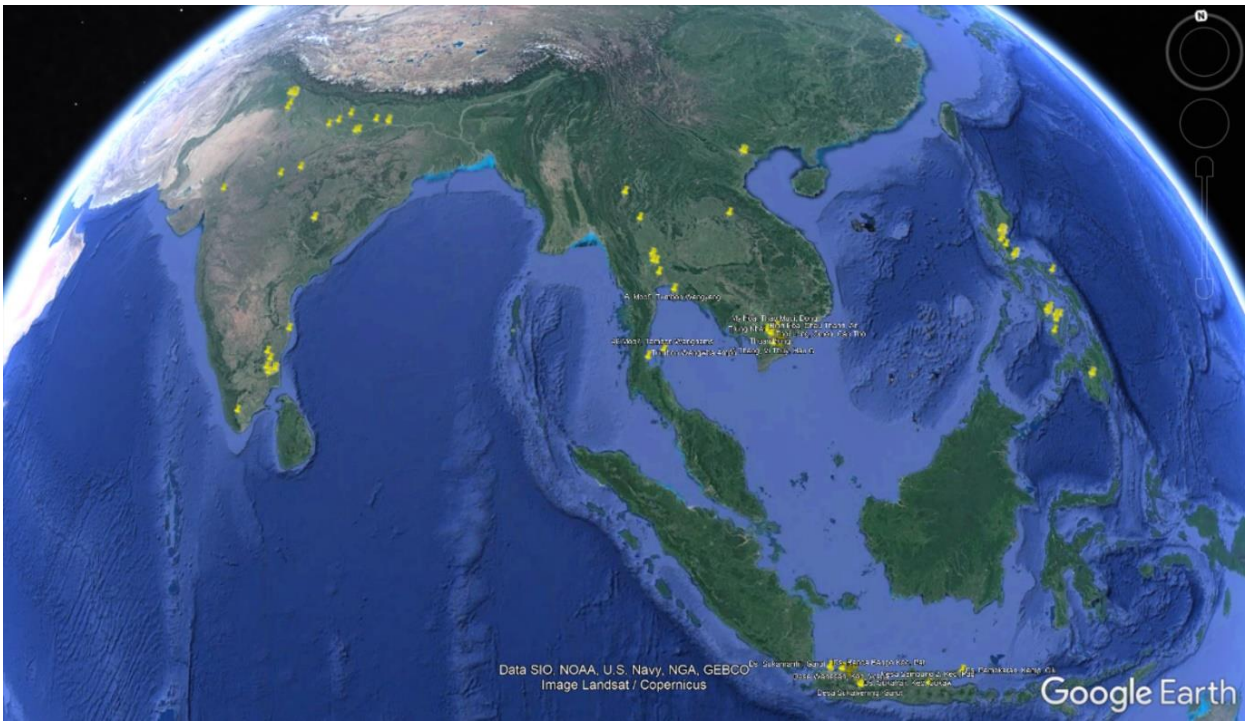

Figure 3.4. Screen shot of Google Earth with located points from field data.

3.2.1. Field data

A dataset consist of the agronomic practices of rice and crop yield was obtained from the International Rice Research Institute (IRRI), Manila, Philippines. The data covers six countries, namely China, India, Indonesia, Philippines, Thailand and Vietnam, for seven years (1987, 1992, 1993, 1996, 1997, 2009 and 2010). The data contains the name of the location or village or province or district, date of planting and harvesting, yield from the field in tonnes per hectare and information regarding agronomic practices in an excel file format. A critical drawback of this data is it does not contain the geographic coordinates. Therefore, the name of the city or village provided in the dataset is searched in google earth and the location was saved. 140 points covering above-mentioned countries were located. A screenshot of google earth with located points are shown in figure 3.4.

3.2.2. Rice cultivation area image file

A raster file shows general extent of rice in Asia was obtained from IRRI. The file was created based on MODIS data compiled from analysis for 2000 to 2012 (Nelson & Gumma, 2015). The map is crated using national statistics, maps and large volume of field-plot data in combination with suite of methods that include spectral matching techniques, decision trees, and ideal temporal profile data banks to rapidly identify and classify rice areas over large spatial extents. The image format is 'TIFF' with resolution of 430 x 430 m. The coordinate system for the image is regular longitude-latitude with WGS 84 datum. The image has only two values; the value zero corresponds to the non-rice cultivation area and one corresponds to the rice cultivation area.

3.2.3. Remote sensing datasets

34 years (from 1982 to 2015) of NDVI and daily average of other climatic input parameters (solar radiation flux, temperature and vapour pressure) was downloaded for the study. The name, source and spatial resolution of the data is given in table 3.1. More details of the data are given in the coming sub-sections.

Table 3.1. Remote sensing input parameters, their source and resolution. The NDVI dataset was downloaded from NASA's ecocast website[a] and the AgERA5 dataset was downloaded from Copernicus climate data store[b]

No	Parameter	Source	Unit	Spatial Resolution	Temporal resolution
1	NDVI	The Climate Data Guide: NDVI: Normalized Difference Vegetation Index-3rd generation		1/12 degree (8 km approx.)	Twice a month
2	Solar radiation flux	AgERA5-Agrometeorological indicators	J m^{-2} day^{-1}	0.1 degree (11 km approx.)	Daily
3	Vapour pressure	AgERA5-Agrometeorological indicators	hPa	0.1 degree (11 km approx.)	Daily
4	Average temperature	AgERA5-Agrometeorological indicators	K	0.1 degree (11 km approx.)	Daily

3.2.3.1. Normalized difference vegetation index (NDVI)

The ecocast.arc.nasa.gov provides global NDVI data from July 1981 to December 2015 (NCAR UCAR, 2018). The images used to create the dataset were captured by the Advanced Very High-Resolution

a. https://ecocast.arc.nasa.gov/data/pub/gimms/3g.v1/

b. https://cds.climate.copernicus.eu/cdsapp#!/dataset/sis-agrometeorological-indicators?tab=overview

Radiometer (AVHRR) sensor, then the data set was created within the framework of Global Inventory Monitoring and Modelling System (GIMMS). The AVHRR sensors started measurements from 1981 and it is still measuring. The sensors are mounted in satellites operated by the National Oceanic and Atmospheric Administration (NOAA) and the European Organization for the Exploitation of Meteorological Satellites (EUMETSAT) (Pinzon & Tucker, 2014). The instruments to have non-overlapping ("visible") channel one (0.58–0.68 μm) and (near-infrared) channel two (0.725–1.10 μm) spectral bands and NDVI is calculated as: (channel 2 − channel 1)/(channel 2 + channel 1). But as per the report of Pinzon & Tucker, (2014), processing of AVHRR NDVI data was very difficult because of several limitations such as vicarious post-launch calibration, atmospheric and cloud correction, and bias correction for the systematic orbital drift during the life of the individual missions . The dataset was developed from the captured images based on Bayesian statistics methods and Sea-Viewing Wide Field-of-view Sensor (SeaWiFS) NDVI dataset. The study characterized the NDVI probability density function through SeaWiFS data and corrected the inconsistencies. The resulted dataset has been crucial to study a variety of global land vegetation processes and how they vary in time. The dataset has a bi-weekly temporal resolution, meaning there will be two images per month and it in NetCDF format. The images have an approximately 8-kilometre resolution. This is one of the longest and oldest satellite datasets, and it is suitable for optimization models like PEMOC. Studies confirm that the AVHRR GIMMS dataset is ideal for long term vegetation studies (Fensholt et al., 2009; Zhang et al., 2020, Tian et al., (2015) and M Marshall, Okuto, Kang, Opiyo, & Ahmed, (2016)).

3.2.3.2. AgERA5 dataset

The other required input parameters are solar radiation flux (J/m²day), vapour pressure (KPa) and average temperature (degC) at 2 m above the surface. These parameters are downloaded from the AgERA5 dataset from the Copernicus programme (*Agrometeorological Indicators from 1979 to Present Derived from Reanalysis*, n.d.). The AgERA5 dataset provides daily surface meteorological data for 1979 to present at a spatial resolution of 0.1° grid. The dataset is derived from the fifth generation of the European Centre for Medium-Range Weather Forecasts (ECMWF) atmospheric reanalysis of global climate known as ERA5. This service is based on the original hourly deterministic ECMWF ERA5 data, at surface level and available at a spatial resolution of 30 km (~0.28125°). Data were aggregated to daily time steps and corrected towards a finer topography at a 0.1° spatial resolution (Boogaard & Grijn, 2019). As per Boogaard & Grijn, (2019), ERA5 is produced using 4D-Var data assimilation and model forecasts in CY41R2 of the ECMWF Integrated Forecast System (IFS), with 137 hybrid sigma/pressure (model) levels in the vertical and the top level at 0.01 hPa. Atmospheric data are available on these levels and they are also interpolated to 37 pressure, 16 potential temperature and 1 potential vorticity level(s) by FULL-POS in the IFS. "Surface or single level" data are also available, containing 2D parameters such as precipitation, top of atmosphere radiation and vertical integrals over the entire depth of the atmosphere. The atmospheric model in the IFS is coupled to a land-surface model (HTESSEL), which produces parameters such as 2m temperature and soil temperatures, and an ocean wave model (WAM), the parameters of which are also designated as surface or single level parameters. The AgERA5 dataset includes daily aggregates of agronomic relevant elements, tuned to local day definitions and adapted to the finer topography. The dataset is comprehensive and long term. It can be used as the input for agroecological studies. The users can directly start the analysis without much processing of data. It is globally covered for all land area. The dataset has a resolution of about 11 kilometres and projected on the regular latitude-longitude grid. The file format is NetCDF-4.

3.2.4. Temperature projections

Global climate projections are climate model simulations which have been generated by multiple independent climate research centres in an effort coordinated by the World Climate Research Program (WCRP) and assessed by the Intergovernmental Panel on Climate Change (IPCC) (*CMIP: Global Climate Projections - Copernicus Knowledge Base - ECMWF Confluence Wiki*, n.d.). The projection is based on IPCC 5th Assessment Report (published in 2013) that "Continued emission of greenhouse gases will cause further

warming and long-lasting changes in all components of the climate system, increasing the likelihood of severe, pervasive and irreversible impacts for people and ecosystems". World Climate Research Program (WCRP) established the Climate Model Intercomparison Project (CMIP) to facilitate Global Circulation Model (GCM) simulations. The fifth phase of CMIP or CMIP5 has scenario experiments using representative concentration pathways (RCPs). RCPs are scenarios of different radiative forcing caused by external drivers such as emissions and concentrations of greenhouse gases (GHGs), aerosols, chemically active gases and change of land use/ land cover (IPCC, 2014). Radiative forcing is the change in the net, downward minus upward, radiative flux (expressed in Watts per square metre; W m^{-2}). The fifth Intergovernmental Panel on Climate Change (IPCC) assessment used four RCPs produced from Integrated Assessment Models as a basis for the climate predictions and projections (Stocker et al., 2013). RCPs usually refer to the portion of the concentration pathway extending up to 2100. The four main pathways are given below.

- RCP 2.6: One pathway where radiative forcing peaks at approximately 3 W m^{-2} before 2100 and then declines (the corresponding ECP assuming constant emissions after 2100). The projection for atmospheric CO_2 concentration for year 2050 is 442.70 ppm and for the year 2100 is 420.89 ppm.
- RCP 4.5 and RCP6.0: Two intermediate stabilization pathways in which radiative forcing is stabilized at approximately 4.5 W m^{-2} and 6.0 W m^{-2} after 2100 (the corresponding ECPs assuming constant concentrations after 2150). The projection for atmospheric CO_2 concentration for year 2050 is 486.54 ppm and for year 2100 is 538.36 ppm corresponds to RCP 4.5. For RCP 6.0, the CO_2 concentration are 477.67 ppm and 669.72 ppm for years 2050 and 2100 respectively.
- RCP 8.5: One high pathway for which radiative forcing reaches greater than 8.5 W m^{-2} by 2100 and continues to rise for some amount of time (the corresponding ECP assuming constant emissions after 2100 and constant concentrations after 2250). As per RCP 8.5, the projected atmospheric CO_2 concentrations are 540.54 ppm and 935.87 ppm for the years 2050 and 2100 respectively.

The global CO_2 concentration projections based on each scenario are available in RCP database website of The International Institute for Applied Systems Analysis (IIASA[a]). This data was downloaded and plotted against years from 2000 to 2100. The graph showing future CO2 concentrations is given in figure 3.5.

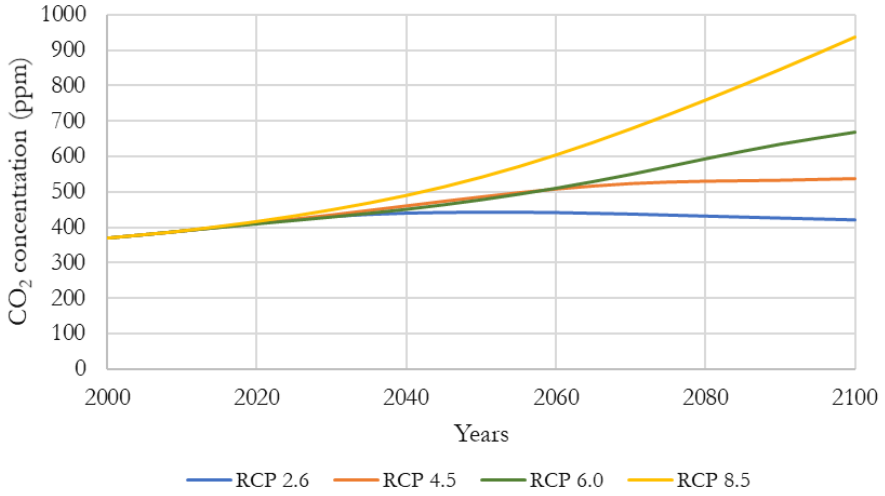

Figure 3.5. Graph showing future CO_2 concentration corresponds to various RCPs up to the year 2100. The data is obtained from the IIASA database[a].

The temperature projections for the years 2050 and 2099 according to RCPs 4.5,6.0 and 8.5 were downloaded from Copernicus climate data store (CDS) (*Agroclimatic Indicators from 1951 to 2099 Derived from*

a. https://tntcat.iiasa.ac.at/RcpDb/dsd?Action=htmlpage&page=compare

Climate Projections, n.d.). RCP 2.6 is excluded from the analysis because there is zero probability to occur (van Vuuren et al., 2011). RCP 2.6 pathway requires the CO_2 emission to start declining from 2020 and become zero at 2100 and also requires, methane emissions (CH_4) to go approximately half of the levels of 2020 (Stocker et al., 2013). The downloaded dataset contains ten days mean daily temperature projections. The dataset has a spatial resolution of 0.5° x 0.5° and projected on the regular latitude-longitude grid.

3.3. Method

A general flowchart of the study is showing in figure 3.6. The first step in the study is to optimize the values of the coefficients in the model using yield data from IRRI, AgERA5 dataset and GIMMS dataset. Since the optimization was not ended up well (the details are explained in the coming sections of this chapter) with yield data, the already optimized values for rice for the United States were used to continue the study. The average yield corresponds to C_3 and C_4 rice was estimated using the average input parameter (NDVI, solar radiation flux, average temperature, vapour pressure deficit) values calculated for 34 years (1982 to 2015) and considered this as the baseline. The results were compared to find the difference in yield between C_3 and C_4 rice. The latitude-wise average values of yield and difference in yield were also calculated to understand the change of yield and change of difference of yield corresponds to latitudinal variations of climate. To find the effect of global warming on crop yield, the average crop yield for C_3 and C_4 rice was estimated using 2050 and 2099 temperature projections based on three RCP scenarios (4.5, 6.0 and 8.5). The results were also compared and difference in yield between C_3 and C_4 rice were calculated. The latitudinal average values and average difference were also calculated. More details about the model and methods are elaborated in the coming sections.

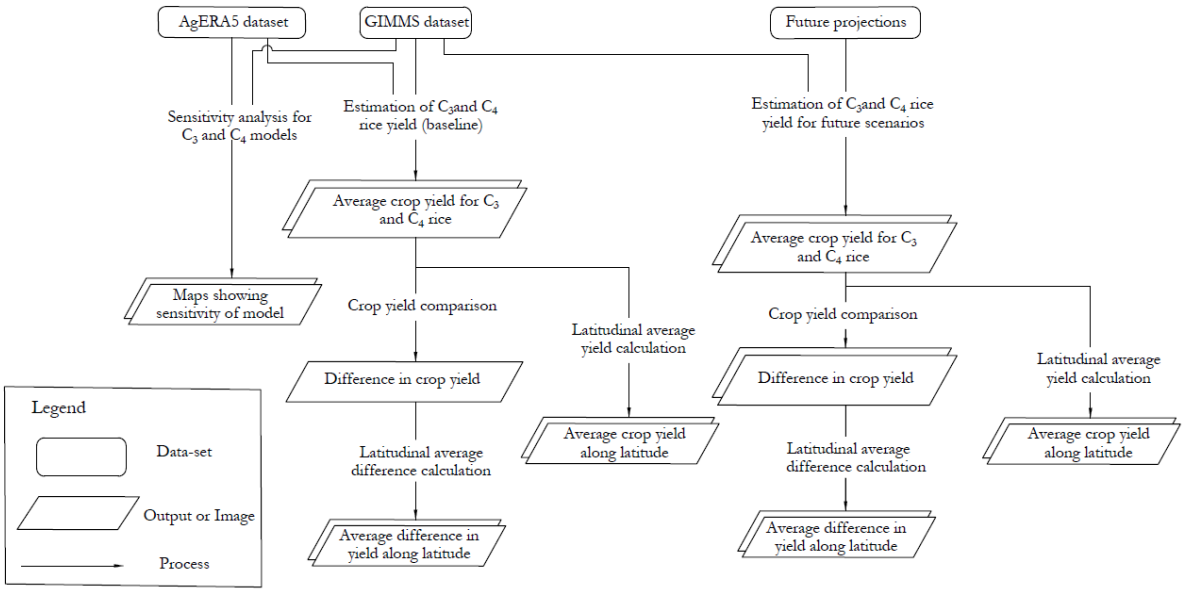

Figure 3.6. Flowchart of the method

3.3.1. Crop yield estimation

The equation to estimate crop yield used in PEMOC is given as below.

$$\text{Crop yield} = \text{Crop growing period}.\, F_{GPP}\, F_{Resp}\, F_{Harv}\, \varepsilon_{max}\, F_{PAR}\, F_T\, F_M\, F_A\, PAR \quad (1)$$

The crop growing period is the day-count from planting to the harvesting of the crop. The value for the crop growing period is taken as 120 days (Gummert & Rickman, 2010). PAR is the photosynthetically active radiation that electromagnetic radiation between 400 nm to 700 nm (Mõttus et al., 2012). Equations or values of other terms, their short descriptions and reference are given in table 3.2.

Table 3.2.Description of different terms in equation (1): F is the conversion factor from carbon to biomass, R is the proportion of GPP allocated to above-ground productivity, HI is the harvest index, W is the moisture content of the grain, Ca is the intercellular CO_2 concentration in mol fraction (340 micro mol/mol), Γ is the CO_2 compensation concentration which has an approximate value of 0.04, NDVI is the seasonal average NDVI value, T_A is the seasonal average temperature, T_{OPT} is the optimal average temperature (25degC), VPD is the seasonal average vapour pressure deficit, $F_{PAR,MAX}$ is the maximum seasonal fraction of photosynthetically active radiation and a_0,a_1, a_2, a_3 and a_4 are constraints, their values were optimized for rice in the United States based on the GPP daily flux measurements by Michael Marshall et al., (2018).

Term	Description	Equation for the term	Reference
F_{GPP}	Conservative fraction for gross daily GPP	F_{GPP} = 63 %	(Sims et al., 2005) (Owen et al., 2007)
F_{Resp}	Fraction for respiration cost	F_{Resp} = 50%	(Ryan, 1991)
F_{Harv}	Fraction for yield from total biomass produced	$F_{Harv} = \frac{F\ R\ HI}{(1\text{-}W)}$	(Wang et al., 2020) (Peng et al., 2014)
ε_{max}	Maximum quantum conversion efficiency	$\varepsilon_{max(\text{for } C_3 \text{ crop})} = 0.08 * (C_a - \Gamma)/(C_a + 2\Gamma)$ $\varepsilon_{max\ (\text{for } C_4 \text{ crop})}: 0.06$	(G. J. Collatz et al., 1991) (G. Collatz et al., 1992)
F_{PAR}	Fraction for photosynthetically active radiation	$F_{PAR} = a_0$ NDVI - a_1	(Potter et al., 1993)
F_T	Fraction for temperature stress	$F_T = \frac{1.1814}{\left(\left(1+e^{a2*(T_{OPT}-10-T_A)}\right)\left(1+e^{a3*(T_A-10-T_{OPT})}\right)\right)}$	(Potter et al., 1993)
F_M	Short-term moisture stress	F_M = 1-a_4 ln (VPD)	(Medlyn et al., 2011)
F_A	Seasonal moisture stress	$F_A = F_{PAR}/F_{PAR,MAX}$	(Michael Marshall et al., 2018)

The fraction of photosynthetically active radiation F_{PAR} is estimated as a linear function of NDVI according to Potter et al., (1993). The carbon assimilated from the absorbed PAR is represented by ε_{max} and the values of ε_{max} for C_3 and C_4 rice were taken different (G. Collatz et al., 1992; G. J. Collatz et al., 1991). To estimate the daily average maximum gross primary production (GPP_{max}), daily average values of parameters are used. The value of GPP_{max} is then converted into gross primary production using F_{GPP} and F_{resp}. The studies of Sims et al., (2005) and Owen et al., (2007) showed strong linearity between gross and maximum daily GPP. Based on their results, the model estimates gross daily GPP as 63% of maximum daily GPP (F_{GPP} = 63%) and that is the same value used for the studies of Michael Marshall et al., (2018). Studies of Michael Marshall et al., (2018) assumes respiration is a conservative fraction (50%) of GPP, therefore the same value is adapted in this study.

To calculate the temperature stress fraction F_T, optimum temperature for rice (T_{OPT}) is taken as 25 degC. Global evaporation modelling studies of Yuan et al., (2010) and regional studies of García et al., (2013) also used 25 degC as the optimum temperature.

The crop yield in tonnes per hectare is calculated by multiplying the average daily GPP by crop growing period and fraction for yield from total biomass produced (F_{Harv}) (Wang et al., 2020). The descriptions and values of F, R, HI and W used to calculate F_{Harv} is given in table 3.3. F is the ratio of biomass produced to the carbon assimilated, R represents the above ground productivity of the crop which is utilized from the GPP, HI is the ratio of economic yield (typically grain) to total above-ground biomass and W is the ratio of weight of water in the grain to the weight of dry mater of grain during the time of harvest (Peng et al., 2014). Over the time, the value of HI has been increased from 0.40 to 0.55~0.62 due to the change from conventional varieties to hybrid verities (Wang et al., 2020). The study used the values of these terms based on previous studies conducted across South and East Asia (Peng et al., 2014; Bastiaanssen & Ali, 2003; Reeves et al., 2005).

Table 3.3. Values of Conversion factor from carbon to biomass (F), proportion of GPP allocated to above-ground productivity (R), harvest index (HI), (in this case, HI for new hybrid verities is used) and moisture content (W)(Wang et al., 2020).

Term	Value
F	1/0.45
R	0.9
HI	0.55
W	0.14

To calculate the short-term moisture stress fraction, the vapour pressure deficit (VPD) is calculated as per Allen et al., (1998) published in the website of FAO. The equations used to calculate VPD are given below.

$$VPD = e_s - e_a \quad (2)$$

Where e_s is mean saturation vapour pressure and e_a is actual vapour pressure. e_s can be calculated using the below equations using air temperature.

$$e^o(T) = 0.6108 \ \exp\left[\frac{17.27\ T}{T + 237.3}\right] \quad (3)$$

Where, $e_o(T)$ is the saturation vapour pressure (kPa)at air temperature T (^oC).

Using equation (3), the e_s can be calculated as below.

$$e_s = \frac{e^o(T_{max}) + e^0(T_{min})}{2} \quad (4)$$

Where T_{max} and T_{min} are average daily maximum and average daily minimum temperature, respectively. Values of e_a is available in AgERA5 dataset.

3.3.2. Optimization of the model

As the name indicates, PEMOC is an optimization model. That means the coefficients in the model equations needs to be optimized with the field data before running it for the entire study area. In the previous study, the model was optimized for various crops (corn, rice, soybean, and winter wheat) across the Contiguous United States and showed the R-squared value of 0.75 with rice when validated (Michael Marshall et al., 2018). In the initial stages of this study, it was proposed to optimize the model and validate

using the field data collected from IRRI. As described in the data section of this chapter, the field data does not contain any coordinates. Therefore, the name of the city or village provided in the dataset is searched in google earth and the location was saved. 140 points covering six countries (China, India, Indonesia, Philippines, Thailand and Vietnam) for seven years (1987, 1992, 1993, 1996, 1997, 2009 and 2010) were located.

These coordinates were plotted with the map of rice-growing areas. It was found that some points fall outside the pixels represents the rice-growing areas. The resolution of the rice mask map is around 430 meters (0.00417 decimal degrees). But NDVI and climatic dataset have coarser resolution (approximately 8 km and 11 km each). Therefore, it was expected that while extracting the pixel value of parameters corresponds to the geocoded locations, it would be representing the rice fields also (figure 3.7).

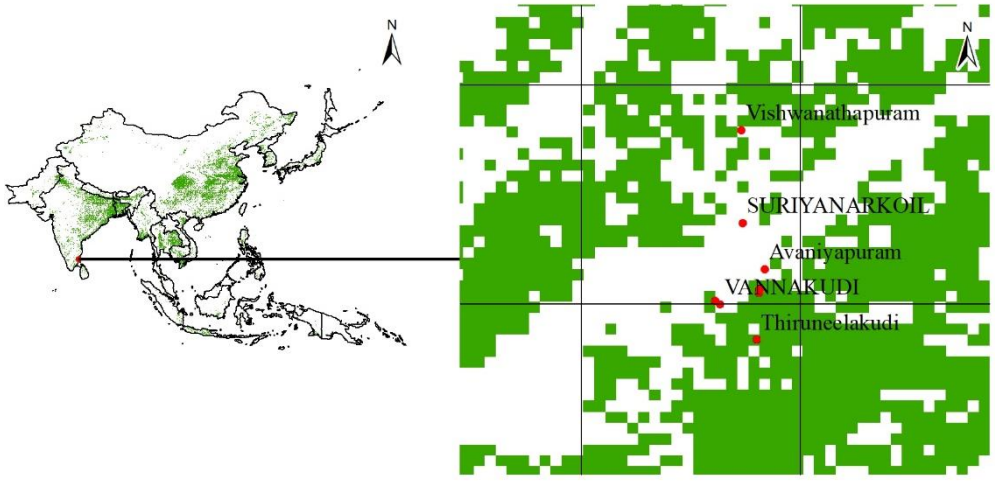

Figure 3.7. Map showing some geocoded locations from where field data was collected at the south of India. Some geocoded locations are fallen outside the rice cultivating area, but it is still inside the same NDVI pixel. Red dots are geocoded locations, green patches are rice cultivation regions and black squares are NDVI pixel.

To proceed with the research, it is expected to see some relationship between the field data and biophysical predictors. The field dataset contains the planting and harvesting dates of each geocoded points. The planting date was considered as start of season (SOS) and the harvesting date was considered as end of the season (EOS). Then, the parameter values (both GIMMS and AgERA5 datasets) between these dates were extracted and averaged using the python language and necessary packages like gdal (Spyder environment and Anaconda distribution). The extracted average values of parameters were stored correspond to the respective point location in CSV format. Even if there are multiple points present in a single grid cell, their planting and harvesting dates (SOS and EOS) were different in most of the cases. Therefore, all the points were selected for parameters extraction irrespective of their position. The R-Squared values between these parameters and the yield were calculated, but they are too small to proceed with optimization. The average parameter values were plotted against the yield with R-squared values and is shown in figure 3.8.

Since the R-squared values between the yield and average parameters are very small and lack of any visible relation between yield and parameters, it is decided to check the relation between the average values of parameter district-wise to the yield. Shapefile containing the district boundaries were downloaded from gdam.org[a]. The polygons which contain the yield data location were selected and saved as separate files.

a. https://gadm.org/download_country_v3.html

It was decided to check the correlation between NDVI and yield first because NDVI is one of the main parameters that drive the model. Then, to proceed further if the correlation is high enough. Seasonal Average NDVI values were calculated bounding to the polygons with and without some thresholds. Researches reported that course resolution of remote sensing dataset can cause faulty results due to the heterogeneity of the pixels (Teluguntla et al., 2015). In this study the pixel resolution is about 9 km. Therefore, the chances are more that the pixel is representing a mixture of land features like paddy field, other vegetation and other natural or manmade features. The thresholds were set as the polygons selected (district) for extraction should contain at least 20 % of rice growing area and each pixel of NDVI raster must have at least 40% rice-growing area. Phenological studies either use 20% threshold or 50 % threshold for extracting phenological parameters and currently many studies used 20% threshold (Huang et al., 2019). The polygons and NDVI pixels that are not passed these criteria were excluded from the extraction. Image of a district in India with rice mask and NDVI mask are shown in figure 3.9. But these methods also did not produce any improvement, instead the R-squared value went lower to 0.01903. The R-squared values between yield and average NDVI with and without threshold is given in table 3.4.

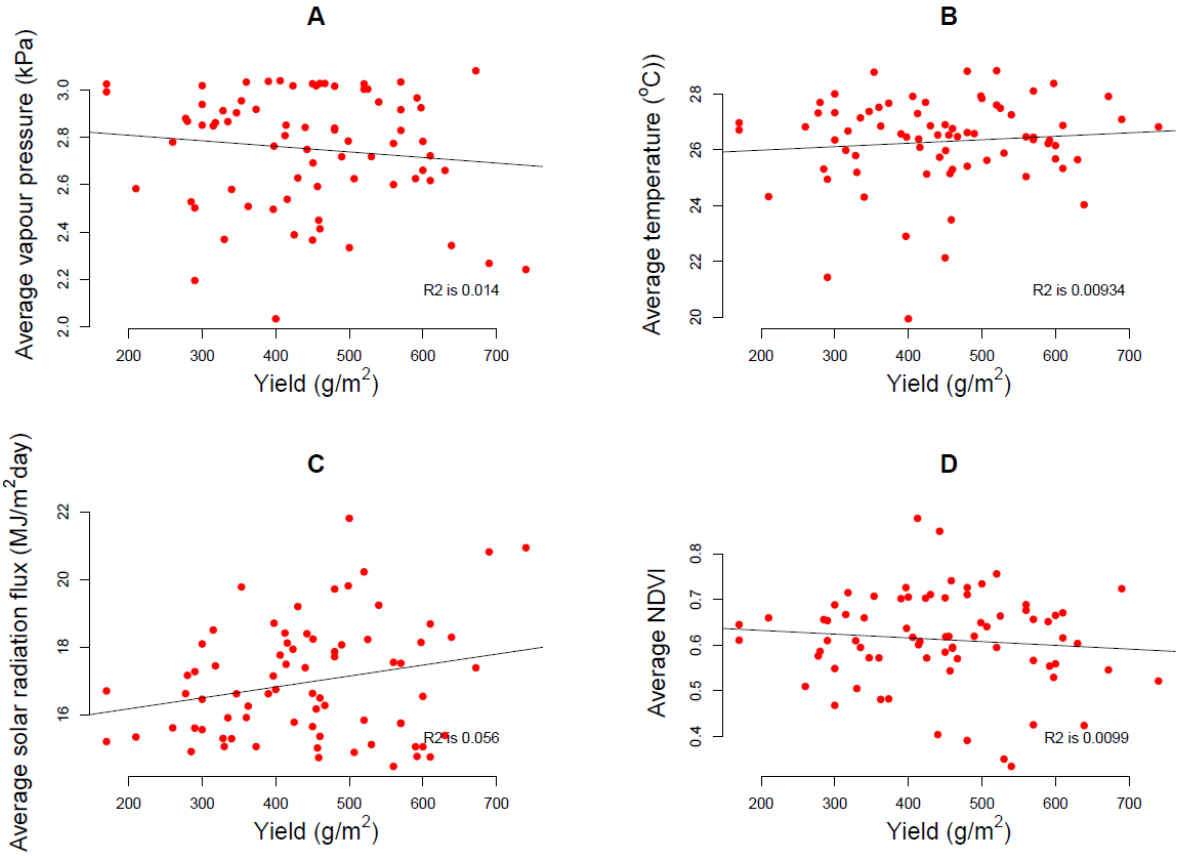

Figure 3.8. Yield v/s average parameter values with r-squared values. A). Yield v/s Average vapour pressure. B). Yield v/s Average temperature. C). Yield v/s Average solar radiation flux. D). Yield v/s Average NDVI

Table 3.4. Coefficient of Determination (R-Squared) values between the average NDVI to the yield extracted district-wise.

	With threshold	**Without threshold**
Coefficient of Determination (R-Squared)	0.01903	0.06997

The R-squared value between the average NDVI and yield without threshold is higher than that of with threshold. The probable cause is the wrong geocoding of location. The sample date collected from the field may not lie in the district boundary. Therefore, there is no relation between NDVI in the geocoded location

and the yield and the difference in the R-squared value may be just coincidental. Since the resulted r-squared values are very low, it was decided not to use the yield data for optimization. Instead, the optimized values of the coefficients for the Contiguous United States by Michael Marshall et al., 2018, will be used to run the model for South and East Asia. The values of the coefficients in PEMOC model are given in the table 3.5. Long-term climatic data for the whole study area will be needed to continue the study. Therefore, the same NDVI and climatic datasets already downloaded will be used in the research.

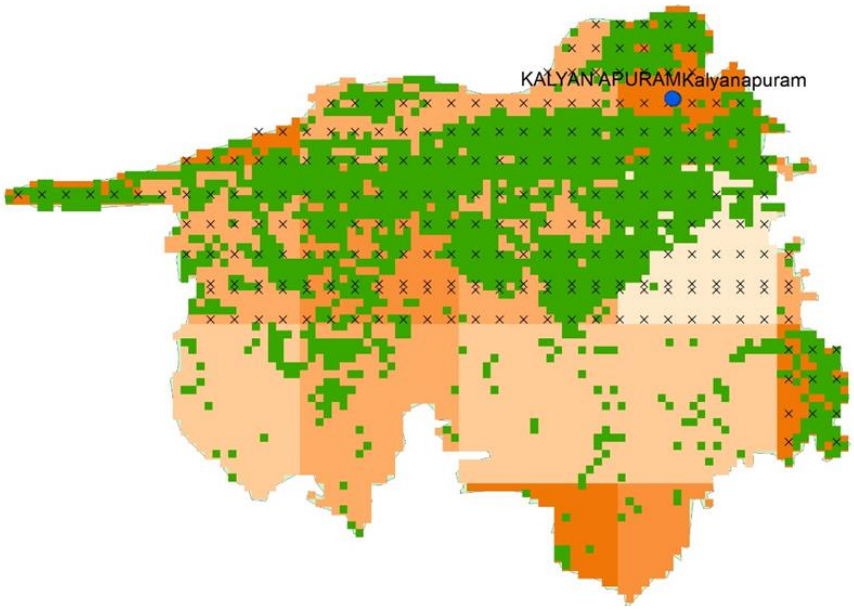

Figure 3.9. A district in India from which the average NDVI values extracted. The big pink or saffron pixels are NDVI; the small green pixels are rice-growing area. The NDVI values averaged from only those pixels covered by at least 40 % rice (the pixels with small 'x's) when the threshold is applied.

Table 3.5. Values of the coefficients in PEMOC model used for the study

Coefficient	a_0	a_1	a_2	a_3	a_4
Value	1.00	0.20	0.17	1.00	0.16

3.3.3. Extraction of parameters for crop yield estimation

All the downloaded datasets (both GIMMS and AgERA5) were saved in the University of Twente's data storage facility due to the large size (around 500gb). The datasets cover the global data. Therefore, it is then clipped to study area using the extent (57° 50' 0.0024" to 168° 4' 59.9988" in longitude and - 16° 49' 59.9988" to 55° 55' 0.0012" in latitude) of rice cultivation map obtained from IRRI and saved in separate folders. The NDVI files were saved as flat binary 16-bit signed integer format (.img format) for using it in TIMESAT to find the start of season (SOS) and end of season (EOS). In South and East Asia main growing period of rice is in the rainy season from June to October, which is the primary season (USDA, 2015). TIMESAT was used to find out SOS and EOS of the primary season.

3.3.3.1. Estimation of the start of season (SOS) and end of season (EOS)

'TIMESAT' is a tool to extract phenological information from satellite image time series (Jönsson & Eklundh, 2004). TIMESAT uses the variation in NDVI values to extract phenological information like SOS and EOS. The processing is based on the least-squares fits to the upper envelope of the NDVI timeseries data. The fitting process gives a primary maximum and sometimes a secondary maxima if the amplitude of the secondary maxima exceeds a certain fraction of the amplitude of the primary maxima. The SOS is defined from the filtered or fitted functions as the point in time for which the value has increased by a

certain percentage of the distance between the left minimum level and the maximum. The EOS is defined in a similar way. The input NDVI images for the whole period must be saved in appropriate format (in this case, the files are saved as flat binary 16-bit signed integer format (.img format)). The GIMMS NDVI images have Bi-weekly temporal resolution (2 images per month). Therefore, there are 24 images per year. The SOS and EOS will be calculated according to the image number.

Each NDVI image file has the same size of 873 rows and 1323 columns. An image list for the whole images was created and saved in the same folder with NDVI. A setting file was also created and saved. A screenshot of the setting is shown in figure 3.10.

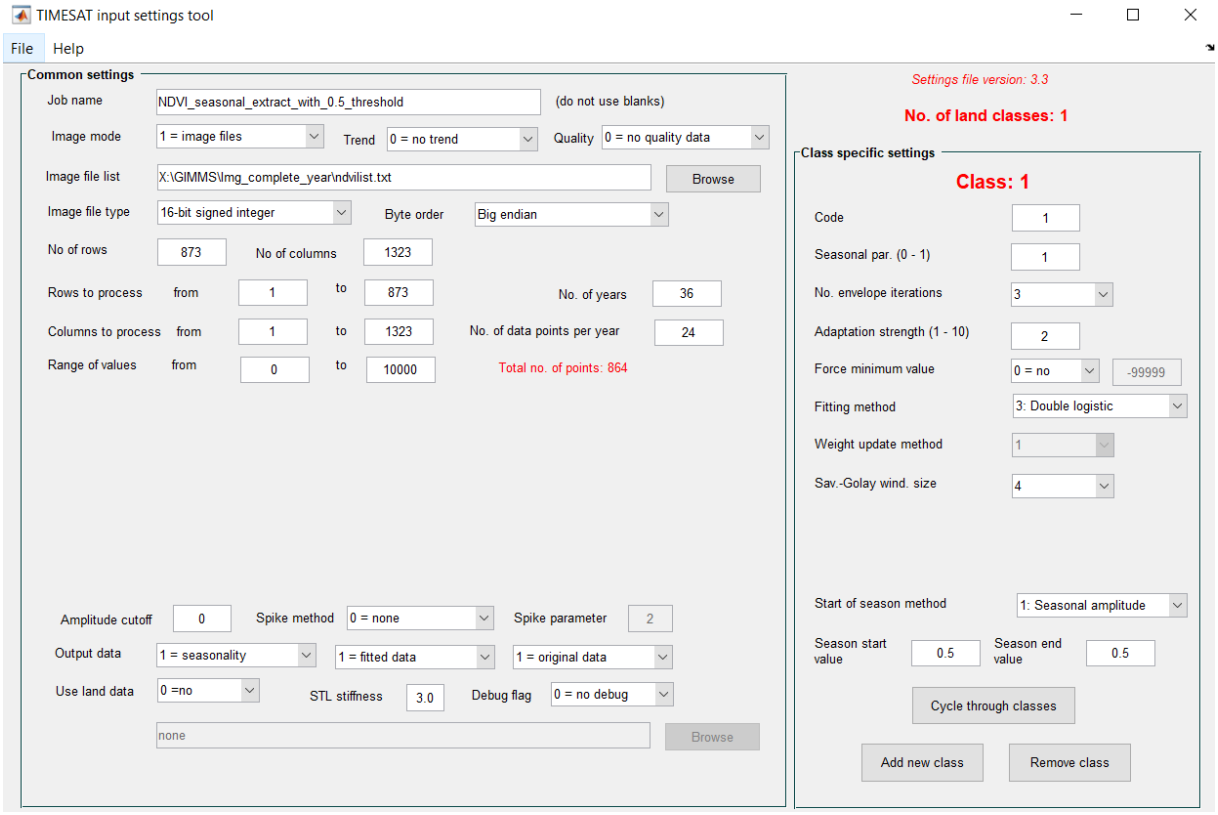

Figure 3.10. TIMESAT Setting for SOS and EOS extract. The fitting method was chosen as Double -logistic and the start and end of season values chosen as 0.5 of the amplitude of the maxima. The number of envelop iterations was selected as 3 to get iterative procedure to get better fit.

TIMESAT has 3 fitting methods to extract phenological parameters. They are Savitzky-Golay, asymmetric Gauss and double logistic. According to Jönsson & Eklundh, (2004), with a plateau indicating that the underlying signal is composed of two vegetation signals, Savitzky- Golay filter performs better, but in noisy time series double logistic is better option. Studies of Hird & McDermid, (2009) also found that double logistic method out-performed other methods in noisy data. Therefore, the double logistic method was chosen over the other two methods. To avoid underestimation and over estimation of SOS and EOS, the season start value and season end value were selected as 0.5 of the amplitude of NDVI curve for each pixel (Jönsson & Eklundh, 2004).

The SOS and EOS for each year were saved separately as .img file from the output produced. They have the same number of rows and columns as the NDVI images. A header file was also created for each img file to open in any GIS or Remote Sensing package. These image files contain pixel values for other places in Asia and a small part of Australia apart from the study area. Therefore, the images were masked to the study area. These masked images are used to extract seasonal average parameters.

3.3.4. Extraction of parameters using python

The average seasonal parameters based on SOS and EOS of each year of the study period were extracted using python language in Spyder environment and Anaconda distribution. As per the script, first, the SOS file and EOS file are opened in python using the gdal package. If the SOS and EOS for a pixel is valid then the images of all parameters (NDVI, solar radiation, temperature and vapour pressure) during the period would be opened, and corresponding pixel values would be extracted and averaged. Since the AgERA5 datasets have daily data, extraction of values during the complete season is time-consuming. Therefore, only five dates were selected during the season and the extraction was performed only for those dates. They are start of season, quartile of season, mid of season, three-quartile of season and end of season, covering the entire season as per the obtained SOS and EOS. The averaged values of the parameters for the season are stored in the corresponding cell location in arrays for different parameters. The arrays have the same number of rows and columns as the SOS and EOS images. The process continues for all the valid SOS and EOS pixels for the entire image. Then the arrays containing the average values of parameters are saved as .tiff images for that year. Then the process continues for the next year to cover the entire study period.

Another python script was written and used to find the average values of parameters for the whole study period. As per the script, the image files containing the seasonal average values for each year are opened. The average values for each pixel for the entire period are calculated and saved as another tiff file. These files are used to estimate the crop yield for C_3 and C_4 rice.

To estimate the future crop yield from 2050 and 2099, the seasonal average projected temperature (as per three RCP scenarios) was used. For this purpose, another python script was written. First, the average SOS and average EOS for the entire study period were calculated and saved. It was assumed that the calculated average values for SOS and EOS would be same in the future. Then using those data, the temperature for five dates between the corresponding SOS and EOS was extracted and averaged and stored as .tiff file.

3.4. Yield estimation

The equation to calculate the crop yield is described in the section 3.3.1 of this chapter (eq. (1)). The yield for C_3 rice and C_4 rice for baseline was estimated using the extracted average values of parameters and the values of optimized coefficients. Similarly, the yield estimation for future scenarios was conducted using the future temperature projections and the average values of parameters for baseline except for temperature with values of optimized coefficients. The crop yield for both baseline and future scenarios was estimated pixel by pixel and saved as .tiff file. Then the output was masked to the rice-growing regions using the rice growing map obtained from IRRI. Now, the maps can be compared to find in which area what crop produces higher yield.

3.5. Yield comparison and Latitudinal plots

To check the difference in C_3 and C_4 rice production, the yield values of C_3 were subtracted from that of C_4 pixel by pixel. This process was done for baseline and future scenarios to understand which crop variety performs better in present and future climatic conditions. If the value is negative, the C_3 crop performs better; else C_4 crop performance is better.

The climate of the study area considerably varies when moving from northern latitude to southern latitude of the study extend (Dando, 2005). To check the variability of crop yield across latitude, the average values of the crops were calculated in each row of the output images and plotted against the corresponding latitude. This can provide an idea where the rice grows more in various agroclimatic conditions. Also, the difference in yield between C_3 and C_4 was averaged row-wise and plotted against the latitude to understand how the difference in crop yield changes when moving along latitude.

3.6. Difference in crop yield - countrywise

The difference in crop yield was estimated country wise for the top eight rice producing county in the study area. The countries are China, India, Bangladesh, Indonesia, Vietnam, Thailand, Myanmar, and Philippines in the decreasing order of yearly rice production as per FAOSTAT. This estimation can provide an idea about which country favours the cultivation of C_4 rice.

3.7. Sensitivity analysis

Sensitivity analysis was carried out in research to identify the most influencing input parameters that control model performance(Herman et al., 2013). Usually, the sensitivity analysis can be classified into two types. They are local sensitivity analysis and global sensitivity analysis. The local method examines the effect of parameter on the result by varying each parameter one at a time between appropriate bounding values. But in real situations, it is highly unlikely to change only one parameter at a time. When one parameter changes, there may or may not be a change in other parameters too, and there may also be some parameter interactions. It can be synergistic or antagonistic. Global sensitivity analysis considers these changes too. The global method assesses the change in output by varying all parameters simultaneously over the entire feasible range (Devak & Dhanya, 2017). In this study, a global sensitivity analysis method called Sobol' sensitivity analysis is adopted. This is a variance-based method that attributes variance in the model output to individual parameters and their interactions. Sobol' method was one of the most accurate and robust methods in non-linear and non-monotonic models (Herman et al., 2013). Also, this method can produce results that are independent of modeler prejudice and non-site specific (Song et al., 2015).

According to Sobol, (2001) and Herman et al., 2013, the attribution of total output variance to individual model parameters and their interactions can be written as below equation (5).

$$D(f) = \sum_i D_i + \sum_{i<j} D_{ij} + \sum_{i<j<k} D_{ijk} + D_{12\ldots p,} \quad (5)$$

Where *D(f)* is the total variance of the output matric f, D_i is first order variance contribution of i^{th} parameter, D_{ij} is the second-order contribution of the interaction between parameters *i* and *j*. $D_{12\ldots p}$ contains all interaction higher than third order, up to p total parameters.

The sensitivity indices can be calculated as below.

$$\text{First-order index: } S_i = \frac{D_i}{D} \quad (6)$$

$$\text{Total-order index: } S_{Ti} = 1 - \frac{D_{\sim i}}{D} \quad (7)$$

First order index measures the fraction of total output variance caused by parameter *i* apart from interactions with other parameters. The total order index is one minus the fraction of total variance attributed to $D_{\sim i}$, representing all parameters except *i*.. The simplest method to rank input variables is to estimate first-order indices and order the variables as per these values (Sobol, 2001).

To find the first-order sensitivity indices pixel by pixel, two matrices A and B will be created for each pixel, each matrix assigned 10000 samples parameter sets within the range of $\pm$ one standard deviation. If f represents the model, then the mean of outputs (f_o) from the parameter set matrix A (θ^A) can be calculated as:

$$f_o = \frac{1}{n}\sum_{s=1}^{n} f(\theta_s^A) \quad (8)$$

Total variance *D,* can be calculated as:

$$D = \frac{1}{n} \sum_{s=1}^{n} [\, f^2(\theta_S^A) - f_o^2] \tag{9}$$

The variance contribution D_i for parameter i can be calculated as:

$$D_i = \frac{1}{n} \sum_{s=1}^{n} [\, f(\theta_s^A)\, f(\theta_{\sim is}^B, \theta_{is}^A) - f_o^2] \tag{10}$$

The parameter sets θ_i are superscripted to indicate which parameters are sampled from which set. The sample set is denoted by the superscript A or B; the parameters taken from that set are denoted either by i (the i^{th} parameter) or $\sim i$ (all parameters except i).

For the current study, the climatic parameters are temperature, solar radiation and vapour pressure deficit. The sensitivity analysis was performed to identify which one of these three parameters is the most influential in each pixel of the study area. A.tiff file was created with three bands corresponding to the sensitivity indices of three parameters and can be shown as red, green and blue (RGB) colour. Red corresponds to sensitivity index of temperature; green corresponds to sensitivity index of vapour pressure deficit and green corresponds to sensitivity index of radiation. This image can provide an idea of the most influencing parameter in different regions of the study area.

4. RESULTS

4.1. Yield estimation

The crop yield for C_3 and C_4 rice was estimated in the rice growing areas of the study area as described in the methodology section for the baseline for seasonal average climatic parameters for the years from 1982 to 2015 and future scenarios (RCPs 4.5, 6.0 and 8.5 for the years 2050 and 2099). The differences between the crop yield of C_3 and C_4 pathways were also calculated pixel by pixel basis. The maps showing the yield estimations for both pathways and the differences in yield for baseline and future scenarios are given in the figures from 4.1 to 4.21.

The difference map for the baseline (figure 4.3) shows heterogeneity around 30° of southeast China, the pixels representing more C_3 (blue) or more C_4 (red) are mixed in this region. In the same map, same latitude around 30°, at the northwest of India, the Punjab region, shows more C_3 production than C_4. At the northern latitudes above 40°, C3 rice has higher production. At the tropics, below 20° to -10°, C_4 rice performs well. When the baseline difference map is compared with the difference maps for the future scenarios (figures 4.6, 4.9, 4.12, 4.15, 4.18 and 4.21), a change from mixed pixels of C_3 and C_4 to more C_4 rice production (red pixels) can be seen in the sub-tropic area around 30° of southeast China and north of India. But for RCP 6.5 for the year 2050, the changes are comparatively less. The Punjab region shows more C_4 production only at the highest emission scenario (RCP 8.5 year 2099). At the southern region of China, Kunming, favours the production of C_3 rice for all climatic conditions.

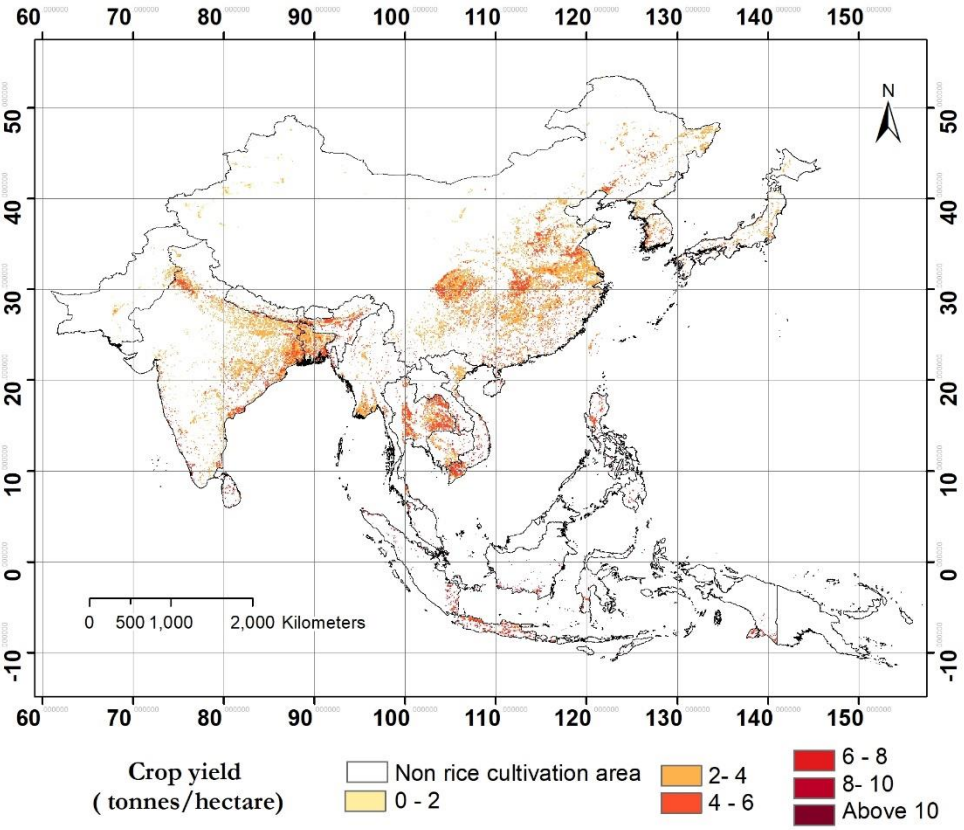

Figure 4.1. Average crop yield estimation of C_3 rice corresponds to baseline (1982-2015).

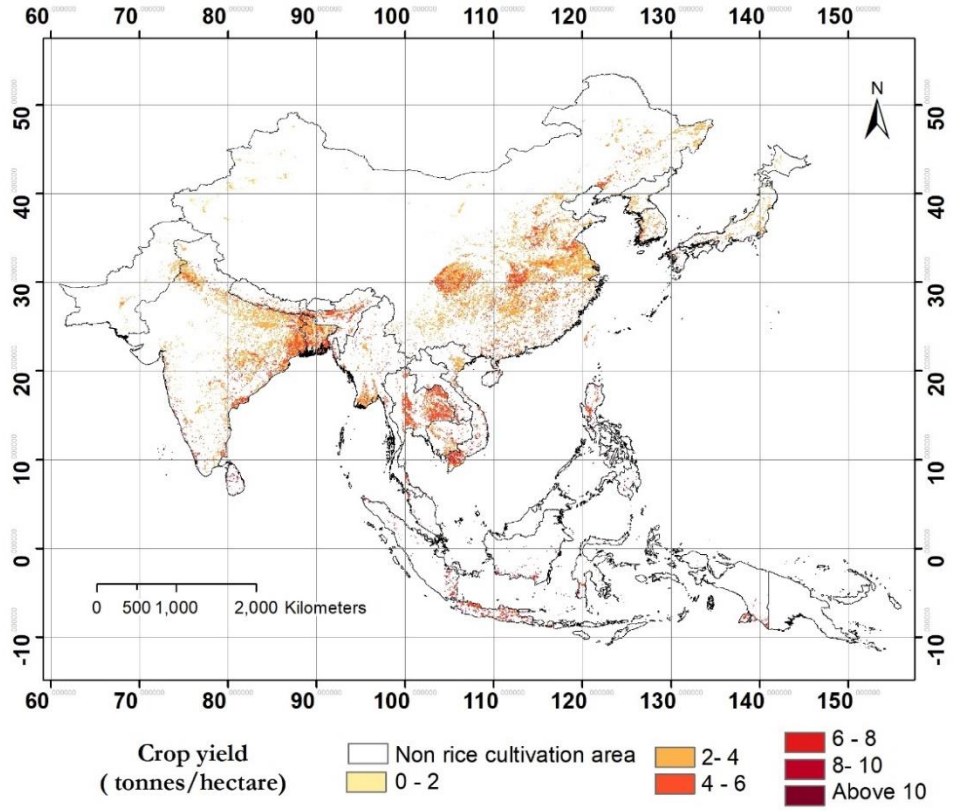

Figure 4.2. Average crop yield estimation of C_4 rice corresponds to baseline (1982-2015).

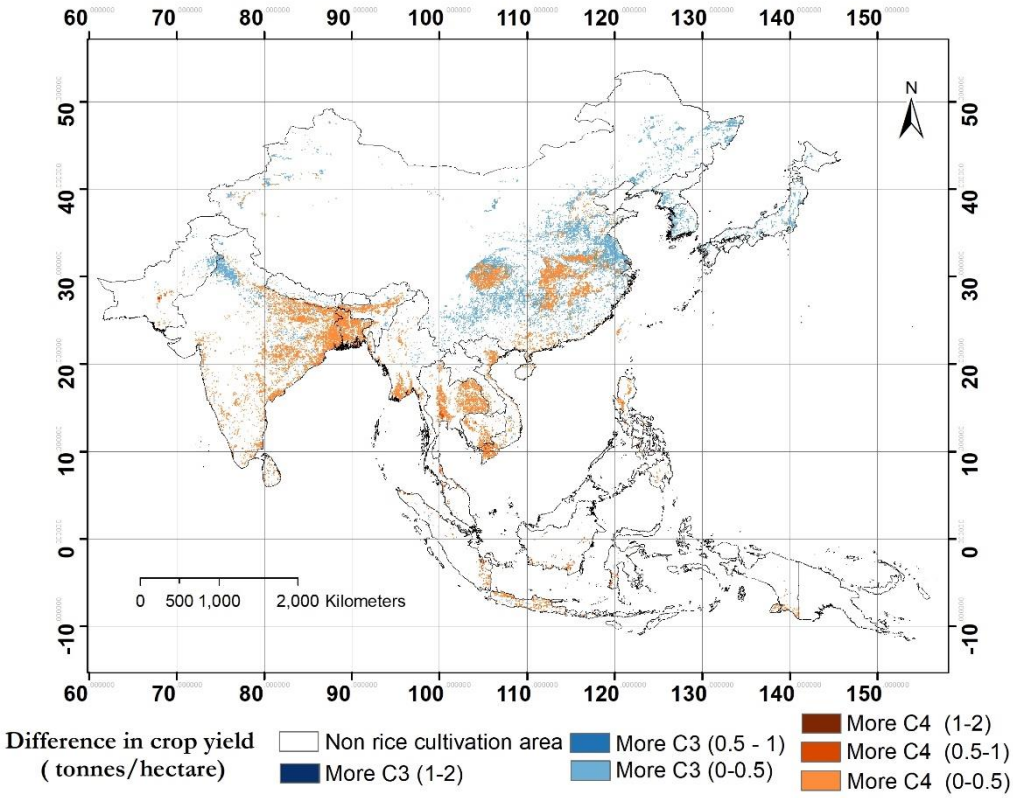

Figure 4.3. Difference between the yield of C_3 and C_4 pathways corresponds to the baseline (1982-2015). The difference between the yield in tonnes/hectare is given inside the parentheses of the legend.

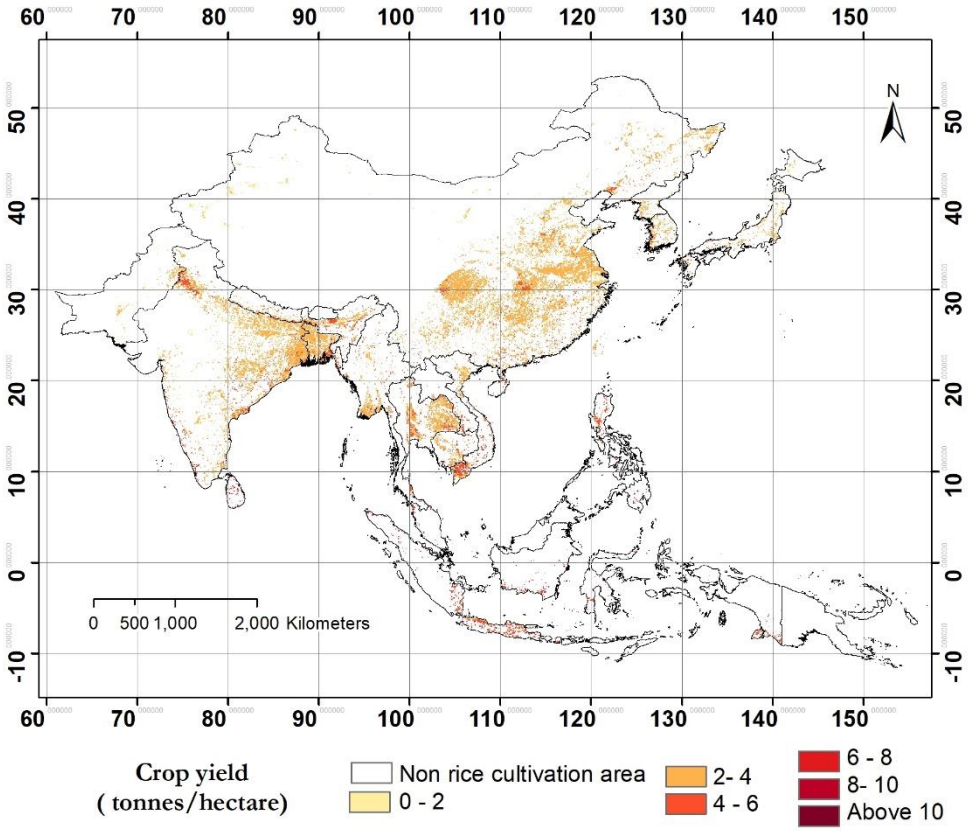

Figure 4.4. Average crop yield estimation of C_4 rice corresponds to RCP 6.0 year 2050.

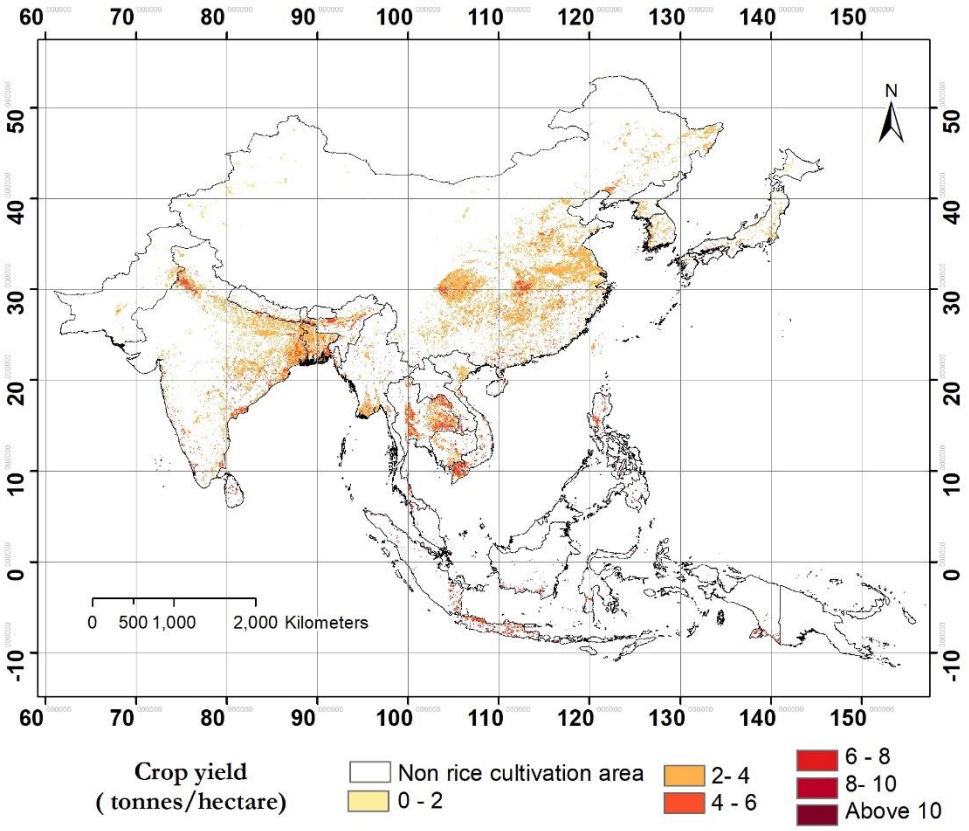

Figure 4.5. Average crop yield estimation of C_4 rice corresponds to RCP 4.5 year 2050.

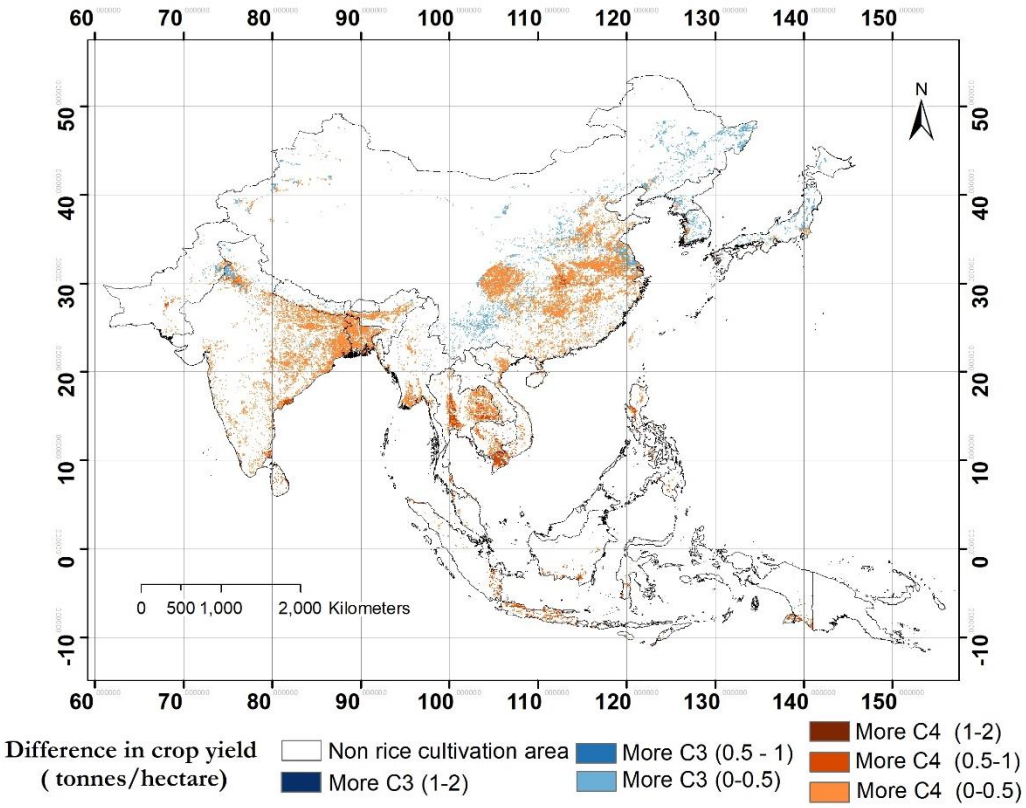

Figure 4.6. Difference between the yield of C_3 and C_4 pathways corresponds to RCP 4.5 year 2050.

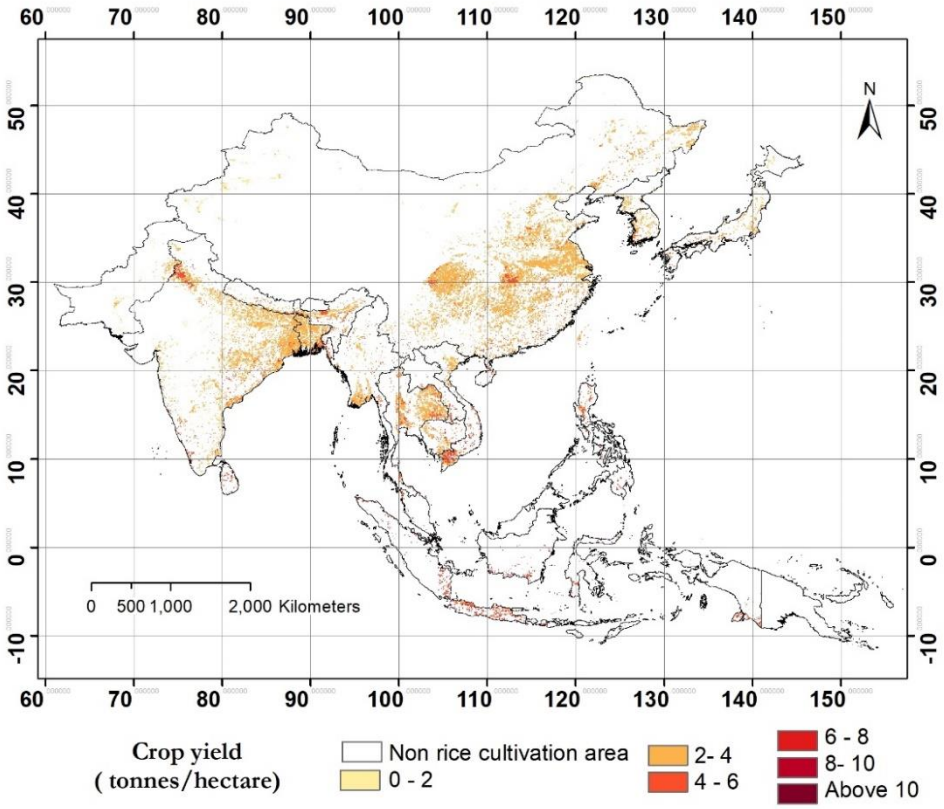

Figure 4.7. Average crop yield estimation of C_3 rice corresponds to RCP 6.0 year 2050.

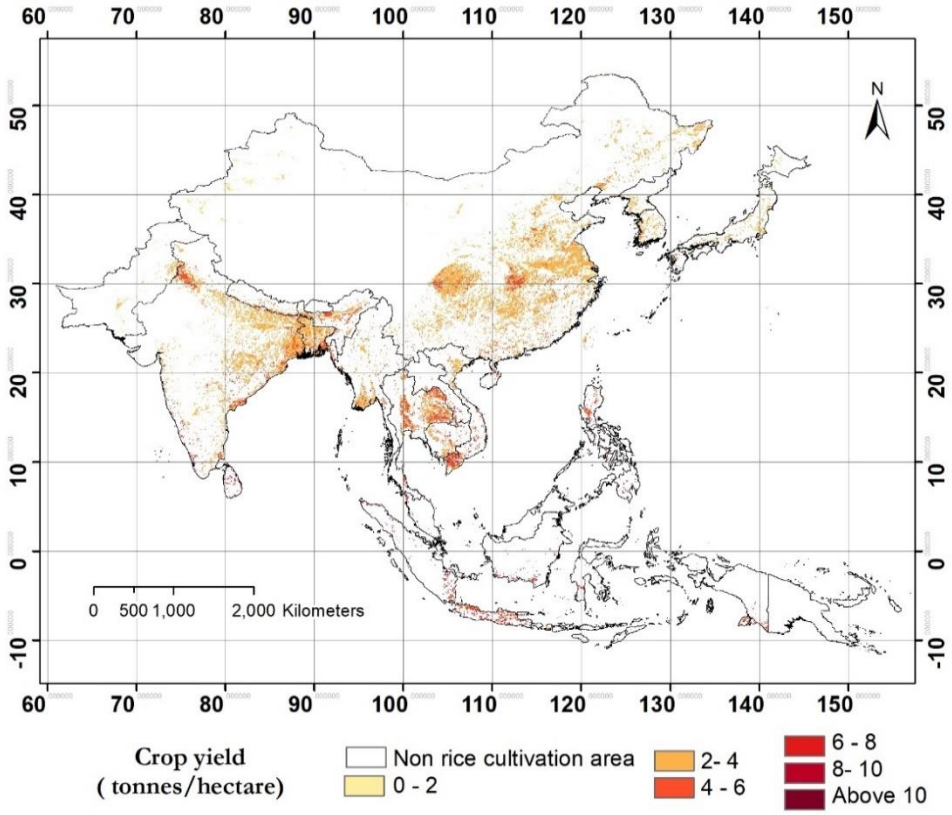

Figure 4.8. Average crop yield estimation of C_4 rice corresponds to RCP 8.5 year 2050.

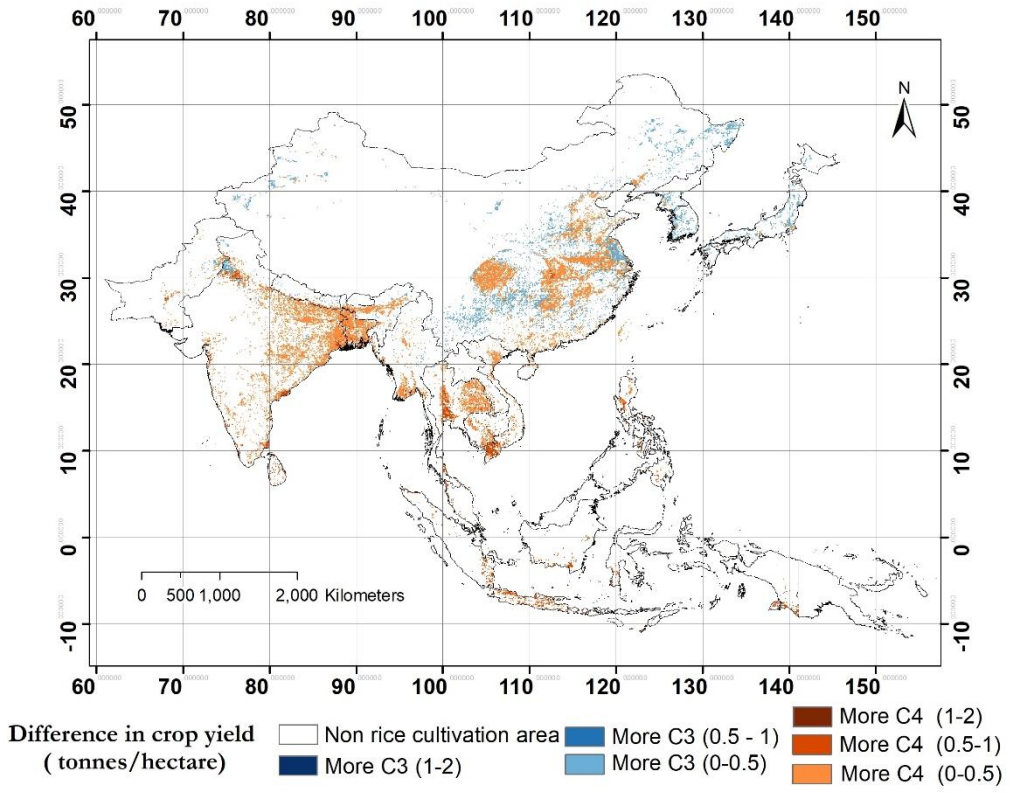

Figure 4.9. Difference between the yield of C_3 and C_4 pathways corresponds to RCP 6.0 year 2050.

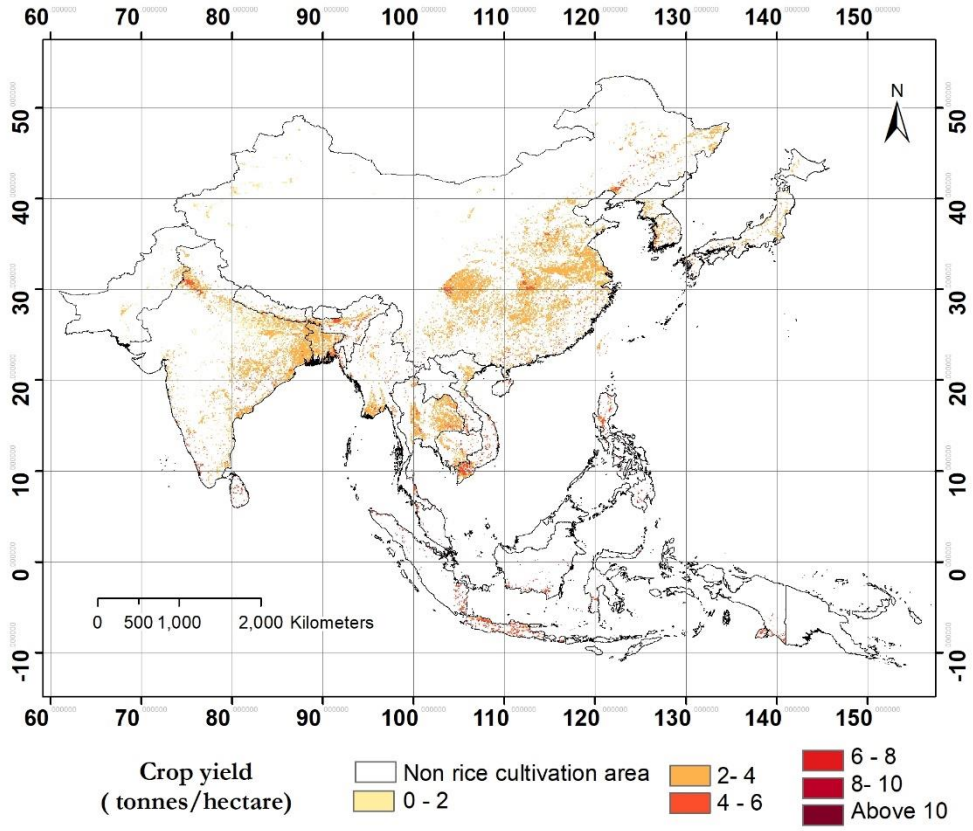

Figure 4.10. Average crop yield estimation of C_3 rice corresponds to RCP 8.5 year 2050.

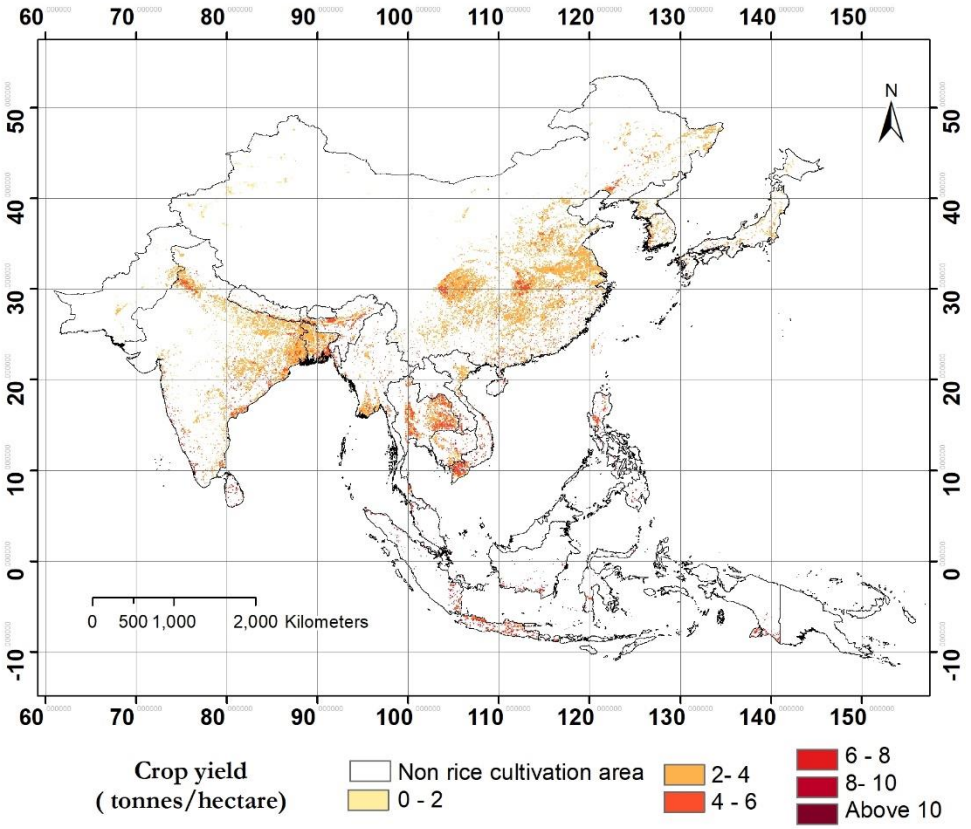

Figure 4.11. Average crop yield estimation of C_4 rice corresponds to RCP 8.5 year 2050

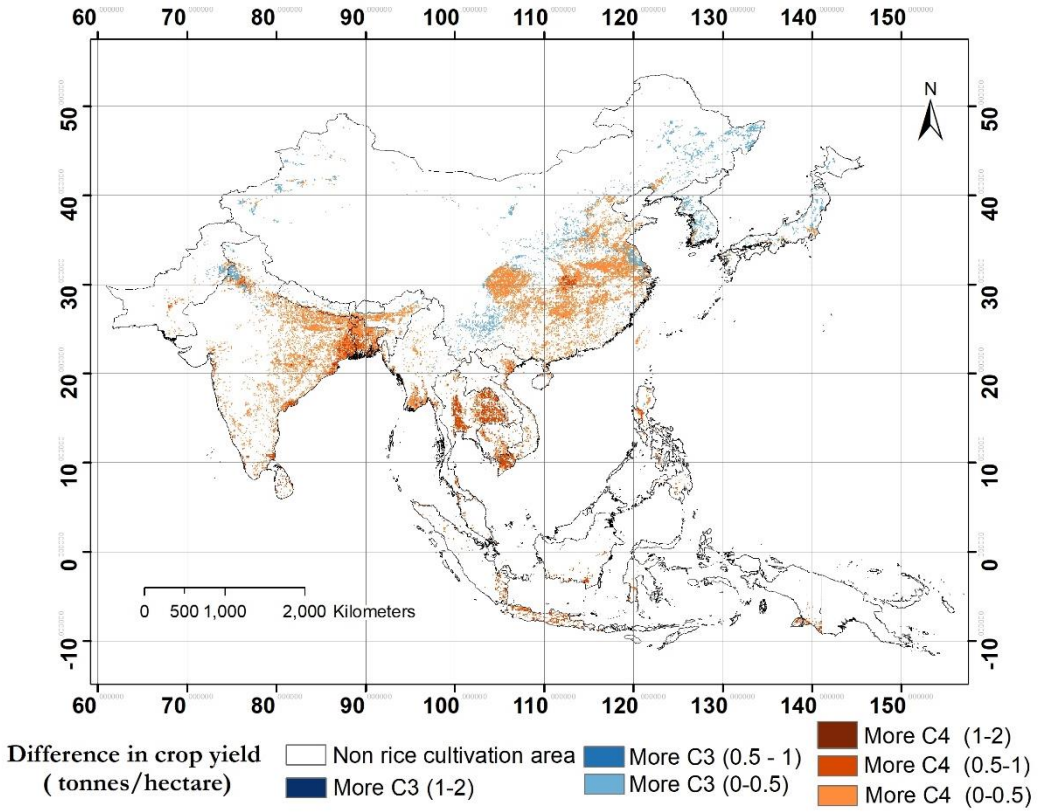

Figure 4.12. Difference between the yield of C_3 and C_4 pathways corresponds to RCP 8.5 year 2050.

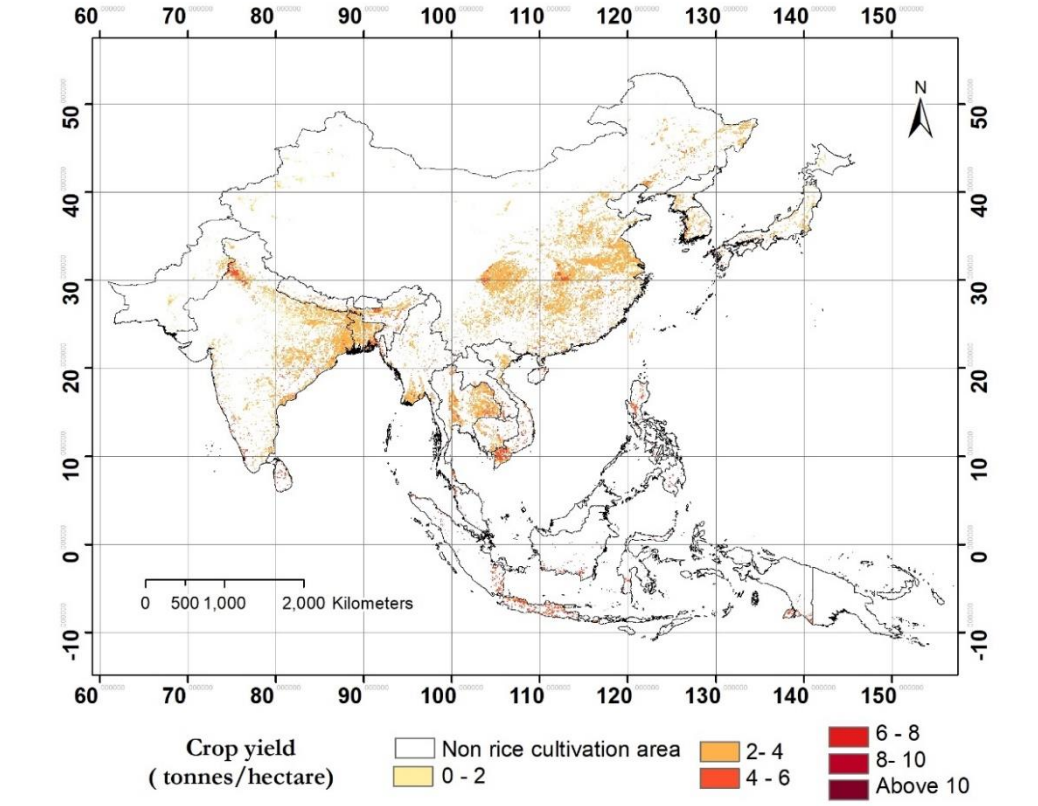

Figure 4.13. Average crop yield estimation of C_3 rice corresponds to RCP 4.5 year 2099.

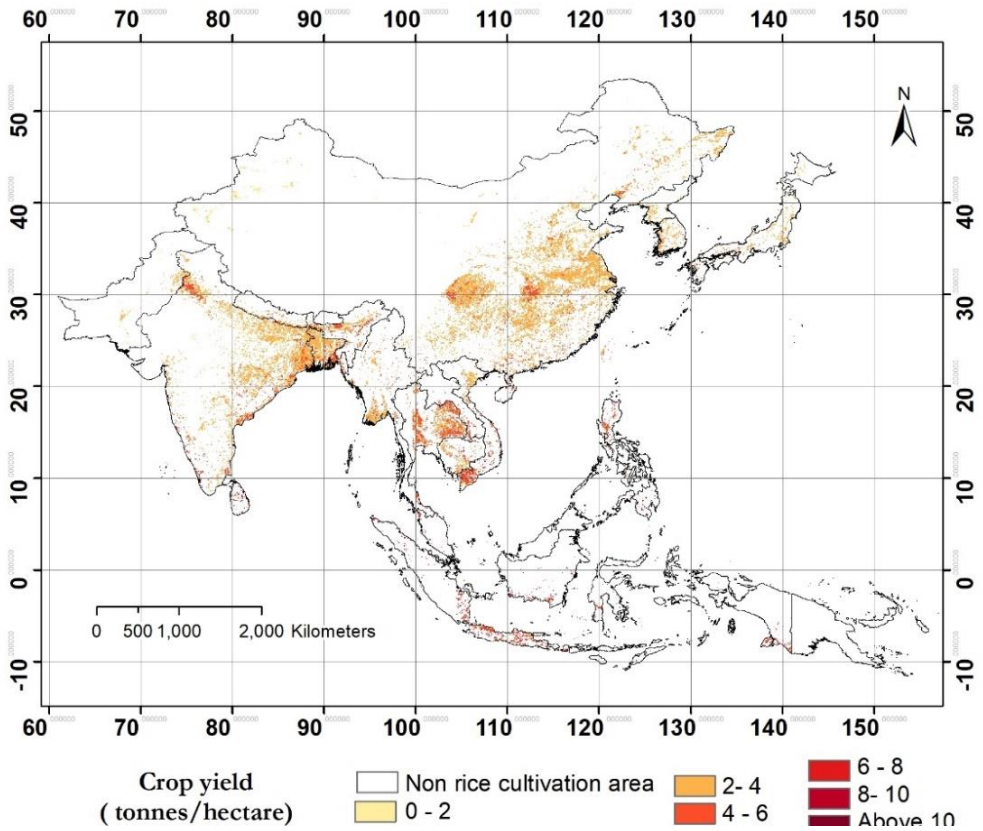

Figure 4.14. Average crop yield estimation of C_4 rice corresponds to RCP 4.5 year 2099.

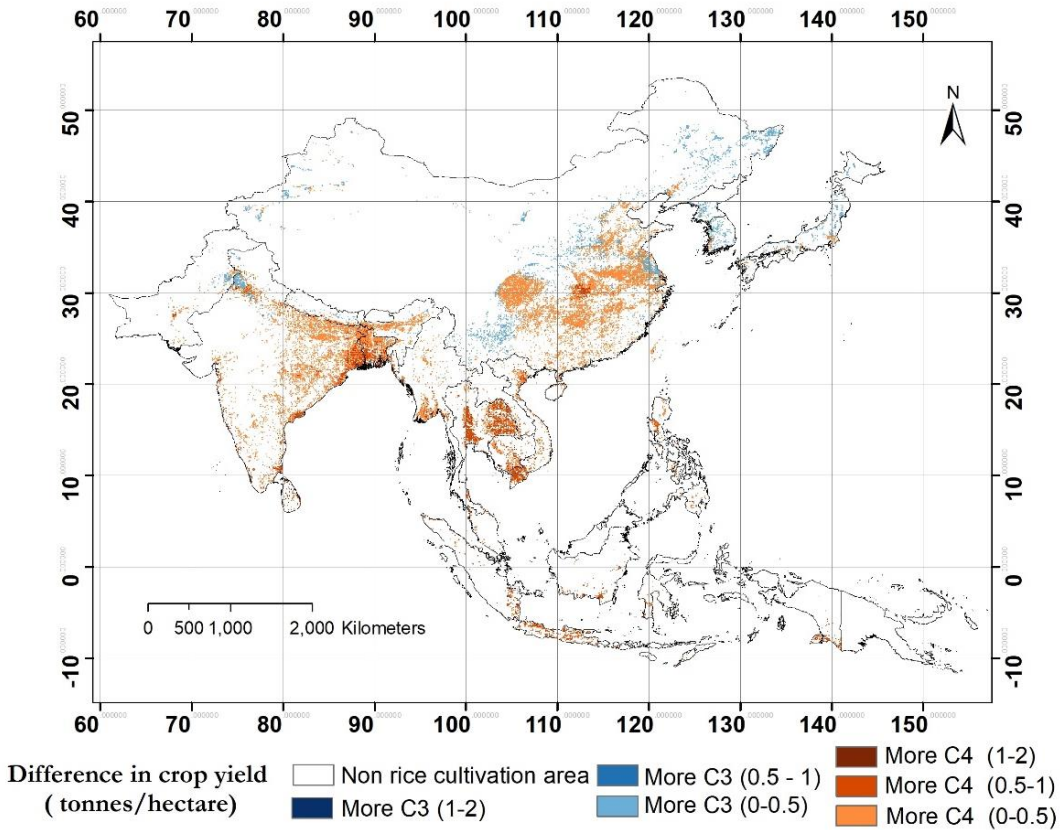

Figure 4.15. Difference between the yield of C_3 and C_4 pathways corresponds to RCP 4.5 year 2099.

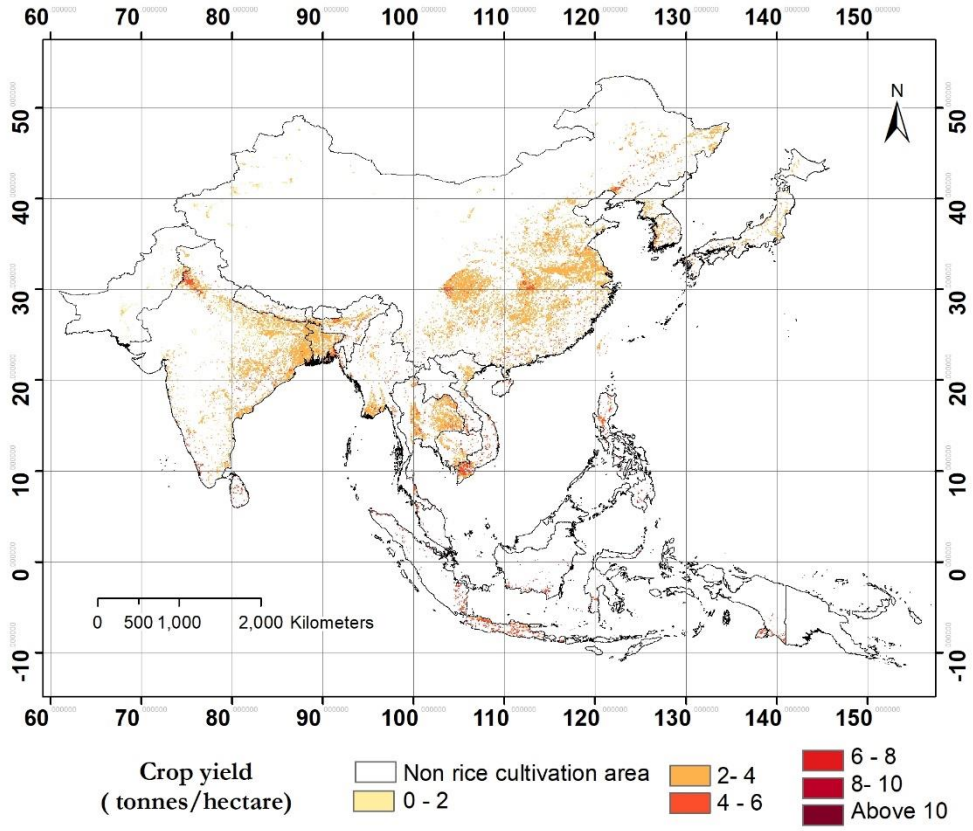

Figure 4.16. Average crop yield estimation of C_3 rice corresponds to RCP 6.0 year 2099.

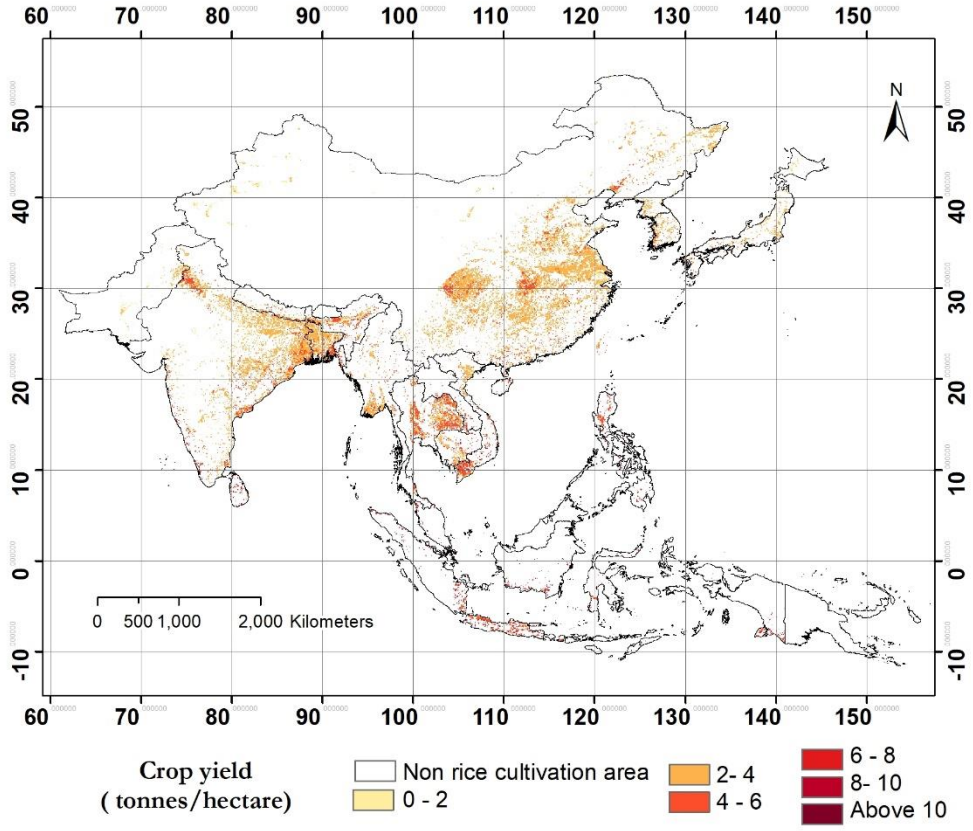

Figure 4.17. Average crop yield estimation of C_4 rice corresponds to RCP 6.0 year 2099.

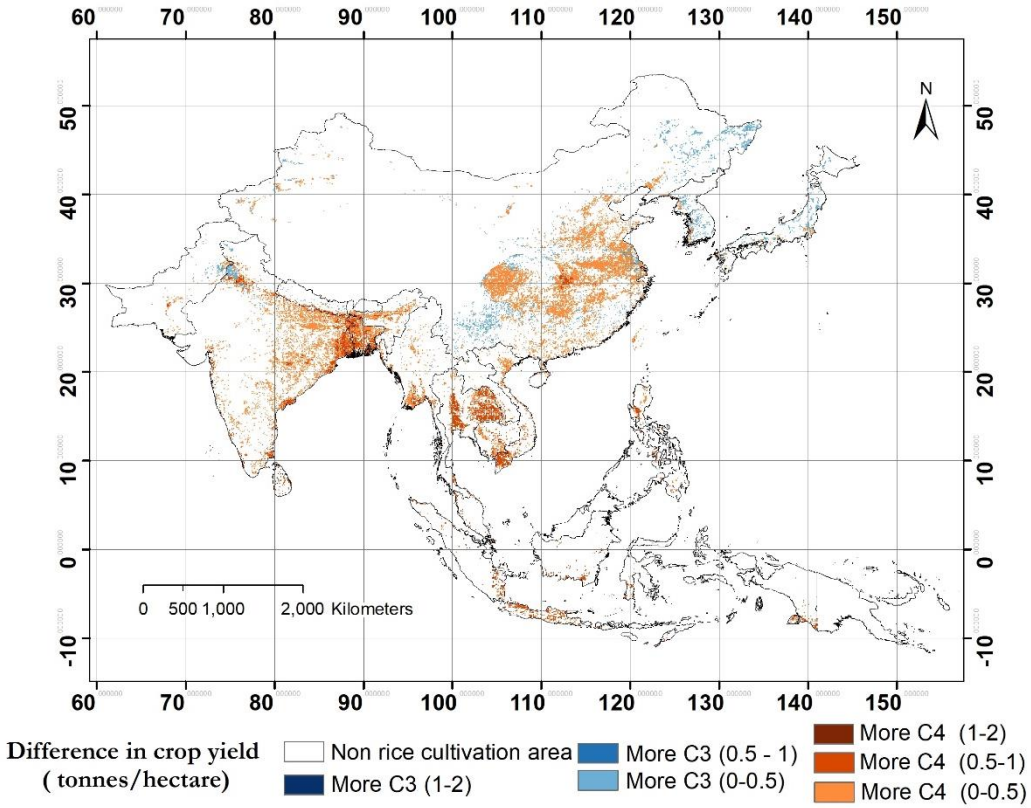

Figure 4.18. Difference between the yield of C_3 and C_4 pathways corresponds to RCP 6.0 year 2099.

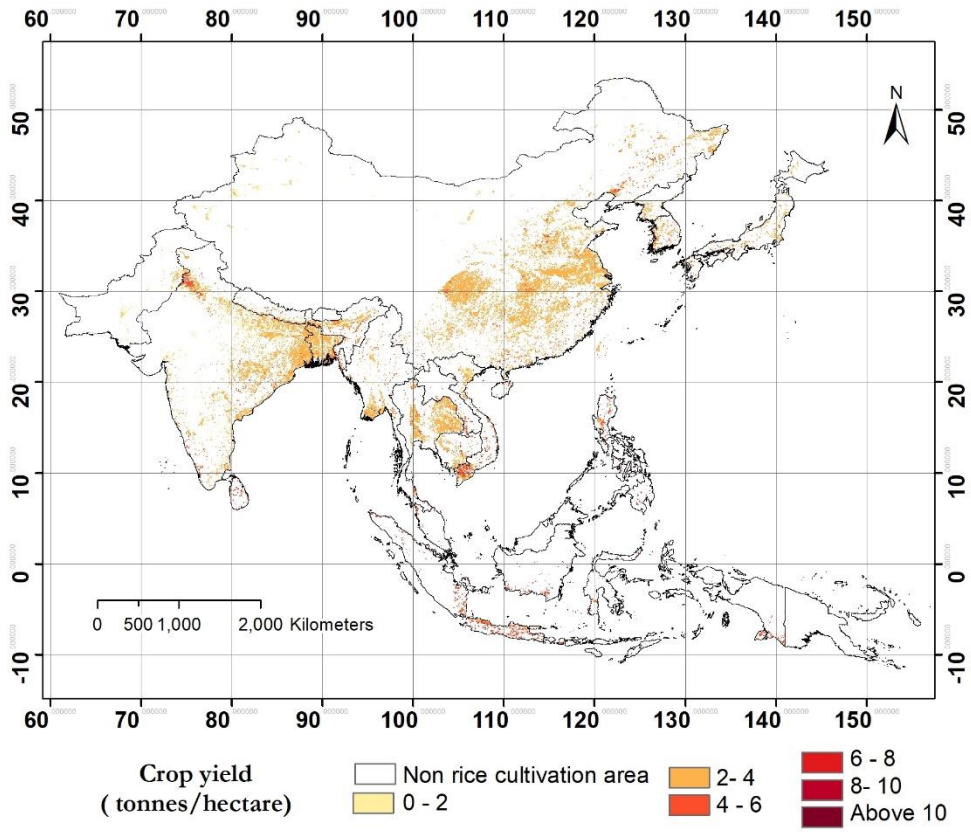

Figure 4.19. Average crop yield estimation of C_3 rice corresponds to RCP 8.5 year 2099.

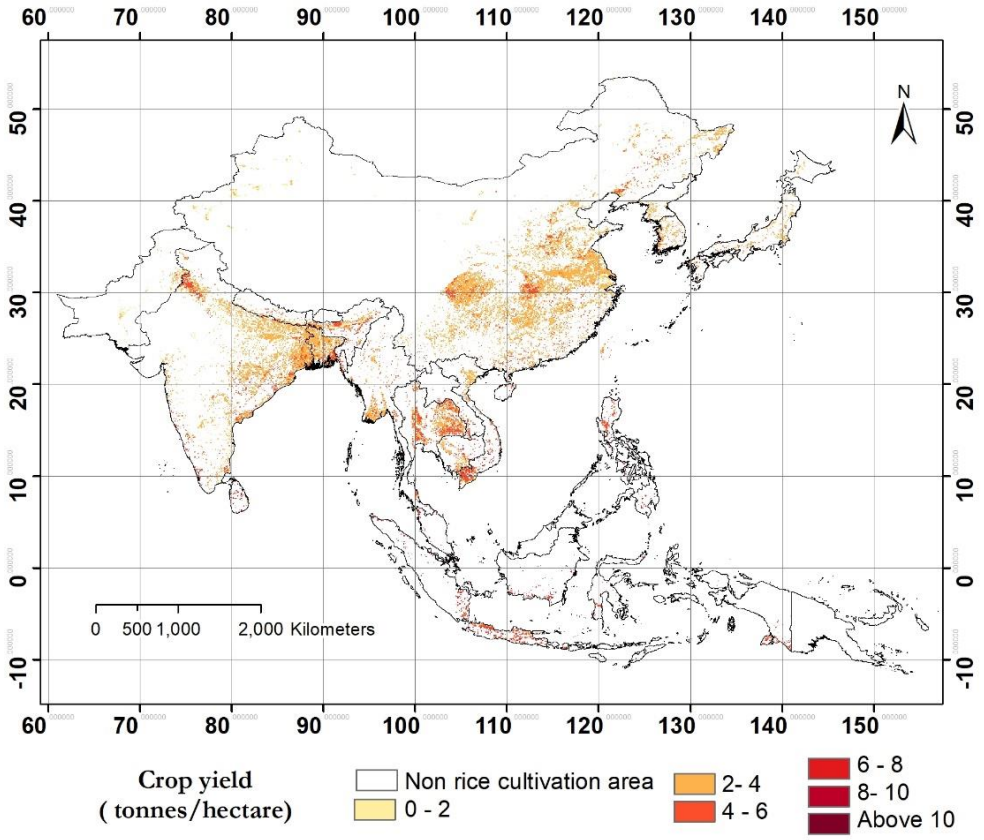

Figure 4.20. Average crop yield estimation of C_4 rice corresponds to RCP 8.5 year 2099.

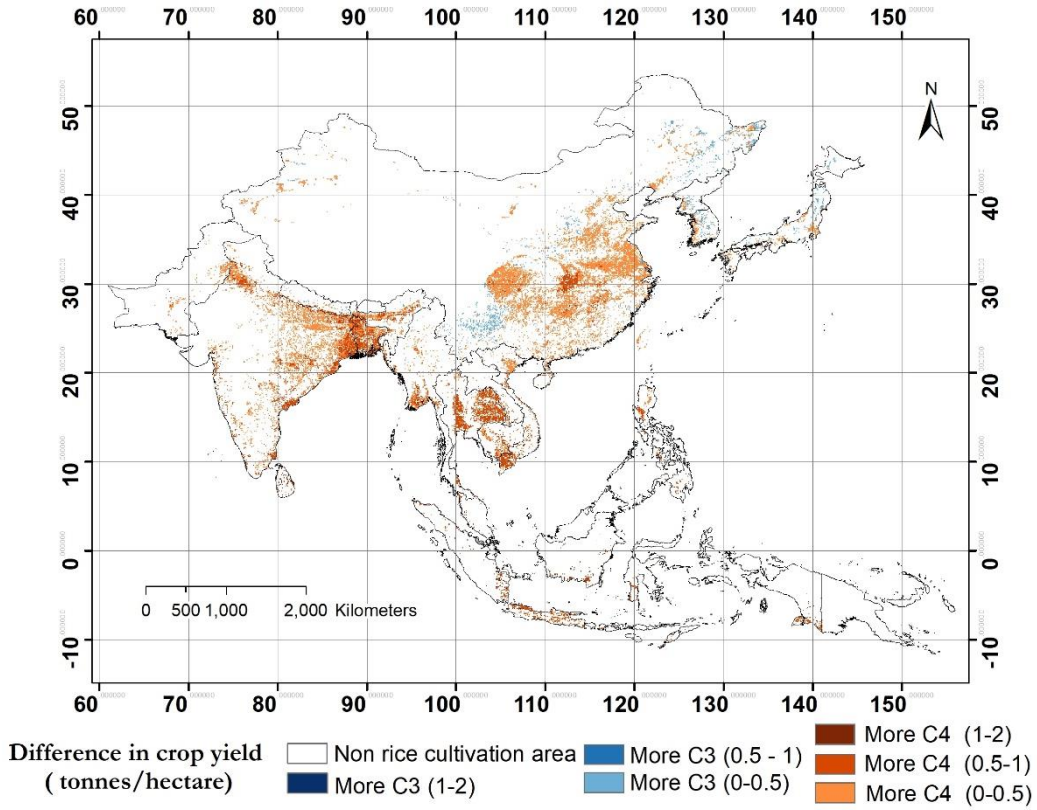

Figure 4.21. Difference between the yield of C_3 and C_4 pathways corresponds to RCP 8.5 year 2099.

4.2. Latitudinal plots

As explained about the study area in the methodology chapter, the climatic conditions such as the temperature and the precipitation, change a lot when moving from the north latitude to south latitude of the study area. The graph showing the seasonal variability of temperature and precipitation are also provided (figures 3.2 and 3,3). The heterogeneity in the study area can be visualized from the map, but the latitudinal plots help to understand average yield along latitude. To see the changes of crop yield of both C_3 rice and C_4 rice along the latitude, the average yield and the standard deviation in each row of the estimated crop yield map for both pathways were calculated. These average values were plotted against the respective latitude values. The latitudinal mean values are shown as the solid lines and the standard deviation values are shown as a ribbon in the plot. The pixel numbers used in the calculation are shown as a bar plot on the right-side. These graphs were produced for all the climatic scenarios and are shown in figure 4.22 and figure 4.23.

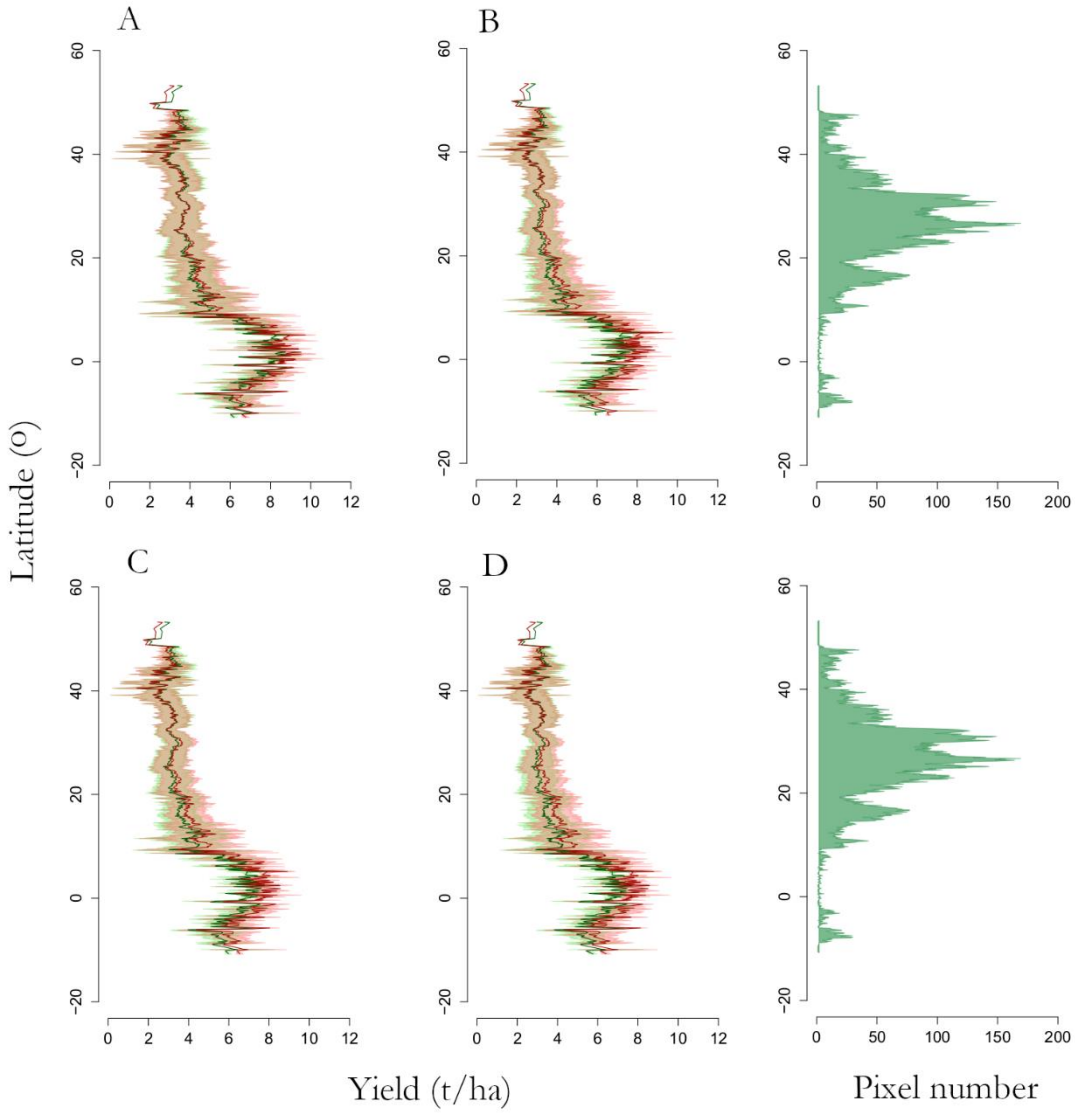

Figure 4.22. Plots showing the average crop yield latitude wise for baseline and future scenarios 2050. A). Plot for baseline (1982-2015). B). Plot for RCP 4.5 for the year 2050. C). Plot for RCP 6.0 for the year 2050. D). Plot for RCP 8.5 for the year 2050. The solid green line represents C_3 yield and the solid maroon line represents C_4 yield, The green and maroon shadows represents the standard deviation of yield for C_3 rice and C_4 rice, respectively. Pixel numbers used in the calculations are shown on the right-side as bar plot.

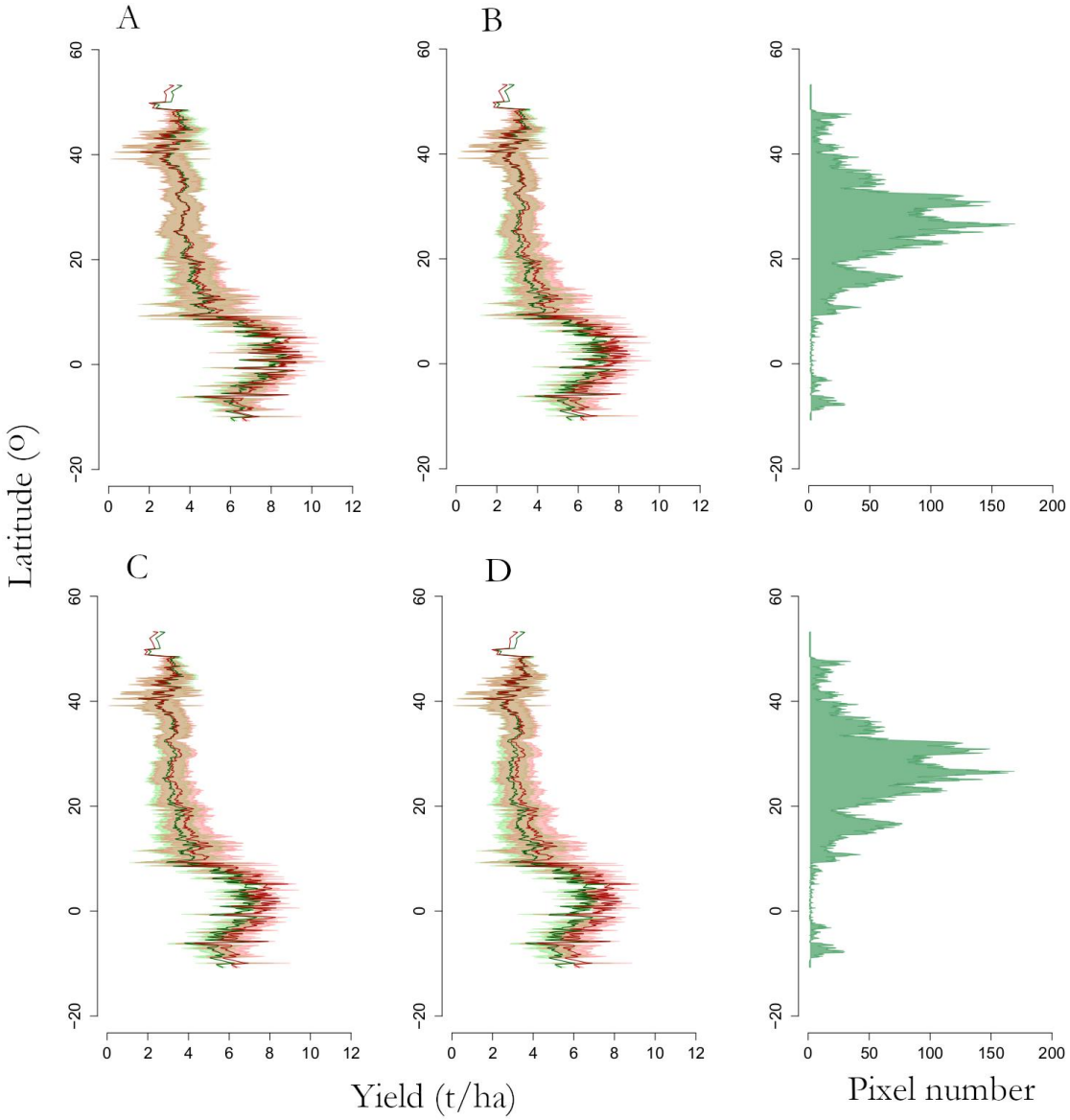

Figure 4.23. Plots showing the average crop yield latitude wise for baseline and future scenarios 2099. A). Plot for baseline (1982-2015). B). Plot for RCP 4.5 for the year 2099. C). Plot for RCP 6.0 for the year 2099. D). Plot for RCP 8.5 for the year 2099. The solid green line represents C_3 yield and solid maroon line represents C_4 yield. The green and maroon shadows represent the standard deviation of yield for C_3 rice and C_4 rice, respectively. Pixel numbers used in the calculations are shown on the right-side as bar plot.

The graphs in the figures 4.22 and 4.23 show increment in production for both C_3 and C_4 rice as approaches the tropics. A sudden positive change can be seen clearly between (+10° and -10° latitudes), but the number of pixels used (corresponding to the rice cultivation area) in the estimation is less.

To understand how much the difference in yield along the latitude changes, average value in each row of the difference map was calculated and plotted against the respective latitude. The negative values represent difference in crop yield where C_3 rice yield is more, and positive values represent the difference in yield where C_4 rice yield is more. The number of pixels used in the calculation is also included in the figure. It is represented as bar plots on the right side of the respective graph. The graphs showing the average difference between C_3 and C_4 rice are shown from figure 4.24 to figure 4.27.

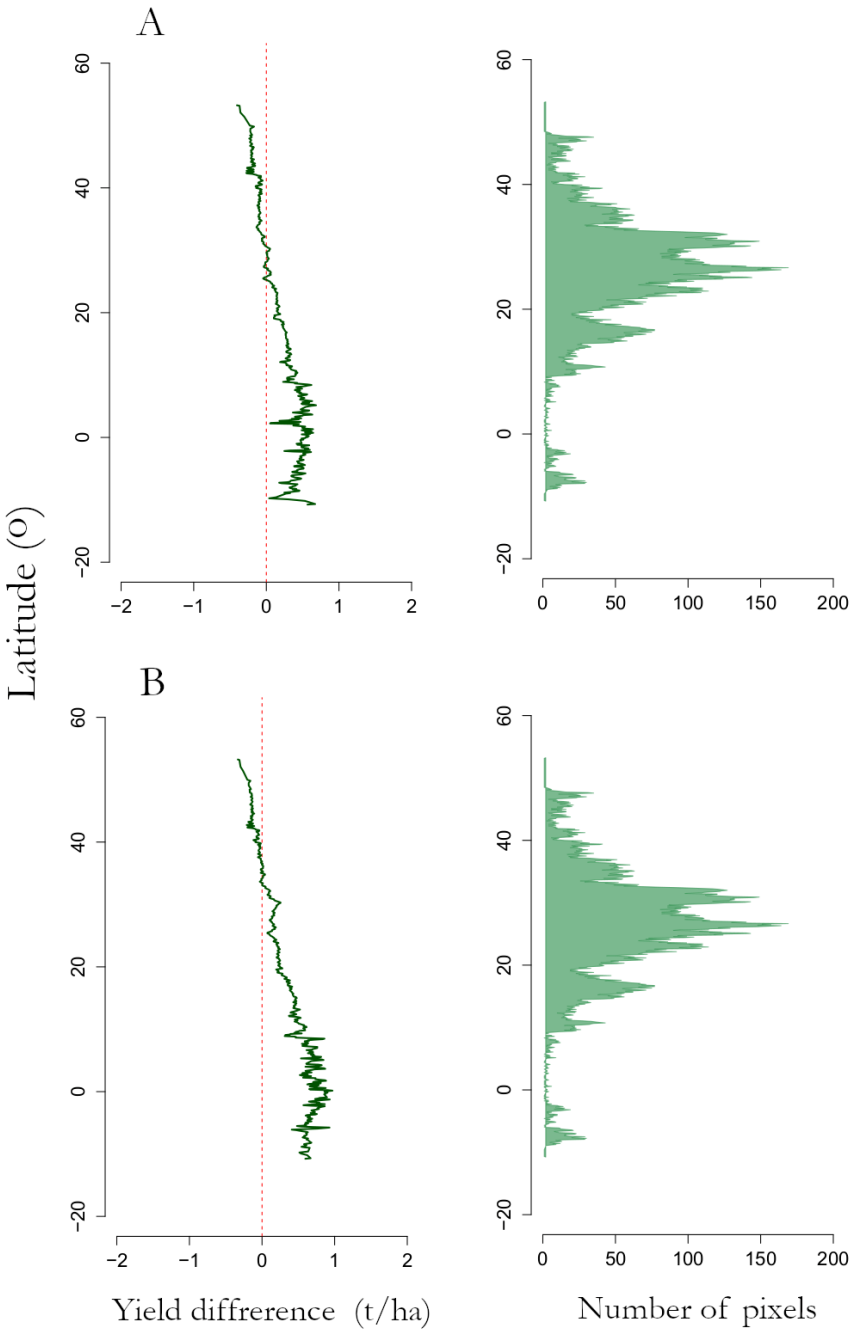

Figure 4.24. Graph showing the average difference in crop yield between C_3 and C_4 rice along latitude. A). corresponds to baseline (1982-2015). B). corresponds to RCP 4.5 for the year 2050. The number of pixels used is represented as bar graphs on the right-side.

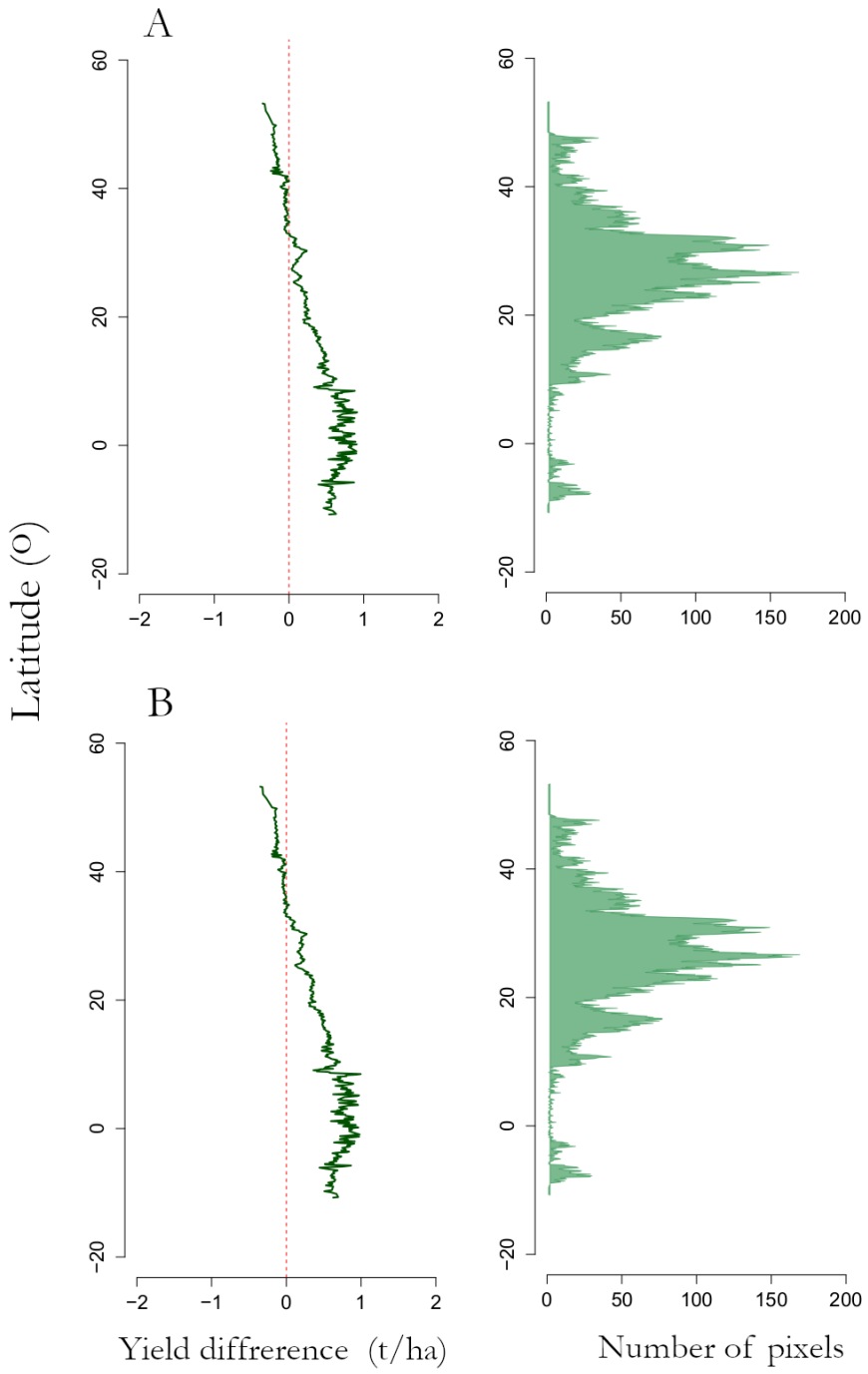

Figure 4.25. Graph showing the average difference in crop yield between C_3 and C_4 rice along latitude. A). corresponds to RCP 6.0 for the year 2050. B). corresponds to RCP 8.5 for the year 2050. The number of pixels used is represented as bar graphs on the right-side.

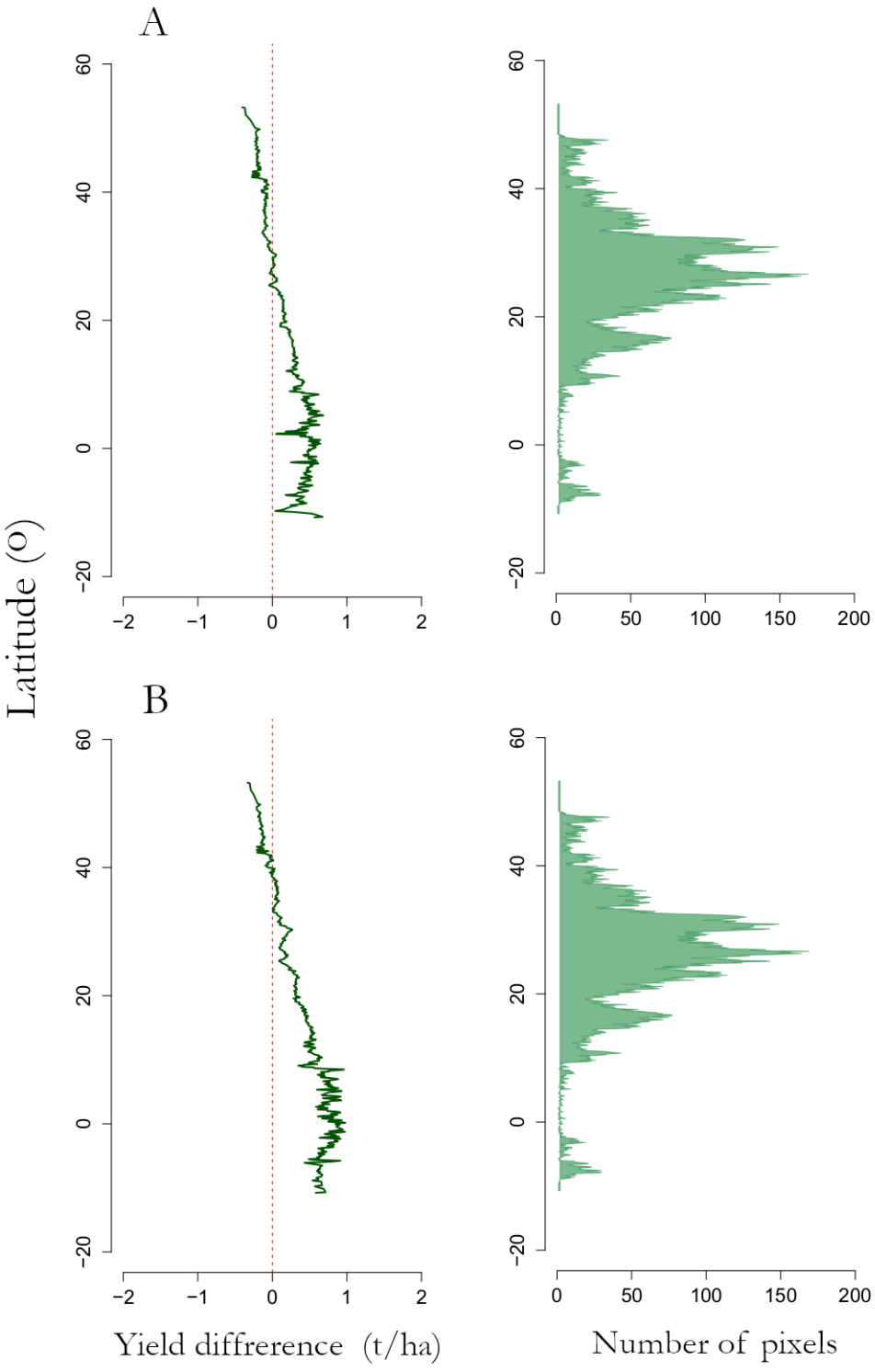

Figure 4.26. Graph showing the average difference in crop yield between C_3 and C_4 rice along latitude. A). corresponds to baseline (1982-2015). B) RCP 4.5 for the year 2099. The number of pixels used is represented as bar graphs on the right-side.

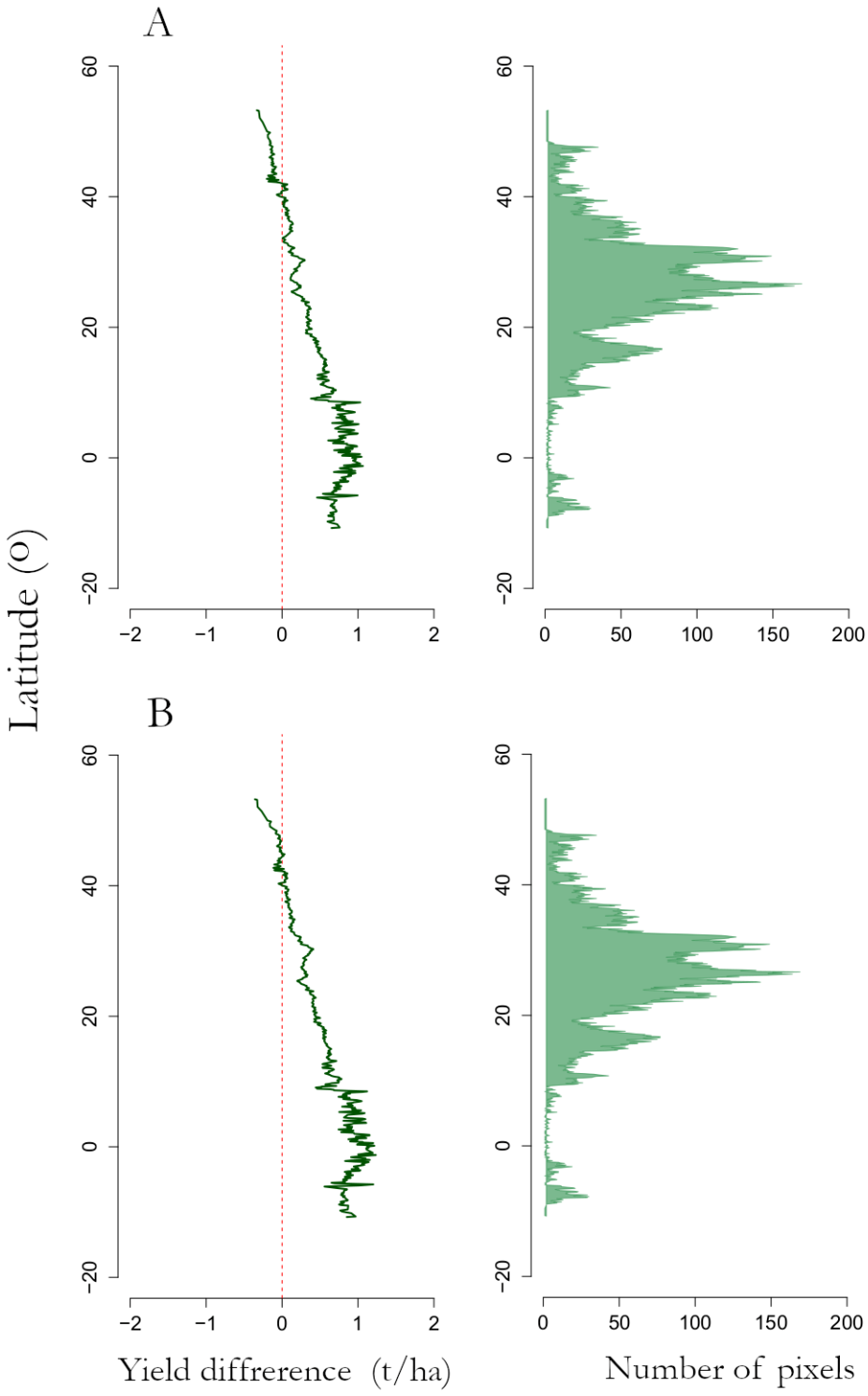

Figure 4.27. Graph showing the average difference in crop yield between C_3 and C_4 rice along latitude corresponds A) RCP 6.0 for the year 2099 B) RCP 8.5 for the year 2099. The number of pixels used is represented as bar graphs on the right-side.

The latitudinal difference plots shown in figures 4.24 to 4.27, reveals the C_4 rice production is more in the tropical region than that of C_3 rice. But at higher latitudes performance of C_3 is better. In the case of baseline, C_3 performs better above 30° and for future scenarios yield is better above 40°.

4.3. Difference in crop yield country-wise

Since the major rice producing countries in the study area spreads across different ago-climatic regions, the county-wise comparison can provide a better understating about which country favours what crop. According to *FAOSTAT*, n.d., the top eight rice producers globally are Bangladesh, China, India, Indonesia, Myanmar, Philippines, Thailand and Vietnam. The average difference between the crop yield of C_3 and C_4 rice in these countries were calculated to check which country favours which crop. Negative values represent C_3 yield and positive value represent C_4 yield. The results are plotted in a bar graph and shown in figure 4.28. The rice cultivating area in million hectare and the rice production in million tonnes for these countries for the year 2019 was obtained from FAOSTAT. The data is plotted and shown in figure 4.29

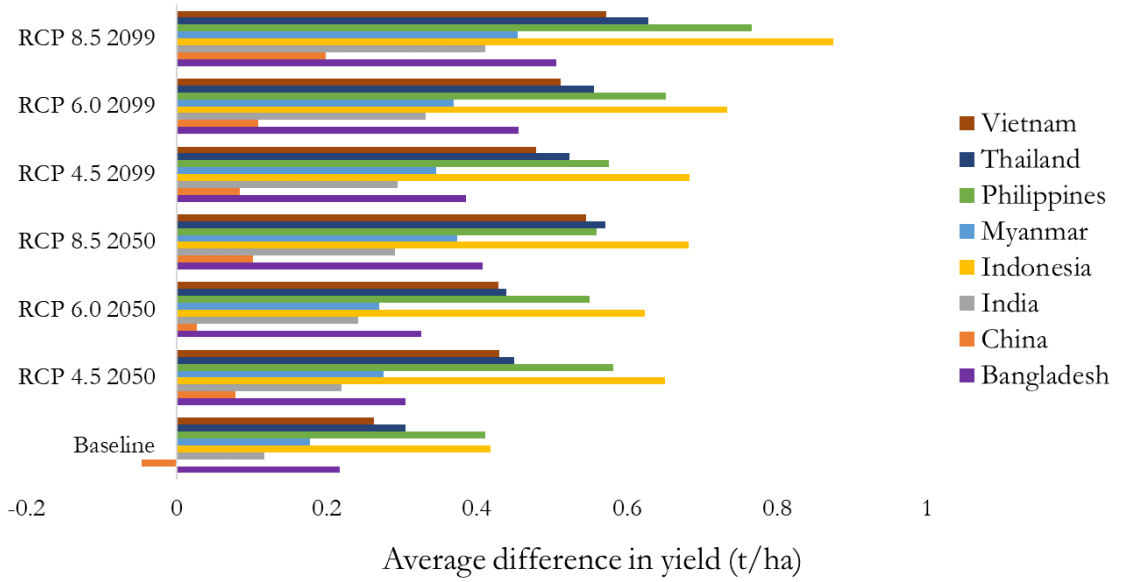

Figure 4.28. The difference in crop yield country-wise for baseline and future scenarios.

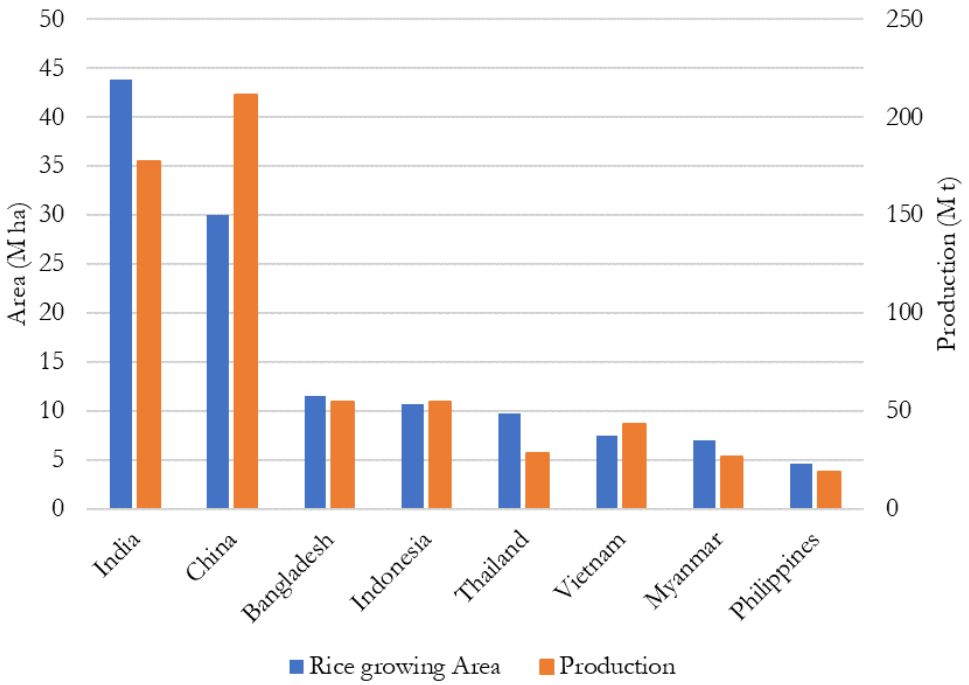

Figure 4.29. The rice cultivation area (M ha) and rice production (M t) for the top eight rice producing countries in the study area for the year 2019 as per FAOSTAT.

From figure 4.28, Indonesia and Philippines are the two countries those are most favour to C_4 rice production. Both countries showed about 0.4 tonnes more production for C_4 rice at baseline. Indonesia showed 0.9 tonnes difference and Philippines showed 0.8 tonnes difference corresponds to RCP 8.5 for 2099. But Indonesia is in the fourth position and Philippines is at the eighth position of global rice production contributing 7.5 % and 2.5 % respectively for the year 2019 as per FAOSTAT, n.d. But the highest producing countries like China and India do not show much support to C_4 rice. Their global production contributions are 28 % and 23.5 % respectively. China gets the least benefit from C_4 rice, the country even showed better performance in C_3 yield at baseline. The other countries show moderate but positive response towards C_4 rice.

From the difference maps and latitudinal plots, above 40^o latitude C_3 rice shows more yield for all climatic conditions, there is not much difference in yield between 30^o and 40^o, then C_4 yield starts to increase as going down (towards south) along the latitude. The difference reaches maximum around the equator, then starts to decrease around -7^o. The maximum difference in yield is between -10^o and $+10^o$. The average values of crop yield difference between these latitudes are shown in table 4.1.

Table 4.1. Average yield difference between C_3 and C_4 rice from -10^o to $+10^o$ latitudes for all climatic scenarios.

Climatic scenarios	**Average crop yield difference (t/ha)**
Baseline	0.446
RCP 4.5 (2050)	0.666
RCP 6.0 (2050)	0.660
RCP 8.5 (2050)	0.724
RCP 4.5 (2099)	0.713
RCP 6.0 (2099)	0.770
RCP 8.5 (2099)	0.898

Pixels used in the analysis between -10^o and $+10^o$ latitudes are about 1427. The image resolution is approximately 9 km. Therefore, the total rice cultivation area in this region is about 115,587 km^2. The most number of pixels used are between 22^o and 32^o degrees, 11990 pixels. It is an approximate area of 971,190 km^2. The average yield difference between 22^o and 32^o latitudes are given in table 4.2 for all the climatic scenarios.

Table 4.2. Average yield difference between C_3 and C_4 rice from 22^o to 32^o for all climatic scenarios.

Climatic scenarios	**Average crop yield difference (t/ha)**
Baseline	0.025
RCP 4.5 (2050)	0.158
RCP 6.0 (2050)	0.129
RCP 8.5 (2050)	0.203
RCP 4.5 (2099)	0.174
RCP 6.0 (2099)	0.204
RCP 8.5 (2099)	0.307

When the average difference values given in table 4.1 and 4.2 are compared, the more rice growing areas (between 22° and 32° latitudes) do not show a big difference in yield between C_3 and C_4 rice. The maximum difference in yield is between -10° and +10° latitudes but the rice growing areas are comparatively lesser.

4.4. Sensitivity analysis

Global sensitivity analysis (Sobol method) was performed to determine the most influencing parameter of the model in the study area, as explained in the methodology. The maps showing the sensitivity of the model to temperature, solar radiation, and VPD for C_3 rice are given in figure 4.30 and for C_4 rice in figure 4.31.

When both the images are compared, there is not much difference in sensitivity of both C_3 and C_4 models to the three parameters across the study area. In both cases of C_3 and C_4, the Punjab area in the northwest part of India is the only place that is more sensitive to temperature (represented in red colour) than the other two parameters. Along the border between India and Nepal both the models show higher sensitivity to VPD (green colour) compare to other parameters. Apart from these areas, the other rice growing areas of south and southeast of India, south and southeast of China, Bangladesh, Thailand, Myanmar, Vietnam, Cambodia, Indonesia, Philippines etc. the models are sensitive to solar radiation (blue colour).

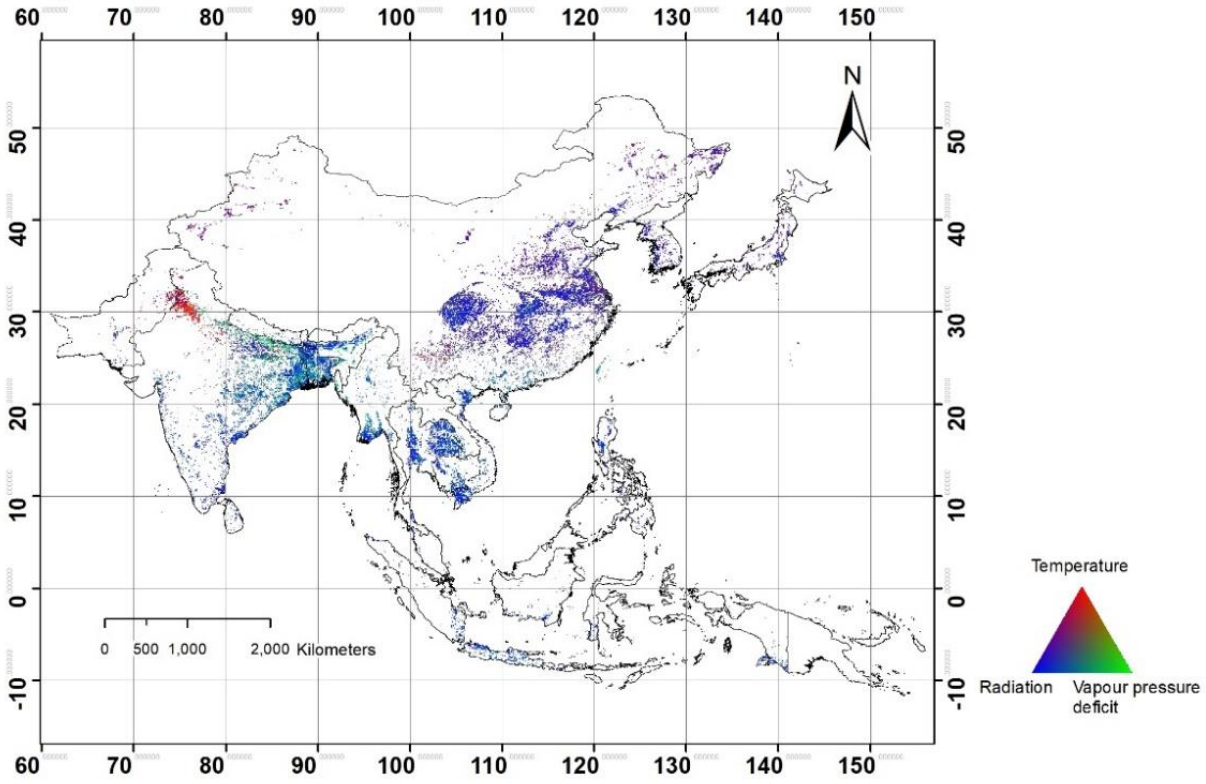

Figure 4.30. Map showing the result of sensitivity analysis of C_3 model for rice-growing areas.

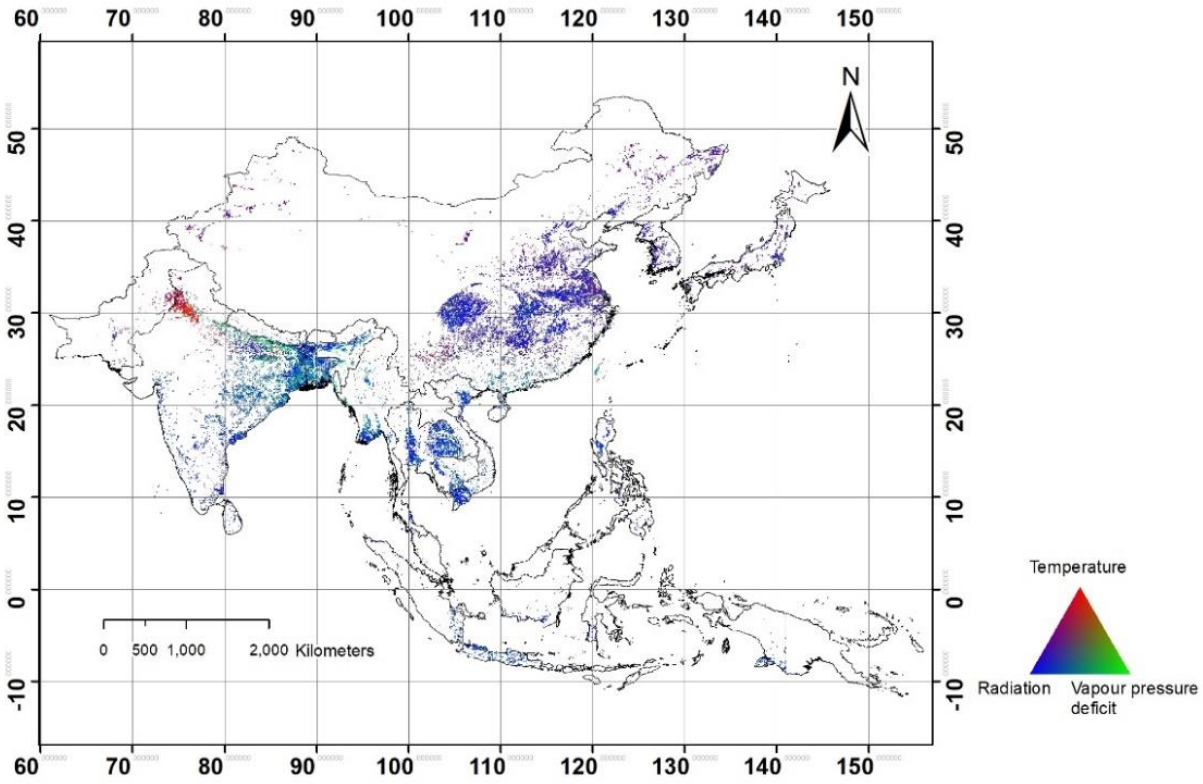

Figure 4.31. Map showing the result of sensitivity analysis of C_4 model for rice-growing areas.

5. DISCUSSIONS

5.1. Yield estimation

Since the study area covers a large portion of Asia and spreading across various ago-climatic conditions, the crop yield estimation of C_3 and C_4 rice also changes across the study area. The area near the Himalayan mountains is cold and temperature drops to below freezing point during winter and reaches an average of 15 degC during summer (Dando, 2005). North, northeast and central parts of China are temperate zones. The northern part of India, south, south-east and southwest parts of China are sub-tropical regions. The coastal areas of south and east Asia are tropical areas. The irrigated lowland rice is grown in wet tropical and sub-tropical regions and rainfed lowland rice is grown near river deltas and coastal regions (*Where Is Rice Grown? - Ricepedia*, n.d.). Places like northeast and northwest china have low temperature, a short growth period, little rainfall, and a lack of water (W. Li et al., 2021). Therefore, the areas suitable for rice cultivation are very few in this region, but still rice is cultivated in some areas as shown in the rice-growing region in the study area section of the methodology chapter as per the map from IRRI.

There are researches which explored the productivity of C_3 and C_4 plants in different climatic and atmospheric conditions such as the studies by Morgan et al., (2011). The research examined the responses of C_3 and C_4 grasses at raised levels of atmospheric CO_2 and higher temperatures, and, crucially, how these conditions might change the plants' water budgets. The result of the study show that higher CO_2 concentration favours the growth of C_3 plants and higher temperature favours the growth of C_4 plants. The study also states that the combination of increase in temperature and increase in CO_2 concentration favours C_4 plants because water use efficiency and nitrogen use efficiency are more in C_4 plants. Studies of Taylor et al., (2014) also showed similar results. The study observed higher C_4 grasses productivity at warmer and drier environment. This higher productivity of C_4 grass at warm and dry environment is due to the conditions during its evolution. The C_3 and C_4 pathways were evolved in completely different atmospheric conditions. The C_3 photosynthesis evolved when the concentration of CO_2 was well above 1000ppm, but later the CO_2 level dropped to around 500 ppm around 32to 25 million years ago, which leads to the evolution of C_4 plants (Langdale, 2011; Ehleringer et al., 1991). Studies also suggest that once the C_4 has evolved, it tends to make the transition into arid habitats with higher temperature as opposed toC_3 plants (Langdale, 2011).

The difference in crop yield for the entire study area for the baseline and future scenarios are shown in the difference map in the result chapter. As described earlier, the higher latitude of the study area has lower temperature (area above 40^o latitude). The annual temperature plot given in the methodology chapter shows that the temperature corresponds to the points located at this region varies around -20 degC at winter to+20 degC at summer. As explained earlier with studies of Morgan et al., (2011) and Langdale, (2011), the productivity of C_3 and C_4 plants are highly depended on temperature. This explains why the C_3 rice production is more compared to C_4 rice above 40^o latitude with all climatic scenarios. Also, as per the studies of Morgan et al., (2011) the CO_2 fertilization in the future favours the C_3 crop in this area since the temperature is mild.

When examine the crop yield maps around 30^o latitude, a lot of heterogeneity (mixed pixels corresponds to more C_3 and C_4 can be seen. In this region, the annual temperature variations are between 10 degC and 30 degC (temperature plot from methodology). In the yield difference map corresponds to baseline, it is very clear that befits of C_3 over C_4 in some areas like Punjab in North of India and south east provinces of China. When compared with future scenarios, most of the areas show change from more C_3 production to more C_4 production except some areas like the Kunming region at the south of China. In the Kunming region, the temperature varies between 8 to 22 degC (from the temperature graph in methodology). This is the

reason C_3 rice befits in Kunming region. But in the other areas around 30^o latitude, it is clear that the elevation in temperature favours the growth of C_4 rice.

In the tropical region (below 20 degree), it is very clear that the current and future conditions are beneficial to the production of C_4 rice. The area between $+10^o$ and -10^o latitude shows maximum difference in crop yield between C_3 and C_4 benefiting C_4 rice. The future increase of temperature has synergistic effect on C_4 yield. It is clearly visible in the latitudinal plots. The maximum gain for C_4 rice is corresponds to the RCP scenario 8.5 for the year 2099.

When compare the yield difference maps, the map that corresponds to RCP 6.0 for the year 2050 shows less pixels of C_4 rice gain (red colour pixels) compared to RCP 4.5 for the year 2050. The CO_2 concentration graph for RCPs given in the methodology shows that the CO_2 concentration corresponding to RCP 4.5 for the year 2050 is greater than RCP 6.0 for the year 2050. Therefore, the corresponding temperature projection is also varied. The temperature projection for RCP 6.0 for the year 2050 is less than RCP 4.5 for the year 2050. That also explains the corresponding yield difference maps. Similarly, The CO_2 concentration correspond to RCP 8.5 for year 2050 and RCP 4.5 for year 2099 are almost equal. Therefore, the temperature projections are also almost same. This leads to the production of nearly the same yield difference map corresponding to RCP 8.5 for year 2050 and RCP 4.5 for year 2099.

5.2. Difference in crop yield country-wise

Average difference of crop yield between C_3 and C_4 rice for top eight rice producing countries (Bangladesh, China, India, Indonesia, Myanmar, Philippines, Thailand and Vietnam) were calculated for baseline and future climatic scenarios. These countries rice production and area harvested are also given in the results. Indonesia and Philippines are two countries that shows the maximum positive gain for C_4 rice for all climatic scenarios. But these countries produce only 7.5 % and 2.5 % of the global rice production, respectively. Indonesia is the only major country which lies between $+10^o$ and -10^o latitude where rice yield for both C_3 and C_4 and yield difference between both the crops were highest. But Indonesia contribute only 6.6 % of the global rice cultivation area (FAOSTAT, n.d.).

As shown in the graph of top rice producing countries in result section, China and India are the top producers contributing 28 % and 23.5 % to global rice production respectively. But both countries do not gain much benefit from C_4 rice. They lack behind all the other six countries. The reason for this is the rice cultivation areas in both countries situated at higher latitudes compare to other countries in the study area. When the latitude is higher, the temperature is lower which leads to the reduction in C_4 rice performance.

Among all climatic scenarios, the least difference between C_3 and C_4 crop yield for the eight countries was corresponds to baseline. China even showed negative difference (more C_3 yield) in baseline. But for the future scenarios, all the countries show positive response toward C_4 yield. At RCP 8.5 for year 2099, country-wise difference between crop yields showed maximum values, Indonesia with maximum benefit and China with least benefit. But the values showed positive gain for C_4 rice in all countries. That means, in the future warm climate C_4 rice can produce more yield compare to the current C_3 rice crop varieties.

5.3. Sensitivity analysis

As shown in the result section, the model is sensitive to radiation in most study areas. But in some smaller areas, the model is sensitive to temperature and VPD. In the northwest region of India near the Pakistan border, Punjab region, the temperature is the most influencing parameter. Compare to other rice-growing areas in the tropics, Punjab receives low amount of rainfall about 555 ± 280 mm annually, but it varies across the region, and has low relative humidity (about 70 % in the rainy season and about 40 % in summer) (ENVIS, n.d.). About 96 % of the cultivation depends on irrigation (ICAR, n.d.). The Thar desert lies on the north side of Punjab. The temperature varies a lot with the seasonal changes. In winter, the mean

temperature is about 10 degC and in summer the temperature rises to 30 degC. Because of these geographical and climatic specialities, the model shows more sensitivity to temperature than the other two parameters (radiation and VPD).

On the northeast side of India near the border of Nepal, the model shows higher sensitivity to VPD. This region lies in the foothills of the Himalayas, covering two states in India (Uttar Pradesh and Bihar). The northern areas of these states receive high rainfall (above 1000 mm) during the monsoon season during July-August, but in the southern areas, the rainfall is comparatively less (Guhathakurta, L, Menon, Prasad, Sable, et al., 2020 a; Guhathakurta, L, Menon, Prasad, Sangwan, et al., 2020 b). The possible reason for this rainfall is the influence of Himalayan mountain ranges causing orographic lift. When the air mass lifted due to a rising terrain, it cools down adiabatically cause rainfall and high relative humidity (RH) (Tada et al., 2016). The RH of the two states fluctuates a lot when the season changes. The average minimum RH is about 30% and average maximum RH is 80%. Because of these reasons, the region is more sensitive to VPD than the other two parameters (temperature and radiation).

All the other remaining study area shows sensitivity to radiation, means the yield estimation mostly influenced by the radiation. This is the reason the model does not estimate the C_4 yield with much improvement in the future scenarios. Most of the study area is sensitive to radiation, but the future yield estimation was carried out with future temperature projections, because the data for the future solar radiation is not available. Therefore, the average solar radiation value corresponds to baseline was also used in the future field estimation.

5.4. Uncertainties in the study

This research produced some interesting results as explained in the result chapter and earlier in this discussion chapter. But the method used in the study is not free from uncertainties. Some of the important issues that need to be explained are given below.

The first issue to describe is the optimization of the model. As explained in the methodology, in the initial stages of study the proposed method was to optimize the model with the available field data to find out the values of coefficient present in the model equation. But the optimization with the yield data could not provide sufficient result. Therefore, the values of the coefficients in the model used was the values optimized for rice using the data from the United States in the previous study. But it is more appropriate to conduct the study with values optimized using the data in the study area.

The next issue to be addressed is about future CO_2 concentration. The temperature projections based on the RCP scenarios are developed based on different emission rate of GHGs and socio-economic aspects (van Vuuren et al., 2011). The concentration of CO_2 plays an important role in this. But in the current research yield estimation for the future scenarios was conducted only the temperature projections. The effect of the future CO_2 concentration on the intercellular CO_2 concentration on plants was not considered, Instead, the current value of intercellular CO_2 concentration (340 micro-mol/mol) was used (Michael Marshall et al., 2018).

One another issue is to consider is about harvest index (HI). HI is the measure of crop production from the total above ground biomass. In the current study it was considers as a constant (0.55) from the studies of Wang et al., (2020). The study also stated that due to use of new high yielding crop varieties the value of HI for rice has been increased from 0.44 to 0.55-0.62. It also depends on many factors like crop variety, crop management practices, climatic condition in the growing area, etc (Pan & Deng, 2007). Therefore, it changes place to place, but for current study value of 0.55 was chosen as HI.

The basic concept of LUE approach is the total biomass produces is directly proportional to the total absorption of photosynthetically active radiation over the growing period(David B. Lobell, 2013). The climatic parameters used in current study to estimate crop yield for C_3 and C_4 are average temperature, solar

radiation and VPD. But the growth and development of plats are also affected by other factors like management practices, crop variety, fertility of soil etc. Since the process to incorporate these factors are complex and they vary place to place (lot of cultivation practices and varieties are localized), the current study does not consider these factors.

5.5. Areas for further research

To reduce the uncertainties in the research some additional work needed to be carry out in the future research. The first thing to be considered is to optimize the model coefficient with data from the study area. Asiaflux is a regional research network in Asia (*AsiaFlux*, n.d.). They have stations in the study area to measure the exchange of CO_2, water and energy between terrestrial ecosystems and the atmosphere daily basis. Two stations of this network situated in paddy fields at Japan and Republic of Korea. The daily GPP measurement in the crop growing season at these stations can be used to optimize the model and proceed with yield estimation of C_3 and C_4 rice for baseline and future scenarios.

As explained in the uncertainty part future CO_2 concentration is not included in the study. Therefore, another major consideration to make in the future work is to include future CO_2 concentration in the model corresponds to different RCP scenarios and conduct the estimation.

6. CONCLUSION

The current study focused on yield estimation and comparison of present C_3 rice variety and future C_4 rice variety across the south and east Asia using the LUE model PEMOC for the baseline climatic condition (1982 to 2015) as well as future temperature projection for the years 2050 and 2099. It was found out that the C_3 rice performs better in higher latitudes (above 40^o) of the study area, the difference in yield is very less between 30^o and 40^o and below 30^o the C_4 rice performs better. The increment of C_4 rice yield is maximum near the equator between $+10^0$ and -10^0 latitudes. The C_4 crop produces more yield in the countries which lie near the equator, like Indonesia and Philippines for all scenarios. But the major rice-producing countries like China and India do not have much benefit in the baseline because of their geographical positions. But the yield estimation corresponds to future scenarios showed all the countries will gain benefits from C_4 rice in the future.

LIST OF REFERENCES

• *Global population - distribution by continent 2019 | Statista*. (n.d.). Retrieved May 12, 2021, from https://www.statista.com/statistics/237584/distribution-of-the-world-population-by-continent/

5 ways to transform our food systems and save the planet | World Economic Forum. (n.d.). Retrieved April 17, 2021, from https://www.weforum.org/agenda/2021/03/5-ways-transform-food-system-sustainable/

Agroclimatic indicators from 1951 to 2099 derived from climate projections. (n.d.). Retrieved May 15, 2021, from https://cds.climate.copernicus.eu/cdsapp#!/dataset/sis-agroclimatic-indicators?tab=overview

Agrometeorological indicators from 1979 to present derived from reanalysis. (n.d.). Retrieved May 15, 2021, from https://cds.climate.copernicus.eu/cdsapp#!/dataset/sis-agrometeorological-indicators?tab=overview

Ahmadi, M., Etedali, H. R., & Elbeltagi, A. (2021). Evaluation of the effect of climate change on maize water footprint under RCPs scenarios in Qazvin plain, Iran. *Agricultural Water Management*, *254*, 106969. https://doi.org/10.1016/j.agwat.2021.106969

Allen, R. G., Pereira, L. S., Raes, D., & Smith, M. (1998). *Crop evapotranspiration-Guidelines for computing crop water requirements-FAO Irrigation and drainage paper 56*. https://www.researchgate.net/publication/235704197_Crop_evapotranspiration-Guidelines_for_computing_crop_water_requirements-FAO_Irrigation_and_drainage_paper_56

Ania, W., & Mark, W. (2012). History of Agricultural Biotechnology: How Crop Development has Evolved | Learn Science at Scitable. *Nature Education Knowledge*, *3*(10), 9. https://www.nature.com/scitable/knowledge/library/history-of-agricultural-biotechnology-how-crop-development-25885295/

AsiaFlux. (n.d.). Retrieved June 30, 2021, from https://www.asiaflux.net/

Asseng, S., Zhu, Y., Wang, E., & Zhang, W. (2015). Crop modeling for climate change impact and adaptation. In *Crop Physiology: Applications for Genetic Improvement and Agronomy: Second Edition* (pp. 505–546). Elsevier Inc. https://doi.org/10.1016/B978-0-12-417104-6.00020-0

Barker, S. A., Bassham, J. A., Calvin, M., & Quarck, U. C. (1956). Intermediates in the photosynthetic cycle. *Biochimica et Biophysica Acta*, *21*(2), 376–377. https://doi.org/10.1016/0006-3002(56)90022-1

Bastiaanssen, W. G. M., & Ali, S. (2003). A new crop yield forecasting model based on satellite measurements applied across the Indus Basin, Pakistan. *Agriculture, Ecosystems and Environment*, *94*(3), 321–340. https://doi.org/10.1016/S0167-8809(02)00034-8

Boogaard, H., & Grijn, G. van der. (2019). *Product User Guide and Specification Data Stream 2 : AgERA5 historic and near real time forcing data Global Agriculture* (Issue April). https://cds.climate.copernicus.eu/cdsapp#!/dataset/sis-agrometeorological-indicators?tab=overview

Challinor, A. J., Watson, J., Lobell, D. B., Howden, S. M., Smith, D. R., & Chhetri, N. (2014). A meta-analysis of crop yield under climate change and adaptation. *Nature Climate Change*, *4*(4), 287–291. https://doi.org/10.1038/nclimate2153

Chen, T., Van Der Werf, G. R., Gobron, N., Moors, E. J., & Dolman, A. J. (2014). Global cropland monthly gross primary production in the year 2000. *Biogeosciences*, *11*(14), 3871–3880. https://doi.org/10.5194/bg-11-3871-2014

Climate change and global warming: Impacts on crop production. (2021). In *Genetically Modified Plants* (pp. 283–296). Elsevier. https://doi.org/10.1016/b978-0-12-818564-3.09991-1

CMIP: Global climate projections - Copernicus Knowledge Base - ECMWF Confluence Wiki. (n.d.). Retrieved June 11, 2021, from https://confluence.ecmwf.int/display/CKB/CMIP%3A+Global+climate+projections

Collatz, G. J., Ball, J. T., Grivet, C., & Berry, J. A. (1991). Physiological and environmental regulation of stomatal conductance, photosynthesis and transpiration: a model that includes a laminar boundary layer. *Agricultural and Forest Meteorology*, *54*(2–4), 107–136. https://doi.org/10.1016/0168-1923(91)90002-8

Collatz, G., Ribas-Carbo, M., & Berry, J. (1992). Coupled Photosynthesis-Stomatal Conductance Model for Leaves of C4 Plants. *Functional Plant Biology*, *19*(5), 519. https://doi.org/10.1071/pp9920519

Covshoff, S., & Hibberd, J. M. (2012). Integrating C 4 photosynthesis into C 3 crops to increase yield potential. In *Current Opinion in Biotechnology* (Vol. 23, Issue 2, pp. 209–214). Elsevier Current Trends. https://doi.org/10.1016/j.copbio.2011.12.011

Dando, W. A. (2005). Asia, climates of siberia, central and East Asia. In *Encyclopedia of Earth Sciences Series*

(pp. 102–114). Springer Netherlands. https://doi.org/10.1007/1-4020-3266-8_19
Delécolle, R., Maas, S. J., Guérif, M., & Baret, F. (1992a). Remote sensing and crop production models: present trends. *ISPRS Journal of Photogrammetry and Remote Sensing*, *47*(2–3), 145–161. https://doi.org/10.1016/0924-2716(92)90030-D
Delécolle, R., Maas, S. J., Guérif, M., & Baret, F. (1992b). Remote sensing and crop production models: present trends. *ISPRS Journal of Photogrammetry and Remote Sensing*, *47*(2–3), 145–161. https://doi.org/10.1016/0924-2716(92)90030-D
Devak, M., & Dhanya, C. T. (2017). Sensitivity analysis of hydrological models: Review and way forward. In *Journal of Water and Climate Change* (Vol. 8, Issue 4, pp. 557–575). IWA Publishing. https://doi.org/10.2166/wcc.2017.149
Dong, J., Lu, H., Wang, Y., Ye, T., & Yuan, W. (2020). Estimating winter wheat yield based on a light use efficiency model and wheat variety data. *ISPRS Journal of Photogrammetry and Remote Sensing*, *160*, 18–32. https://doi.org/10.1016/j.isprsjprs.2019.12.005
Doraiswamy, P. C., Hatfield, J. L., Jackson, T. J., Akhmedov, B., Prueger, J., & Stern, A. (2004). Crop condition and yield simulations using Landsat and MODIS. *Remote Sensing of Environment*, *92*(4), 548–559. https://doi.org/10.1016/j.rse.2004.05.017
Doraiswamy, Paul C, Moulin, S., Cook, P. W., & Stern, A. (2003). Crop yield assessment from remote sensing. In *Photogrammetric Engineering and Remote Sensing* (Vol. 69, Issue 6, pp. 665–674). https://doi.org/10.14358/PERS.69.6.665
Ehleringer, J. R., Sage, R. F., Flanagan, L. B., & Pearcy, R. W. (1991). Climate change and the evolution of C4 photosynthesis. In *Trends in Ecology and Evolution* (Vol. 6, Issue 3, pp. 95–99). Elsevier Current Trends. https://doi.org/10.1016/0169-5347(91)90183-X
ENVIS. (n.d.). *ANNUAL AVERAGE RAINFALL BY DISTRICTS IN PUNJAB (in mm)*. Retrieved June 18, 2021, from http://punenvis.nic.in/index3.aspx?sslid=3870&subsublinkid=3599&langid=1&mid=1
Ermakova, M., Danila, F. R., Furbank, R. T., & von Caemmerer, S. (2020). On the road to C4 rice: advances and perspectives. *Plant Journal*, *101*(4), 940–950. https://doi.org/10.1111/tpj.14562
European Environment Agency. (2017). *Copernicus Land Monitoring Service - EU-DEM*. *3436*, Permalink: 7860bc42f4c1494599f1e135c832788c. https://land.copernicus.eu/
FAO. (n.d.). *Cereals & Grains | Inpho | Food and Agriculture Organization of the United Nations*. Retrieved November 1, 2020, from http://www.fao.org/in-action/inpho/crop-compendium/cereals-grains/en/
FAO. (2008). An Introduction to the Basic Concepts of Food Security Food Security Information for Action. In *EC - FAO Food Security Programme*. http://www.fao.org/docrep/013/al936e/al936e00.pdf
FAO. (2009). Global agriculture towards 2050. *High-Level Expert Forum*.
FAO. (2015). *Food for all - World food summit - Agricultural machinery worldwide*. http://www.fao.org/3/x0262e/x0262e06.htm
FAO. (2017). *Methodology for Estimation of Crop Area and Crop Yield under Mixed and Continuous Cropping Publication prepared in the framework of the Global Strategy to improve Agricultural and Rural Statistics* (Issue March).
FAO. (2019). *SOFI 2019*. The State of Food Security and Nutrition in The World. http://www.fao.org/state-of-food-security-nutrition
FAOSTAT. (n.d.). *FAOSTAT*. Retrieved September 15, 2020, from http://www.fao.org/faostat/en/#data/QC/visualize
Fensholt, R., Rasmussen, K., Nielsen, T. T., & Mbow, C. (2009). Evaluation of earth observation based long term vegetation trends - Intercomparing NDVI time series trend analysis consistency of Sahel from AVHRR GIMMS, Terra MODIS and SPOT VGT data. *Remote Sensing of Environment*, *113*(9), 1886–1898. https://doi.org/10.1016/j.rse.2009.04.004
Fick, S. E., & Hijmans, R. J. (2017). WorldClim 2: new 1-km spatial resolution climate surfaces for global land areas. *International Journal of Climatology*, *37*(12), 4302–4315. https://doi.org/10.1002/joc.5086
GADM. (n.d.). Retrieved May 16, 2021, from https://gadm.org/download_country_v3.html
García, M., Sandholt, I., Ceccato, P., Ridler, M., Mougin, E., Kergoat, L., Morillas, L., Timouk, F., Fensholt, R., & Domingo, F. (2013). Actual evapotranspiration in drylands derived from in-situ and satellite data: Assessing biophysical constraints. *Remote Sensing of Environment*, *131*, 103–118. https://doi.org/10.1016/j.rse.2012.12.016
Goal 2: Zero Hunger – United Nations Sustainable Development. (n.d.). Retrieved October 28, 2020, from https://www.un.org/sustainabledevelopment/hunger/

Guhathakurta, P., L, S. B., Menon, P., Prasad, A. K., Sangwan, N., & Advani, S. C. (2020). *Observed Rainfall Variability and Changes Over Bihar State*.

Guhathakurta, P., L, S. kumar B., Menon, P., Prasad, A. K., Sable, S. T., & Advani, S. C. (2020). *Observed Rainfall Variability and Changes Over Uttar Pradesh State*.

Gummert, M., & Rickman, J. F. (2010). *When to harvest - IRRI Rice Knowledge Bank*. http://www.knowledgebank.irri.org/training/fact-sheets/item/when-to-harvest-fact-sheet

Herman, J. D., Kollat, J. B., Reed, P. M., & Wagener, T. (2013). Technical Note: Method of Morris effectively reduces the computational demands of global sensitivity analysis for distributed watershed models. *Hydrology and Earth System Sciences*, *17*(7), 2893–2903. https://doi.org/10.5194/hess-17-2893-2013

Hird, J. N., & McDermid, G. J. (2009). Noise reduction of NDVI time series: An empirical comparison of selected techniques. *Remote Sensing of Environment*, *113*(1), 248–258. https://doi.org/10.1016/j.rse.2008.09.003

Hoefsloot, P., Ines, A., Dam, J. Van, Duveiller, G., Kayitakire, F., & Hansen, J. (2012). *Combining Crop Models and Remote Sensing for Yield Prediction: Concepts, Applications and Challenges for Heterogeneous Smallholder Environments*. https://doi.org/10.2788/72447

Hoogenboom, G., Porter, C. H., Boote, K. J., Shelia, V., Wilkens, P. W., Singh, U., White, J. W., Asseng, S., Lizaso, J. I., Moreno, L. P., Pavan, W., Ogoshi, R., Hunt, L. A., Tsuji, G. Y., & Jones, J. W. (2019). *The DSSAT crop modeling ecosystem* (pp. 173–216). https://doi.org/10.19103/as.2019.0061.10

Huang, X., Liu, J., Zhu, W., Atzberger, C., & Liu, Q. (2019). The optimal threshold and vegetation index time series for retrieving crop phenology based on a modified dynamic threshold method. *Remote Sensing*, *11*(23), 2725. https://doi.org/10.3390/rs11232725

ICAR. (n.d.). *Punjab*. Retrieved June 18, 2021, from https://icar.org.in/files/state-specific/chapter/99.htm

IIASA. (2015). *RCP Database*. Versión 2.0.5. Representative Concentration Pathways (RCPs). International Institute for Applied Systems Analysis. https://tntcat.iiasa.ac.at/RcpDb/dsd?Action=htmlpage&page=about

IPCC. (2014). IPCC DDC Glossary. In *IPCC Fifth Assessment Report*. https://www.ipcc-data.org/guidelines/pages/glossary/glossary_r.html

IRRI. (2011). *Importance of Rice*. Knowledge Bank. http://www.knowledgebank.irri.org/ericeproduction/Importance_of_Rice.htm

JICA. (2010). *RICE CULTIVATION HANDBOOK*. https://www.jica.go.jp/activities/issues/agricul/approach/ku57pq00002m21du-att/handbook_01.pdf

Jönsson, P., & Eklundh, L. (2004). TIMESAT - A program for analyzing time-series of satellite sensor data. *Computers and Geosciences*, *30*(8), 833–845. https://doi.org/10.1016/j.cageo.2004.05.006

Langdale, J. A. (2011). C 4 Cycles: Past, present, and future research on C 4 photosynthesis. *Plant Cell*, *23*(11), 3879–3892. https://doi.org/10.1105/tpc.111.092098

Li, W., Zhao, S., Chen, Y., Wang, Q., & Ai, W. (2021). State of China's Climate in 2020. *Atmospheric and Oceanic Science Letters*, 100048. https://doi.org/10.1016/j.aosl.2021.100048

Li, X., Zhu, Z., Zeng, H., & Piao, S. (2016). Estimation of gross primary production in China (1982-2010) with multiple ecosystem models. *Ecological Modelling*, *324*, 33–44. https://doi.org/10.1016/j.ecolmodel.2015.12.019

Lin, H. C., Coe, R. A., Paul Quick, W., & Bandyopadhyay, A. (2019). Climate-resilient future crop: Development of c4 rice. In *Sustainable Solutions for Food Security: Combating Climate Change by Adaptation* (pp. 111–124). Springer International Publishing. https://doi.org/10.1007/978-3-319-77878-5_6

Lobell, D. B., Hicke, J. A., Asner, G. P., Field, C. B., Tucker, C. J., & Los, S. O. (2002). Satellite estimates of productivity and light use efficiency in United States agriculture, 1982-98. *Global Change Biology*, *8*(8), 722–735. https://doi.org/10.1046/j.1365-2486.2002.00503.x

Lobell, David B. (2013). The use of satellite data for crop yield gap analysis. *Field Crops Research*, *143*, 56–64. https://doi.org/10.1016/j.fcr.2012.08.008

Lobell, David B., Schlenker, W., & Costa-Roberts, J. (2011). Climate trends and global crop production since 1980. *Science*, *333*(6042), 616–620. https://doi.org/10.1126/science.1204531

Marshall, M, Okuto, E., Kang, Y., Opiyo, E., & Ahmed, M. (2016). Global assessment of Vegetation Index and Phenology Lab (VIP) and Global Inventory Modeling and Mapping Studies (GIMMS) version 3 products. *Biogeosciences*, *13*, 625–639. https://doi.org/10.5194/bg-13-625-2016

Marshall, Michael, Tu, K., & Brown, J. (2018). Optimizing a remote sensing production efficiency model for macro-scale GPP and yield estimation in agroecosystems. *Remote Sensing of Environment*,

217(August), 258–271. https://doi.org/10.1016/j.rse.2018.08.001
Meacham-Hensold, K. (2020). The difference between C3 and C4 plants. In *Realizing Increased Photosynthetic Efficiency*. https://ripe.illinois.edu/blog/difference-between-c3-and-c4-plants
Medlyn, B. E., Duursma, R. A., Eamus, D., Ellsworth, D. S., Prentice, I. C., Barton, C. V. M., Crous, K. Y., De Angelis, P., Freeman, M., & Wingate, L. (2011). Reconciling the optimal and empirical approaches to modelling stomatal conductance. *Global Change Biology*, *17*(6), 2134–2144. https://doi.org/10.1111/j.1365-2486.2010.02375.x
Monteith, J. L. (1977). Climate and the efficiency of crop production in Britain. In *Trans. R. Soc. Lond. B* (Vol. 281).
Morgan, J. A., Lecain, D. R., Pendall, E., Blumenthal, D. M., Kimball, B. A., Carrillo, Y., Williams, D. G., Heisler-White, J., Dijkstra, F. A., & West, M. (2011a). C4 grasses prosper as carbon dioxide eliminates desiccation in warmed semi-arid grassland. *Nature*, *476*(7359), 202–205. https://doi.org/10.1038/nature10274
Morgan, J. A., Lecain, D. R., Pendall, E., Blumenthal, D. M., Kimball, B. A., Carrillo, Y., Williams, D. G., Heisler-White, J., Dijkstra, F. A., & West, M. (2011b). C4 grasses prosper as carbon dioxide eliminates desiccation in warmed semi-arid grassland. *Nature*, *476*(7359), 202–205. https://doi.org/10.1038/nature10274
Mõttus, M., Sulev, M., Baret, F., Lopez-Lozano, R., & Reinart, A. (2012). Photosynthetically Active Radiation: Measurement photosynthesis/photosynthetic(ally) active radiation (PAR) measurement and Modeling photosynthesis/photosynthetic(ally) active radiation (PAR) modeling. In *Encyclopedia of Sustainability Science and Technology* (pp. 7902–7932). Springer New York. https://doi.org/10.1007/978-1-4419-0851-3_451
Müller, C., Elliott, J., Chryssanthacopoulos, J., Deryng, D., Folberth, C., Pugh, T. A. M., & Schmid, E. (2015). Implications of climate mitigation for future agricultural production. *Environmental Research Letters*, *10*(12), 125004. https://doi.org/10.1088/1748-9326/10/12/125004
NCAR UCAR. (2018). *NDVI: Normalized Difference Vegetation Index-3rd generation: NASA/GFSC GIMMS | NCAR - Climate Data Guide*. https://climatedataguide.ucar.edu/climate-data/ndvi-normalized-difference-vegetation-index-3rd-generation-nasagfsc-gimms
Nelson, A., & Gumma, M. K. (2015). A map of lowland rice extent in the major rice growing countries of Asia. *IRRI*, 37.
Nguy-Robertson, A., Suyker, A., & Xiao, X. (2015). Modeling gross primary production of maize and soybean croplands using light quality, temperature, water stress, and phenology. *Agricultural and Forest Meteorology*, *213*, 160–172. https://doi.org/10.1016/j.agrformet.2015.04.008
NOAA. (n.d.). *NOAA's Office of Satellite and Product Operations*.
Owen, K. E., Tenhunen, J., Reichstein, M., Wang, Q., Falge, E., Geyer, R., Xiao, X., Stoy, P., Ammann, C., Arain, A., Aubinet, M., Aurela, M., Bernhofer, C., Chojnicki, B. H., Granier, A., Gruenwald, T., Hadley, J., Heinesch, B., Hollinger, D., … Vogel, C. (2007). Linking flux network measurements to continental scale simulations: Ecosystem carbon dioxide exchange capacity under non-water-stressed conditions. *Global Change Biology*, *13*(4), 734–760. https://doi.org/10.1111/j.1365-2486.2007.01326.x
Pan, X., & Deng, Q. (2007). Review on crop harvest index. *Acta Agriculturae Universitatis Jiangxiensis*.
Papademetriou, M. K. (2000). RICE PRODUCTION IN THE ASIA-PACIFIC REGION : ISSUES AND PERSPECTIVES. In *FAO report*. http://www.fao.org/3/x6905e/x6905e04.htm
Peng, D., Huang, J., Li, C., Liu, L., Huang, W., Wang, F., & Yang, X. (2014). Modelling paddy rice yield using MODIS data. *Agricultural and Forest Meteorology*, *184*, 107–116. https://doi.org/10.1016/j.agrformet.2013.09.006
Photorespiration (article) | Photosynthesis | Khan Academy. (n.d.). Retrieved October 18, 2020, from https://www.khanacademy.org/science/biology/photosynthesis-in-plants/photorespiration--c3-c4-cam-plants/a/c3-c4-cam-plants
Pinzon, J., & Tucker, C. (2014). A Non-Stationary 1981–2012 AVHRR NDVI3g Time Series. *Remote Sensing*, *6*(8), 6929–6960. https://doi.org/10.3390/rs6086929
Potter, C. S., Randerson, J. T., Field, C. B., Matson, P. A., Vitousek, P. M., Mooney, H. A., & Klooster, S. A. (1993). Terrestrial ecosystem production: A process model based on global satellite and surface data. *Global Biogeochemical Cycles*, *7*(4), 811–841. https://doi.org/10.1029/93GB02725
Reeves, M. C., Zhao, M., & Running, S. W. (2005). Usefulness and limits on MODIS GPP for estimating wheat yield. *International Journal of Remote Sensing*, *26*(7), 1403–1421. https://doi.org/10.1080/01431160512331326567
Rice productivity - Ricepedia. (n.d.). Retrieved May 30, 2020, from http://ricepedia.org/rice-as-a-crop/rice-

productivity
Rosenzweig, C., Karoly, D., Vicarelli, M., Neofotis, P., Wu, Q., Casassa, G., Menzel, A., Root, T. L., Estrella, N., Seguin, B., Tryjanowski, P., Liu, C., Rawlins, S., & Imeson, A. (2008). Attributing physical and biological impacts to anthropogenic climate change. *Nature*, *453*(7193), 353–357. https://doi.org/10.1038/nature06937
Roser, Max and Ortiz-Ospina, E. (2013). *Global Extreme Poverty - Our World in Data*. OurWorldInData.Org. https://ourworldindata.org/extreme-poverty
Running, S. W., Thornton, P. E., Nemani, R., & Glassy, J. M. (2000). Global Terrestrial Gross and Net Primary Productivity from the Earth Observing System. In *Methods in Ecosystem Science* (pp. 44–57). Springer New York. https://doi.org/10.1007/978-1-4612-1224-9_4
Ryan, M. G. (1991). *Effects of Climate Change on Plant Respiration* (Vol. 1, Issue 2).
Sage, R. F., & Zhu, X. G. (2011). Exploiting the engine of C 4 photosynthesis. *Journal of Experimental Botany*, *62*(9), 2989–3000. https://doi.org/10.1093/jxb/err179
Simkin, A. J., López-Calcagno, P. E., & Raines, C. A. (2019). Feeding the world: Improving photosynthetic efficiency for sustainable crop production. In *Journal of Experimental Botany* (Vol. 70, Issue 4, pp. 1119–1140). Oxford University Press. https://doi.org/10.1093/jxb/ery445
Sims, D. A., Rahman, A. F., Cordova, V. D., Baldocchi, D. D., Flanagan, L. B., Goldstein, A. H., Hollinger, D. Y., Misson, L., Monson, R. K., Schmid, H. P., Wofsy, S. C., & Xu, L. (2005). Midday values of gross CO2 flux and light use efficiency during satellite overpasses can be used to directly estimate eight-day mean flux. *Agricultural and Forest Meteorology*, *131*(1–2), 1–12. https://doi.org/10.1016/j.agrformet.2005.04.006
Sinclair, T. R., Purcell, L. C., & Sneller, C. H. (2004). Crop transformation and the challenge to increase yield potential. *Trends in Plant Science*, *9*(2), 70–75. https://doi.org/10.1016/j.tplants.2003.12.008
Sobol, I. M. (2001). Global sensitivity indices for nonlinear mathematical models and their Monte Carlo estimates. *Mathematics and Computers in Simulation*, *55*(1–3), 271–280. https://doi.org/10.1016/S0378-4754(00)00270-6
Socio-Economic Data and Scenarios. (2019, November 4). https://sedac.ciesin.columbia.edu/ddc/ar5_scenario_process/RCPs.html
Song, X., Zhang, J., Zhan, C., Xuan, Y., Ye, M., & Xu, C. (2015). Global sensitivity analysis in hydrological modeling: Review of concepts, methods, theoretical framework, and applications. In *Journal of Hydrology* (Vol. 523, pp. 739–757). Elsevier. https://doi.org/10.1016/j.jhydrol.2015.02.013
Stocker, T. F., Qin, D., Plattner, G. K., Tignor, M., Allen, S. K., Boschung, J., Nauels, A., Xia, Y., Bex, V., & Midgley, P. M. (2013). *IPCC, 2013: Climate Change 2013: The Physical Science Basis. Contribution of Working Group I to the Fifth Assessment Report of the Intergovernmental Panel on Climate Change*. https://www.ipcc.ch/report/ar5/wg1/
Tada, R., Zheng, H., & Clift, P. D. (2016). Evolution and variability of the Asian monsoon and its potential linkage with uplift of the Himalaya and Tibetan Plateau. In *Progress in Earth and Planetary Science* (Vol. 3, Issue 1, p. 4). Springer Berlin Heidelberg. https://doi.org/10.1186/s40645-016-0080-y
Taylor, S. H., Hulme, S. P., Rees, M., Ripley, B. S., Ian Woodward, F., & Osborne, C. P. (2010). Ecophysiological traits in C_3 and C_4 grasses: a phylogenetically controlled screening experiment. *New Phytologist*, *185*(3), 780–791. https://doi.org/10.1111/j.1469-8137.2009.03102.x
Taylor, S. H., Ripley, B. S., Martin, T., De-Wet, L. A., Woodward, F. I., & Osborne, C. P. (2014). Physiological advantages of C4 grasses in the field: A comparative experiment demonstrating the importance of drought. *Global Change Biology*, *20*(6), 1992–2003. https://doi.org/10.1111/gcb.12498
Teluguntla, P., Ryu, D., George, B., Walker, J. P., & Malano, H. M. (2015). Mapping flooded rice paddies using time series of MODIS imagery in the Krishna River Basin, India. *Remote Sensing*, *7*(7), 8858–8882. https://doi.org/10.3390/rs70708858
The C4 Rice Project. (n.d.). Retrieved April 19, 2021, from https://c4rice.com/
Tian, F., Fensholt, R., Verbesselt, J., Grogan, K., Horion, S., & Wang, Y. (2015). Evaluating temporal consistency of long-term global NDVI datasets for trend analysis. *Remote Sensing of Environment*, *163*, 326–340. https://doi.org/10.1016/j.rse.2015.03.031
USDA. (2015). *Southeast Asia: 2015/16 Rice Production Outlook at Record Levels*. https://ipad.fas.usda.gov/highlights/2015/06/Southeast_Asia/Index.htm
van Vuuren, D. P., Edmonds, J., Kainuma, M., Riahi, K., Thomson, A., Hibbard, K., Hurtt, G. C., Kram, T., Krey, V., Lamarque, J. F., Masui, T., Meinshausen, M., Nakicenovic, N., Smith, S. J., & Rose, S. K. (2011). The representative concentration pathways: An overview. *Climatic Change*, *109*(1), 5–31.

https://doi.org/10.1007/s10584-011-0148-z
Von Caemmerer, S., Quick, W. P., & Furbank, R. T. (2012). The development of C4 rice: Current progress and future challenges. In *Science* (Vol. 336, Issue 6089, pp. 1671–1672). https://doi.org/10.1126/science.1220177
Wang, F., Wang, F., Wang, F., Hu, J., Hu, J., Xie, L., Xie, L., Yao, X., & Yao, X. (2020). Rice yield estimation based on an NPP model with a changing harvest index. *IEEE Journal of Selected Topics in Applied Earth Observations and Remote Sensing*, *13*, 2953–2959. https://doi.org/10.1109/JSTARS.2020.2993905
Weiss, M., Jacob, F., & Duveiller, G. (2020). Remote sensing for agricultural applications: A meta-review. *Remote Sensing of Environment*, *236*, 111402. https://doi.org/10.1016/j.rse.2019.111402
Where is rice grown? - Ricepedia. (n.d.). Retrieved May 13, 2021, from https://ricepedia.org/rice-as-a-crop/where-is-rice-grown
WHO EMRO | Food security | Nutrition. (n.d.). Retrieved February 22, 2021, from http://www.emro.who.int/nutrition/food-security/
Xiao, X., Hollinger, D., Aber, J., Goltz, M., Davidson, E. A., Zhang, Q., & Moore, B. (2004). Satellite-based modeling of gross primary production in an evergreen needleleaf forest. *Remote Sensing of Environment*, *89*(4), 519–534. https://doi.org/10.1016/j.rse.2003.11.008
Xin, Q., Gong, P., Yu, C., Yu, L., Broich, M., Suyker, A. E., & Myneni, R. B. (2013). A production efficiency model-based method for satellite estimates of corn and soybean yields in the midwestern US. *Remote Sensing*, *5*(11), 5926–5943. https://doi.org/10.3390/rs5115926
Yang, P., Prikaziuk, E., Verhoef, W., & van der Tol, C. (2020). SCOPE 2.0: A model to simulate vegetated land surface fluxes and satellite signals. *Geoscientific Model Development Discussions*, *October*, 1–26. https://doi.org/10.5194/gmd-2020-251
Yuan, W., Chen, Y., Xia, J., Dong, W., Magliulo, V., Moors, E., Olesen, J. E., & Zhang, H. (2015). Estimating crop yield using a satellite-based light use efficiency model. *Ecological Indicators*, *60*, 702–709. https://doi.org/10.1016/j.ecolind.2015.08.013
Yuan, W., Liu, S., Yu, G., Bonnefond, J. M., Chen, J., Davis, K., Desai, A. R., Goldstein, A. H., Gianelle, D., Rossi, F., Suyker, A. E., & Verma, S. B. (2010). Global estimates of evapotranspiration and gross primary production based on MODIS and global meteorology data. *Remote Sensing of Environment*, *114*(7), 1416–1431. https://doi.org/10.1016/j.rse.2010.01.022
Yuan, W., Liu, S., Zhou, G., Zhou, G., Tieszen, L. L., Baldocchi, D., Bernhofer, C., Gholz, H., Goldstein, A. H., Goulden, M. L., Hollinger, D. Y., Hu, Y., Law, B. E., Stoy, P. C., Vesala, T., & Wofsy, S. C. (2007). Deriving a light use efficiency model from eddy covariance flux data for predicting daily gross primary production across biomes. *Agricultural and Forest Meteorology*, *143*(3–4), 189–207. https://doi.org/10.1016/j.agrformet.2006.12.001
Zan, M., Zhou, Y., Ju, W., Zhang, Y., Zhang, L., & Liu, Y. (2018). Performance of a two-leaf light use efficiency model for mapping gross primary productivity against remotely sensed sun-induced chlorophyll fluorescence data. *Science of the Total Environment*, *613–614*, 977–989. https://doi.org/10.1016/j.scitotenv.2017.09.002
Zero Hunger | World Food Programme. (n.d.). Retrieved April 15, 2021, from https://www.wfp.org/zero-hunger?utm_source=google&utm_medium=cpc&utm_campaign=7170000079041288&gclid=Cj0KCQjwyN-DBhCDARIsAFOELTm_MqtwD-0PdV7og3rQ2pMEe2bFG0jyjEDQ4HTF8F3vzHF3x_b4AlUaAk2lEALw_wcB&gclsrc=aw.ds
Zhang, J., Zhao, J., Wang, Y., Zhang, H., Zhang, Z., & Guo, X. (2020). Comparison of land surface phenology in the Northern Hemisphere based on AVHRR GIMMS3g and MODIS datasets. *ISPRS Journal of Photogrammetry and Remote Sensing*, *169*, 1–16. https://doi.org/10.1016/j.isprsjprs.2020.08.020
Zhou, X., Zheng, H. B., Xu, X. Q., He, J. Y., Ge, X. K., Yao, X., Cheng, T., Zhu, Y., Cao, W. X., & Tian, Y. C. (2017). Predicting grain yield in rice using multi-temporal vegetation indices from UAV-based multispectral and digital imagery. *ISPRS Journal of Photogrammetry and Remote Sensing*, *130*, 246–255. https://doi.org/10.1016/j.isprsjprs.2017.05.003